Designing Wave-measuring Instruments

by

David Joel Chen

Submitted to the Department of Ocean Engineering
in Partial Fulfillment of the Requirements for the Degree of
Master of Science
at the
Massachusetts Institute of Technology
May 1994

Signature of Author _____
Department of Ocean Engineering
May 6, 1994

Certified by _____
Professor Jerome Milgram
Thesis Supervisor

Accepted by _____
Professor A. Douglas Carmichael
Chairman, Department of Ocean Engineering Graduate Committee

Designing Wave-measuring Instruments

by

David Joel Chen

Submitted to the Massachusetts Institute of Technology on May 6, 1994,
in partial fulfillment of the requirements for the degree of
Master of Science in Ocean Engineering

Abstract

The accurate measurement of water waves is an essential need of many experiments in the realm of ocean engineering. For instance, the study of non-linear wave-wave interactions requires an excellent ability to discern a variety of wave frequencies which have wave amplitudes that can vary over a few orders of magnitude. Similarly, the study of how surface films attenuate wave propagation requires a dependable means of tracking changes in wave amplitudes. One final example of a wave gauge application is the determination of the sea wave directional spectrum in a ship's wake by using a multi-channel saltwater gauge. In all cases, a reliable set of wave gauges is necessary for the quantification of the dynamics of a changing water surface.

The design of one such set of wave-measuring instruments has been based on resistive/conductive techniques utilizing surface-piercing wires. There are variations in this design based on whether freshwater or saltwater waves are being measured.

The performance of this set of wave gauges has been evaluated in terms of linearity, sensitivity, and repeatability. Furthermore, on a system level, both the accuracy and precision of the gauges in estimating wave amplitudes and frequencies have been analyzed in controlled laboratory situations. Spectral analyses, both in the frequency and wavenumber domains, have yielded encouraging results about the ability of these wave-measuring instruments to perform effectively in their particular applications.

Thesis supervisor: Dr. Jerome Milgram
Title: Professor of Ocean Engineering

Acknowledgements

I would very much like to thank my labmates in the MIT Marine Instrumentation and Computation Laboratory, whose help and support have been essential to the completion of my research project. Not only have they provided me with a supportive atmosphere, but each individual has also contributed an important part to the wave gauge development.

In particular, I would like to thank John Mass first for writing the signal processing code necessary for the autocorrelation and spectra calculations and second for helping me to test and debug the wave gauges (especially in regard to power supplies). Next, I would like to thank Noah Eckhouse for writing the data acquisition software, building the mechanical oscillator needed for my bucket tests, and being the impeccable lab manager. In addition, I owe my thanks to Hasan Olmez for all his FFT code and his helping me to understand it. I would also like to thank Greg Thomas for showing me how to discipline myself to do a few pages of thesis work each day. Finally, I would like to thank Soren Jensen both for machining the central rod for my "circular harp" and for being a fellow graduate student who let me know I was not alone in my struggles at MIT.

Furthermore, I am grateful to Professor Jerome Milgram for being my thesis advisor as well as my academic advisor. His guidance and insight always spurred my project along.

Finally, I would like to thank Rebecca for all her support and understanding, especially when it came to those very late nights at work.

Support for this thesis was provided in part by the following grants from the Office of Naval Research: Grant #N00014-93-1-0726, Grant #N00014-94-1-0236, Grant #N00014-89-J-1185, and Grant #N00014-89-J-1499.

Table of Contents

List of Figures

List of Tables

Designing Wave-measuring Instruments

1. Introduction

It is often useful to be able to quantify accurately the heights and frequencies of water waves. The design and development of such a wave-measuring instrument can be based on a variety of concepts, ranging from optical techniques to capacitive and resistive techniques. There are many criteria by which the effectiveness of these techniques can be judged, and each of these techniques has its advantages and disadvantages. Based on many design considerations, the wave gauge designs considered here for measuring water waves ranging in amplitude from a fraction of a millimeter to tens of centimeters are variations on a resistance or conductance technique. In this resistance/conductance technique, there are differences in the design which depend on whether freshwater or saltwater waves are being measured. The fundamental idea behind the freshwater wave gauge design is the measurement of conductance changes between two probe wires that pierce the water's surface. The fundamental idea behind the saltwater wave gauge design, is the measurement of resistance changes in a single probe wire that is "grounded" at one end by the saltwater. In the former case, the conductance between the two wires is linearly related to the water level across the probe pair; and in the latter case, the effective resistance of the probe wire changes linearly with water level. By monitoring these conductive/resistive changes and then amplifying and filtering their associated signals appropriately, these wave gauge circuits can transform linearly a wave height into an analog voltage output.

1.1. Background

The motivation for developing various freshwater and saltwater wave gauges stemmed from the experimental needs of the MIT Marine Instrumentation and Computation Laboratory. In particular, a reliable set of freshwater gauges was required as instrumentation for the laboratory's wave tank facility. In addition, a set of long-wire freshwater wave gauges was required for a wave-wave interaction experiment taking place in a wave facility in Canada. Finally, a multi-channel saltwater wave gauge was to be developed for measuring the short-wave directional spectrum in a piece of the ocean's surface. Although each of these needs has been distinct, the research in designing effective wave gauges has been relevant to all of these applications.

1.2. Objective

The primary objective of this wave gauge research has been to produce wave gauges that are accurate, sensitive, and repeatable in their capacity for measuring waves. Secondary considerations have been ease of usage, flexibility in performing modifications, and instrument ruggedness. Finally, for each particular wave gauge application, there have been particular design constraints to be met, such as frequency response and gain characteristics.

2. Theory

2.1. Modeling the behavior of conductors in water

To design an effective probe amplifier, it is crucial to understand the behavior of the probe wires in the water. To that end, it is useful to develop a physical model on which the design can be based. These models guide the wave gauge designs by providing insight into the behavior of conductors in both saltwater and freshwater.

The model of a saltwater probe is based on the electric field behavior of a single wire conductor which pierces a volume of saltwater. Figure 2.1 illustrates cross-sections of the model in cylindrical space; part a) of the figure is a top-view, and part b) of the figure is a side-view.

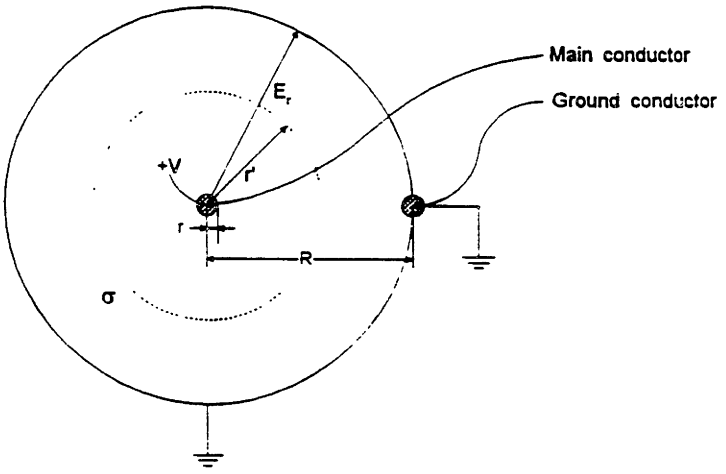

a) Top View Cross-section

Figure 2.1: A Model of the Behavior of Conductors in Water
a) Top View

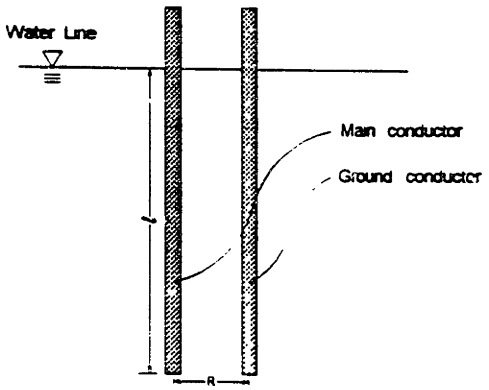

b) Side View Cross-section

Figure 2.1: A Model of the Behavior of Conductors in Water
b) Side View

The model's purpose is to provide an estimate of the effective resistance between the wire and some grounding plate in the water, given the submerged length of the wire, the effective radial distance from the conductor to ground, and the conductivity of the water (See Equation 2.1). A derivation of Equation 2.1, which relates all of these variables, can be found in Appendix A.

$$R_{probe} = \left(\frac{1}{2\pi\sigma l}\right) \times \ln\left(\frac{R}{r}\right) \qquad [2.1]$$

where σ = water conductivity in mhos/cm
l = length of submerged wire in cm
R = radial distance from the conductor to ground in cm
r = radius of the conductor in cm (in this case, 0.0056 cm)

Knowledge of these relationships yields information about the relative importance of the intrinsic wire resistance compared to the resistance through the water. For saltwater, which has a relatively large conductivity (0.035 mho/cm with S = 25‰ and T = 20°C), it is found that the effective resistance in the water path is low compared to the high resistance (27Ω/ft) of the nichrome wire itself (See Equation 2.2).

For fourteen inches of submerged 36 AWG nichrome wire, a resistance comparison yields...

$$\left(\frac{1}{2\pi(0.035 mho/cm)(2.54 cm/in)(14 in)}\right)\ln\left(\frac{1cm}{0.0056cm}\right) << \left(\frac{27\Omega}{ft}\right)\left(\frac{ft}{12in}\right)(14in)$$

or **0.66Ω** (Res. through water) << **31.5Ω** (Res. through submerged wire) [2.2]

Consequently, it follows that the design of a saltwater wave gauge can be based on an exposed wire resistance that changes linearly with wave height. With the saltwater grounded, the resistance of the probe is dominated by the resistance of the exposed portion of the nichrome wire. Thus, as the water level changes, the effective resistance of the wire, assuming uniformity, varies linearly.

The model of the freshwater probe is very similar to that of the saltwater probe. However, instead of having one surface-piercing wire and a ground plate, there is a pair of surface-piercing wires. The same concentric model in Figure 2.1 can thus be used, taking into account, however, the fact that the effective ground path is only a fraction of the total outer cylinder area (See Figure 2.2).

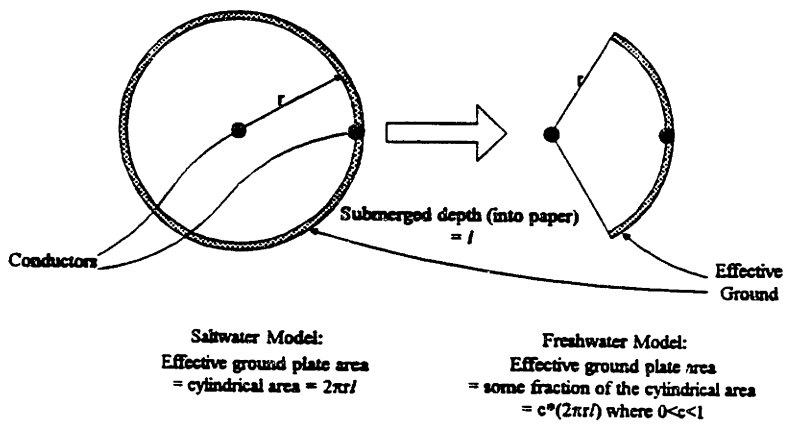

Figure 2.2: Top View Cross-section of Conductor Models

Empirically, the effective ground plate area is found to be roughly one third of the total cylindrical area (i.e. c = 0.33). Utilizing the relationship given by Equation 2.1 and remembering to scale up the result by a factor of three (i.e. 1/c), it is found that the effective resistance in the freshwater path is no longer negligible compared to the resistance in the nichrome wire. In fact, the conductivity of freshwater (0.00045 mho/cm with S near zero and T = 20°C) is sufficiently low such that the resistance in the water path dominates that of the wire.

Performing a calculation similar to that of Equation 2.2, it is found that in the case of the short-wire freshwater gauges, the resistance through the water is **1830Ω**, and the intrinsic wire resistances of the wet and dry portions are **5.3Ω** and **12.4Ω**, respectively. For this case, the submerged length and the exposed length of wire are assumed to be three centimeters per wire and seven centimeters per wire, respectively.

In the long-wire case, 30 AWG copper wire is used, so the resistance calculations now assume an intrinsic wire resistance of 0.3Ω/ft and a wire radius of 0.013 cm. Furthermore, the submerged length and the exposed length of wire are each assumed to be fifty centimeters per wire. Accordingly, for the long-wire freshwater gauges, the resistance through the water is **92Ω**, and the intrinsic resistances of the submerged and exposed wire portions are **0.98Ω** each. Thus, in both freshwater cases, the resistance through the water dominates all other resistances. Consequently, the wave height is linearly proportional to the effective **conductance** of the probe; that is to say, the wave height is inversely proportional to the effective resistance of the probe.

Another way to visualize the freshwater probe is to imagine the sunken portion of the probe pair as a chain of resistors in parallel (See Figure 2.3).

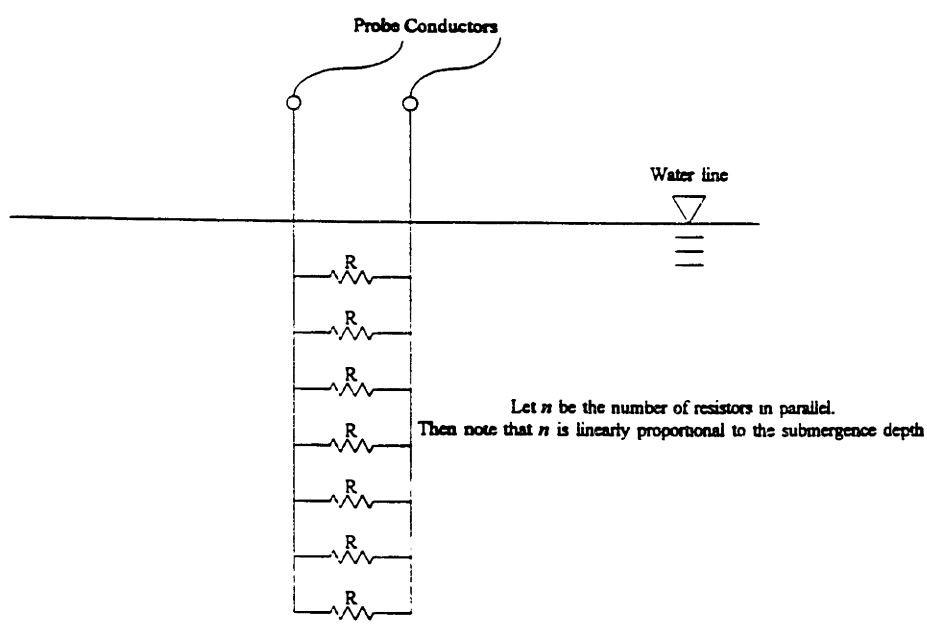

Figure 2.3: Resistor Model of Freshwater Probes

As the water level increases, the number of resistors in parallel increases, thus causing the overall resistance to decrease. Equation 2.3 shows how the overall resistance is inversely proportional to the number of resistors, or wave height.

$$Res(n) = \frac{1}{\left(\frac{1}{R}+\frac{1}{R}+\frac{1}{R}+\ldots\right)} = \frac{1}{n\times\left(\frac{1}{R}\right)} = \frac{R}{n} \qquad [2.3]$$

An advantage of these analytical models is their simplicity; a disadvantage, however, may be the neglecting of factors which could affect the accuracy of the models. For instance, electric field considerations due to edge effects have been completely ignored in our analytical models. Thus, a broader numerical analysis has also been performed in an attempt to provide a more accurate prediction of conductor behavior. The basic concept, omitting many details, is to discretize a three-dimensional volume and then solve Laplace's equations for node voltages throughout that volume, given the appropriate boundary conditions on the probe wires. The results of these numerical studies are consistent with the predictions of the analytical models; therefore, the analytical models are acceptable models for designing wave gauges.

2.2. Circuit theory for the probe amplifiers

The design for the probe amplifier of the saltwater wave gauge is relatively straightforward. The surface-piercing single probe wire acts as a resistor in the bottom leg of a voltage divider (see Figure 2.4).

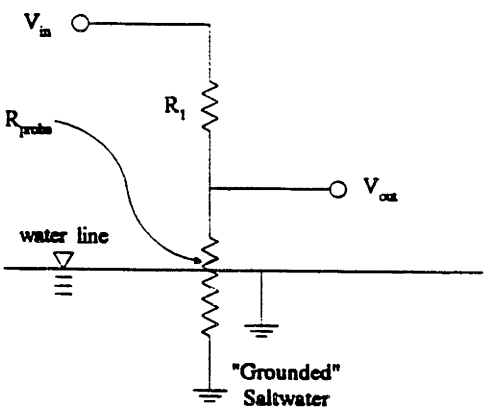

Note: R_{probe} is the resistance of the dry portion of the probe only

Figure 2.4: Divider circuit for the saltwater probe

Given a large enough resistor in the top leg, the changing resistance of the probe due to surface elevation changes maps linearly via constants, V_{in} and R_1, into a changing voltage level (see Equation 2.4).

$$V_{out} = V_{in} \times \left(\frac{R_{probe}}{R_1 + R_{probe}} \right) \approx V_{in} \times \left(\frac{R_{probe}}{R_1} \right) \text{ for large } R_1 \qquad [2.4]$$

The probe amplifier for the freshwater wave gauge is somewhat more sophisticated. Figure 2.5 contains a schematic for the design.

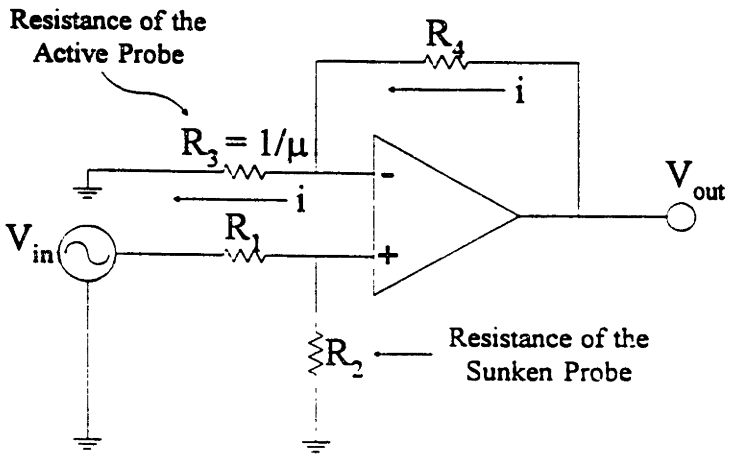

μ is the conductance between the two probe wires of the active probe and is linearly proportional to the water level

Figure 2.5: Freshwater Probe Amplifier Design

Circuit analysis yields the final result relating probe conductance to output voltage (Equation 2.8).

From the circuit,

$$E = V_{in} \times \left(\frac{R_2}{R_1+R_2} \right) \qquad [2.5]$$

$$i = \frac{E}{R_3} = \frac{V_{in}}{R_3} \times \left(\frac{R_2}{R_1+R_2} \right) \qquad [2.6]$$

$$V_{out} = E + iR_4 \qquad [2.7]$$

Now, substituting Eqn.2.5 and Eqn.2.6 into Eqn.2.7,

$$V_{out} = V_{in} \times \left(\frac{R_2}{R_1+R_2}\right) \times \left[1 + \frac{R_4}{R_3}\right]$$

Finally, letting μ represent the inverse of R_3, the equation becomes:

$$V_{out} = V_{in} \times \left(\frac{R_2}{R_1+R_2}\right) \times [1 + \mu R_4]$$

$$\approx V_{in} \times \left(\frac{R_2 R_4}{R_1}\right) \times \mu \quad \text{for large } R_1 \text{ and } R_4 \qquad [2.8]$$

The output voltage is directly proportional to μ (the probe conductance), which is proportional to the water level on the probe wires. Linearity is preserved once again. Of particular interest in the design of the freshwater probe amplifier is the inclusion of a second probe pair, which is completely submerged. The purpose of this sunken probe pair is to compensate for changes in water conductivity. If, for example, the water conductivity changes, say, $R_3' = kR_3$ and $R_2' = kR_2$ where k is some constant, then Equation 2.8 will yield the same result for large R_1 and R_4. That is, the factor of k cancels out because the active probe and the sunken probe have inverse influences on the output voltage.

One final note of importance is the fact that for both wave gauges, the excitation voltage, V_{in}, is a constant-amplitude AC signal. A constant DC voltage is not used because electrolysis of the water would occur, and hydrogen and oxygen bubbles would form on the probes, thus causing electrically insulated regions.

2.3. Signal processing for the saltwater instrument

The saltwater wave gauge is a sixty-four channel instrument that measures surface elevations at sixty-four points evenly spaced on the perimeter of a twenty-centimeter diameter circle. The surface elevation data collected by this instrument is processed to determine the short-wave directional spectrum. In the end, numerical processing yields a plot of variance (or energy) density versus wave number in the x-direction (k_x) and wave number in the y-direction (k_y). This plot of the two-dimensional spectrum provides information on the energy (or squared magnitudes) associated with various wave numbers in various directions of propagation. The array is sized to measure the short waves responsible for L, C, and X-band radar scattering by the sea surface.

Equation 2.9 contains the basic Fourier transform relation between the spectrum in wave number (k_x, k_y) space and the spatial autocorrelation function in Cartesian (x, y) space. This equation illustrates the basic concept behind how the spectrum is calculated given the autocorrelation function, which is determined by knowledge of the average products of surface elevations for a sets of spatial pairs.

$$S_\zeta(k_x, k_y) = \frac{1}{(2\pi)^2} \int_{-\infty}^{\infty} \int_{-\infty}^{\infty} R_\zeta(x, y) e^{-i(k_x x + k_y y)} dx dy \qquad [2.9]$$

3. Design

3.1. Design specifications

There are many design considerations necessary in the design of wave gauges. These considerations range from physical requirements on the probes to electrical requirements on the wave gauge electronics.

3.1.1. Physical requirements on the probes

The four primary criteria by which various types of probe wires are considered are wire size, wire strength, wire corrosion resistance, and wire electrical resistance. A small wire size is important because it is desirable to minimize the effects of meniscus flipping. Water's adhesion to the probe interferes with the measurement of very small waves. In particular, this adhesion effect is greater with a larger probe surface area. Wire strength is important in the context of the instrument ruggedness. Corrosion resistance is important for measurement repeatability as well as instrument ruggedness, especially in a saltwater environment. Finally, the wire's electrical resistance is important in terms of how the waves are being measured. That is, for saltwater waves, it is desirable to have high-resistance wire; whereas, for freshwater waves, it is desirable to have low-resistance wire.

In the case of the saltwater wave gauge, 36 AWG nichrome wire has been chosen because it is small in diameter, strong in tension, resistant to corrosion, and high in electrical

resistance (27 Ω/ft). In the case of the freshwater wave gauges, 30 AWG copper wire has been chosen for long-wire gauges, and 36 AWG nichrome wire has been chosen for short-wire gauges. In both freshwater cases, the resistance associated with the exposed portion of the probe wires should be small. In the long-wire case, copper wire (0.3 Ω/ft) has been selected (at the expense of increased susceptibility to corrosion) to insure that the resistance of the exposed portion is small; in the short-wire case, nichrome wire can still be used because the exposed portion of wire is constrained to be small due to short wire lengths.

3.1.2. Electrical design constraints

Just as important as the physical requirements are the electrical design constraints. These constraints guide the wave gauge designs by providing a framework of design goals to be met. Such design goals are linearity, sensitivity, repeatability, signal-to-noise ratio, frequency response, and flexibility.

A linear circuit response insures that an accurate calibration can be done to relate output voltage to measured wave height. Linearity is desirable because it allows a simple conversion from units of voltage to units of wave height. If the gauge response were nonlinear, then converting voltage data to wave height data would require knowledge of the exact operating point on the probe wire. In other words, the same change in wave height would generate different changes in output voltages depending on which section of the probe wire was being wetted by waves. Thus, a nonlinear calibration curve would demand

complicated conversion calculations, which would depend on knowing which instantaneous slopes corresponded to which operating points.

Sensitivity is important because for some short waves, it is desirable to be able to measure wave heights on the order of one millimeter. Repeatability, moreover, insures that calibrations done earlier can still be used confidently in later experimental runs. Yet another design goal is a high signal-to-noise ratio. Low noise levels are desirable because noise fundamentally sets a limit on wave gauge sensitivity. In addition, frequency responses should be constructed to cater to specific experimental needs by preserving a good dynamic range in output for all our wave frequencies of interest. For example, in one given application, it was necessary to attenuate the amplitudes of lower-frequency primary waves by roughly two orders of magnitude so that they would be comparable to those of higher-frequency waves which needed to be measured. In such a way, the output dynamic range could be optimized. Finally, the circuit design should be flexible enough so that it can be configured for different applications. Gains, offsets, and filter cut-off frequencies would ideally be easily adjustable.

3.2. Design implementation

3.2.1. Mechanical devices

There are two implementations of the freshwater wave gauge design. The first set of freshwater wave gauges has been designed for use as instrumentation for the wave tank facility in the Marine Instrumentation and Computation Laboratory. Because the wave

amplitudes generated in this facility are a few centimeters high at most, and often smaller, the probe wires for this set of gauges are relatively short (roughly ten centimeters). The sunken probe portions of the gauges are mounted horizontally under the water surface. Figure 3.1 illustrates the arrangement.

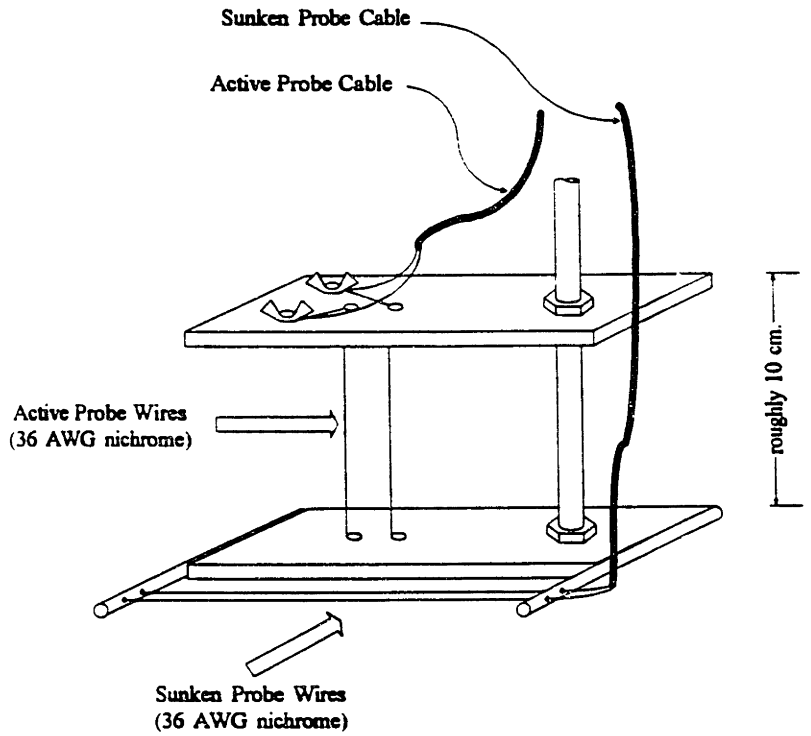

Figure 3.1: Short-wire Freshwater Wave Gauge

In contrast, the second implementation of the freshwater design is made for use in larger wave environments. The active probe portions of these gauges are one meter in length, and the sunken probe wires are roughly half a meter each. Both sets of probes are mounted

vertically for convenience. Figure 3.2 shows the mechanical device used for this long-wire gauge.

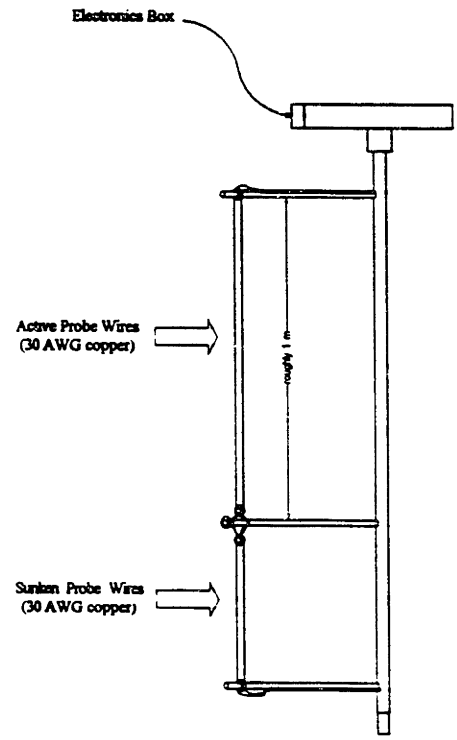

Figure 3.2: Long-wire Freshwater Wave Gauge

Because the purpose of the saltwater wave gauge is to determine the short-wave directional spectrum with good directional resolution, the instrument has many channels, in this case sixty-four. Consequently, the mechanical device for the saltwater gauge is perhaps the most sophisticated in design. Figure 3.3 contains a diagram of the device; part a) is a top view, and part b) is a side view.

The saltwater apparatus consists of two circular disks connected by a stainless steel rod. The top disk is clear plastic, and the bottom disk is stainless steel, since the bottom ends of the wave gauge wires are to be grounded. Sixty-four nichrome wires are strung from top

to bottom along a circular perimeter. The wires are tensioned by springs that attach to eyebolts which screw into threaded holes in the top plate. The bottoms of all the wires, the bottom disk, and the central rod are all grounded electrically to circuit ground. The tops of all the wires are soldered to wires with spade lugs that fit in between two nuts on the lower threaded portion of each eyebolt (i.e. the portion under the top disk). On the higher threaded portion of each eyebolt (i.e. the portion above the top disk) are two more nuts which hold spade lugs from multi-conductor shielded cables that connect to an electronics interface board. There are four such sixteen-conductor cables which connect to the interface board.

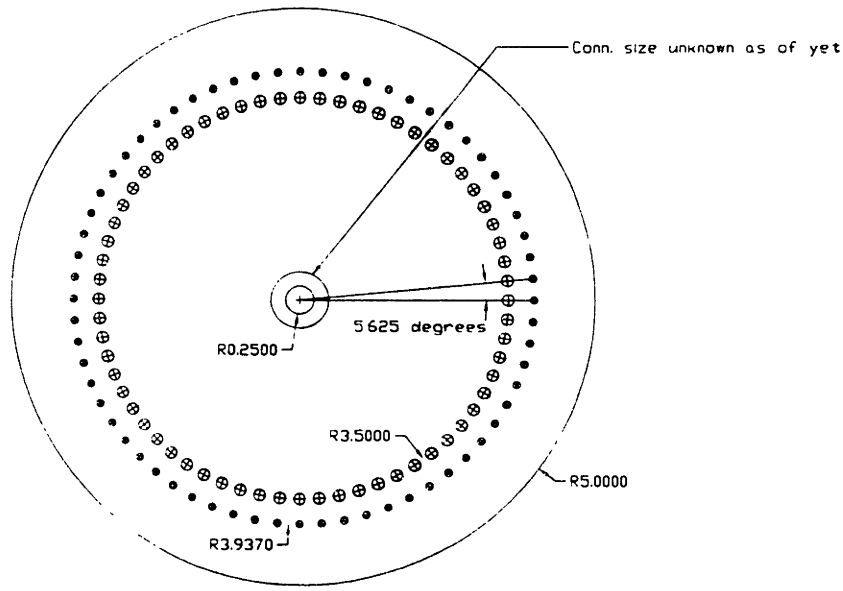

Figure 3.3: Saltwater Wave Gauge Mechanical Device
a) Top View

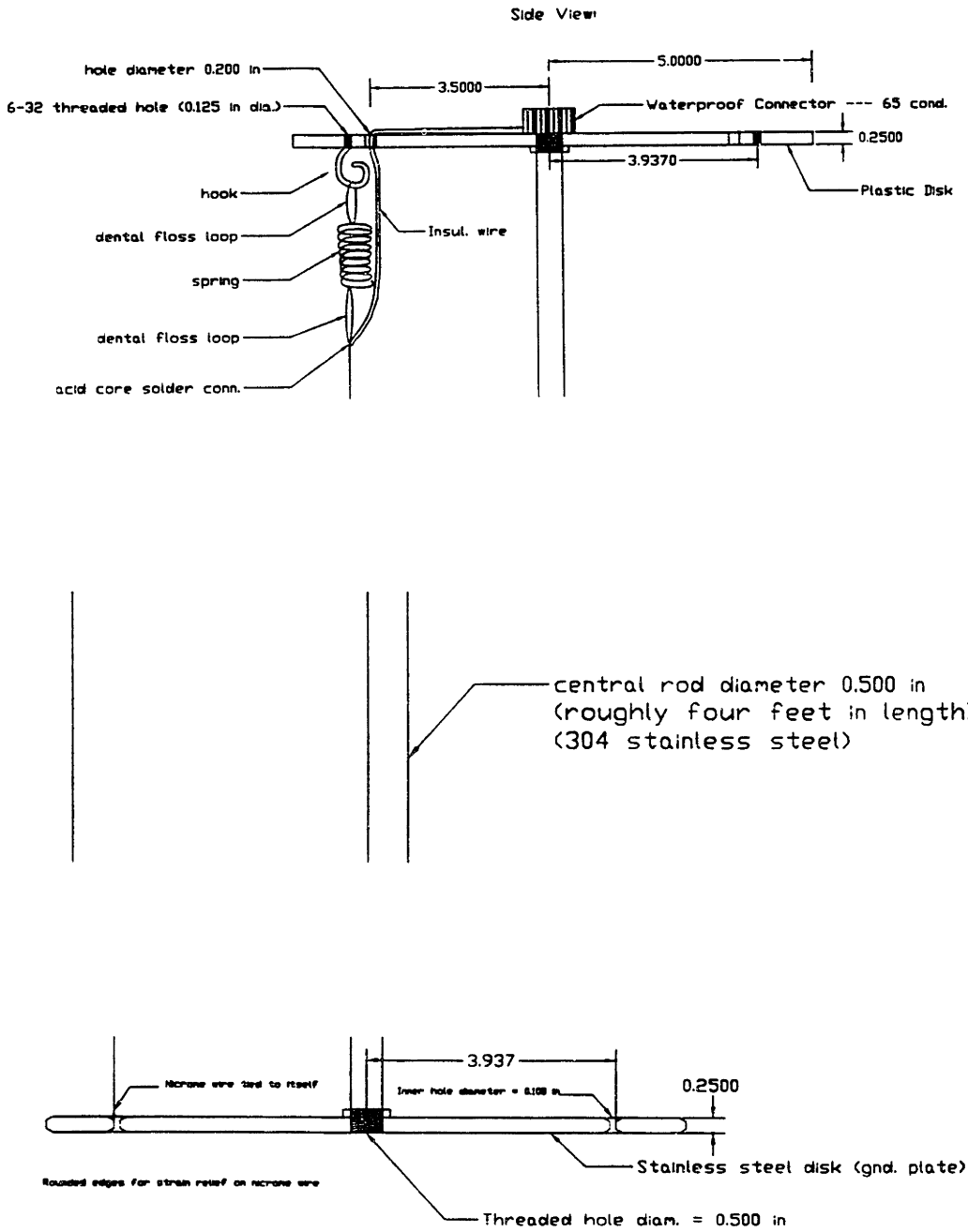

Figure 3.3: Saltwater Wave Gauge Mechanical Device
b) Side Views

3.2.2. Circuit design implementation

The electronics for the short-wire freshwater wave gauges consist of four hand-wired boards which are housed in a metal case. A case lid provides access to all the electronics. BNC coaxial cables supply the connection between wave probes (active and sunken) and circuitry. The long-wire electronics, on the other hand, consist of printed circuit boards, one for each gauge. These boards are individually mounted inside of extruded aluminum cases located at the top of each set of wave probes. Adjustment potentiometers and switches are accessible through holes drilled into the sides of these cases.

The implementation of the saltwater wave gauge electronics is somewhat more sophisticated and can be divided into the analog front-end circuitry, the interface board, and the data acquisition hardware. The analog front-end circuitry performs the signal conditioning necessary for converting wave heights to output voltages. This circuitry is implemented through four printed circuit boards, each containing the electronics necessary for sixteen wave gauge channels. The interface board adds a bit more low-pass filtering but is primarily used as a connection board to both the "circular harp" of wires (which provides the inputs) and the data acquisition boards. Finally, the role of the data acquisition boards is to scan the sixty-four channels and log the data to be processed through software.

3.2.2.1. Analog front-end circuitry

The design of the analog front-end for both freshwater and saltwater cases can be organized into six main sections: 1) the driving oscillator, 2) the probe amplifier, 3) the RMS-to-DC conversion, 4) the trim offset with gain, 5) the filters, and 6) the post-amplifier. Figure 3.4 contains an analog front-end block diagram. Detailed circuit schematics for all the gauges can be found in Appendix B.

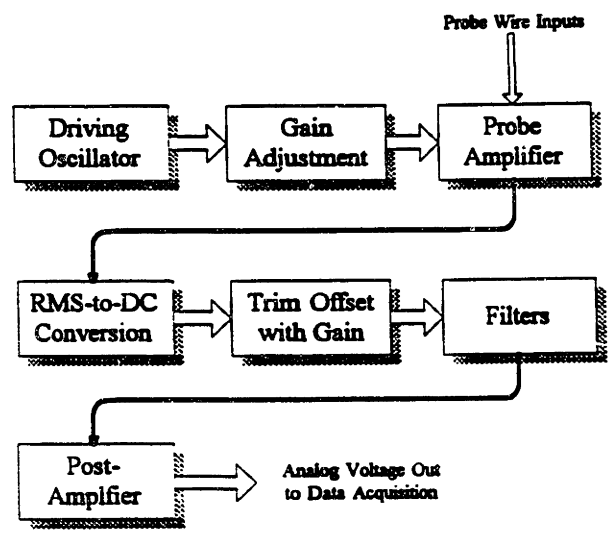

Figure 3.4: Wave Gauge Circuitry Block Diagram

1. The Driving Oscillator

The first stage of the circuit consists of a signal-generator integrated circuit, which generates a constant amplitude sine wave which serves as the input into the probe amplifier. An AC input signal is used instead of a DC signal because it is desirable to avoid polarizing the water, which has the negative effect of generating interfering hydrogen bubbles on the probes. The frequency of the oscillator is set roughly to 10 kilohertz. Furthermore, a potentiometer on the oscillator output allows the amplitude of the sine wave to be adjusted.

2. The Probe Amplifier

The freshwater probe amplifier is an operational amplifier with two voltage divider branches. Each divider branch contains a probe pair. There is a main probe and a sunken probe. The main probe pierces the water's surface, and its conductance varies linearly with changing surface heights; the sunken probe is completely submerged and acts to eliminate drifts in output voltage due to changes in water conductivity by introducing a compensating gain. In essence, changes in water level cause variations in the main probe's resistance, which in turn cause variations in amplification of the controlled sine-wave input. In other words, the sine-wave input is amplitude-modulated by shifting water levels on the main probe.

The saltwater probe amplifier contains only one probe divider branch. In the saltwater case, the effective resistance of the wire itself is what varies linearly with wave height. Amplitude modulation is achieved in a way similar to that of the freshwater gauge.

3. The RMS-to-DC Conversion

The RMS-to-DC converter simply serves as an envelope detector; it translates the amplitude-modulated AC signal into an output whose voltage varies directly with changes in water level on the main probe.

4. The Trim Offset with Gain

Because the output of the RMS-to-DC converter contains a voltage offset attributable to some average immersion length of the main probe, it is desirable to have a trim offset stage so that "zeroing" of the output voltage can be accomplished. Thus, during calibration, any convenient water level can be chosen to represent the zero-voltage level. In addition, this stage contributes another factor of amplification.

5. The Filters

For the long-wire freshwater gauges, there are three distinct filter stages: 1) a second-order Butterworth high-pass filter with a cut-off frequency of 1.94 Hz, 2) a second-order Butterworth low-pass filter with a cut-off frequency of 23.4 Hz, and 3) a combined 1-pole low-pass/1-pole high-pass filter (with cut-off frequencies of 34 Hz and 0.34 Hz, respectively). The function of the low-pass filter poles is to reduce high-frequency noise that may be coupled into the circuit. The function of the high-pass filter poles, on the other

hand, is to scale the magnitudes of waves at certain frequencies of interest. The goal is to attenuate more strongly the higher-amplitude, lower-frequency waves so that the lower-amplitude, higher-frequency waves are not "masked." The range of frequencies of interest (roughly 0.2 to 2 Hz) has consequently been designed to fall on the slope of our high-pass filters. Switches, furthermore, have been added so that all the high-pass poles may be bypassed, if desired. It is desirable, for instance, to turn the high-pass filtering off when probe calibrations are being performed.

For the short-wire freshwater wave gauges, there are also three filter stages cascaded together. The first stage consists of a selectable second-order Butterworth high-pass filter with a cut-off frequency of 0.34 Hz. The remaining two filter stages are both second-order Butterworth low-pass filters with cut-off frequencies at 23.4 Hz. The cutoff frequencies of both the high-pass and the low-pass filters have been designed so that the frequency response will be the highest in gain within a maximally flat passband of 1 to 10 Hz. Unlike the long-wire gauges, the object of the laboratory wave gauges is not to operate on a frequency response slope; the amplitudes of waves generated in the tank generally do not vary from each other by orders of magnitude, so frequency-dependent attenuation is not an essential design constraint. The primary purpose of these filters is to eliminate unwanted high and low frequencies so that the signal-to-noise ratio will be maximized for signals within the passband.

Finally, with respect to the saltwater wave gauge filters, there are also three filter stages. In this case, the first stage is a second-order Butterworth low-pass filter with a cut-off frequency at 9.65 Hz, and the two remaining stages are selectable second-order Butterworth high-pass filters with cut-off frequencies at 6.03 Hz and 7.23 Hz, respectively. Although the

current instrument is a laboratory prototype, it has been designed for expected wave levels in the ocean. Consequently, the instrument is designed to attenuate as much as possible any low frequency waves outside the frequency range of interest. Because low frequency ocean waves can be rather large in amplitude, the high-pass filter cut-off frequencies have been set as high as possible without sacrificing the signal strengths of the frequencies of interest; in other words, there is a compromise with maximum gain at about seven Hertz. To discount very large swells in the ocean, the instrument will be mounted on a buoy that will follow the larger ocean waves.

6. The Post-amplifier

The final stage in the circuit is variable post-amplification. A potentiometer allows for gain adjustments in the final output.

3.2.2.2. The interface board

The primary purpose of the interface board is to connect the analog front-end circuit boards to the "circular harp" and to the data acquisition boards. In addition, there are single-pole low-pass filters on the outputs to reduce unwanted high-frequency noise.

3.2.2.3. Data acquisition

The acquisition of data on sixty-four saltwater wave gauge channels has been achieved by utilizing two IBM PC-compatible, "plug-in", analog I/O boards produced by ComputerBoards, Inc. These boards are the CIO-DAS16 and the CIO-DAS48, which can sample sixteen and forty-eight single-ended voltages, respectively. Both boards use twelve-bit A/D conversion. The sampling rate is set for each channel at twenty samples per second, twice the frequency of the highest wave frequency of interest (10 Hz). The data acquisition boards scan all sixty-four channels nearly instantaneously, wait for a twentieth of a second, and then sample again. The current sampling rate is not set higher for the reason of data management. Because there are sixty-four channels, the amount of data acquired can be quite enormous when many sets of scans are performed.

Freshwater data acquisition is achieved in the same way, but with less channels in use.

3.2.3. System configuration

Figure 3.5 contains an overall drawing of how all the various sections of the saltwater wave gauge instrument are interconnected.

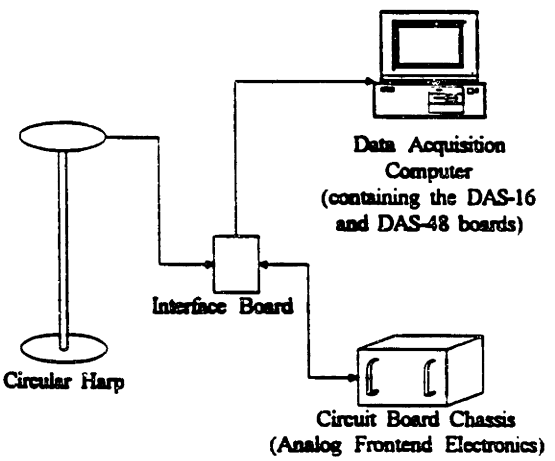

Figure 3.5: Saltwater Instrument System Configuration

Because there are sixty-four channels associated with the saltwater instrument, the issue of powering the analog front-end circuit boards is a major concern. Each circuit board, which contains sixteen channels, draws approximately 0.33 amperes at a regulated supply

voltage of +12 volts and another 0.33 amperes at a regulated supply voltage of -12 volts. Thus, the power supply for the instrument must be able to source at least 1.5 amperes on each of the regulated voltage lines. Noise from the supply should also be considered carefully. The idea of using DC-DC converters, one mounted on each board, has been abandoned precisely because of noise problems caused by interference among the four DC-DC converters.

Another concern, perhaps even more important, is the issue of cabling. The main issue with cabling is noise control. Because there are so many signal lines, both input and output, the cabling becomes necessarily dense for ease of handling. This line density increases the susceptibility of the gauge to interference problems due to cross-talk between signals, and thus, there is a lot of care exercised in shielding. The current implementation utilizes two types of cables, ribbon cable and multi-conductor shielded cable. Ribbon cables are used to connect each printed circuit board to the interface board and to connect the interface board to the data acquisition boards. The multi-conductor shielded cable is used to connect the probe wires on the "circular harp" to the interface board. The ribbon cable lengths are minimized.

3.3. Software

3.3.1. Data acquisition software

Data sampling is cascaded so that after the sixteen channels of the DAS-16 board are read, the forty-eight channels of the DAS-48 are read and so forth. All sixty-four channels are scanned nearly instantaneously, and each scan is taken one twentieth of a second apart. Thus, for each channel, there is an effective sampling rate of twenty data samples per second. All data points are in volts and are given to three decimal places, and four to five significant figures.

3.3.2. Signal processing software

The signal processing software consists of all the code necessary for processing the raw data files generated by the data acquisition system. For a given experiment, there are two kinds of raw data. The first kind is DC calibration data, and the second kind is wave data.

A raw calibration data file consists of sixty-four columns of sixty data samples each. Each calibration file contains three seconds worth of data for each channel at a given calibration height. The first step in processing these raw calibration data files is to average the sixty output values in each of the sixty-four columns for each data file. A calibration file is then generated by combining into a table these rows of average values so that each row represents the sixty-four average outputs for a given calibration height. Finally, one column

of calibration height values is added to the beginning of the sixty-four output data columns to complete the processed calibration file. Then, another program performs a linear least squares fit of each output data column to the calibration height column. In such a way, calibration slopes in volts per inch can be determined for each of the sixty-four channels. The values of these slopes are written to an output file, which is read as an input file by a volt-to-inch conversion program.

This conversion program takes as input not only the file of calibration slopes but also a raw wave data file. Each wave data file consists of sixty-four columns of five-hundred twenty data samples each (i.e. 520 rows). In other words, given that the sampling rate is twenty samples per second, twenty six seconds of data are collected for each channel. The function of the conversion program is to convert a raw wave data file, whose data points are given in volts, into a processed wave data file, given in inches. Each column (or channel) is, of course, normalized by the appropriate calibration slope, which is calculated by the least squares program.

Next, to account for the individual voltage offset of each channel, the DC component, or average, of each column of data is subtracted out from each data value in that column. In such a way, it can be insured that all the channels share the same operating point. The importance of having a shared operating point stems from the fact that a varied distribution of operating points would be misconstrued as an underlying waveform in both the autocorrelation function and the final spectrum.

Finally, the signal processing is performed on a workstation and can be separated into three distinct stages. The first stage is configuring the processed data files into an input

format which the signal analysis software can handle. For a particular data run, a data file containing sixty-four columns each composed of five-hundred twenty data points (in inches) is converted to five-hundred twenty scan files which each contain sixty-four wave height values (converted to centimeters). The second stage of processing then consists of taking these scan files and performing autocorrelation calculations with them. The last stage is using this autocorrelation information to generate the directional spectrum.

The essence of the signal analysis (the second two stages) is performed by two programs: "sw_auto.c" and "dfsum.f". The C and Fortran code for these two programs can be found in Appendix G.

The first program, "sw_auto.c", takes as inputs a set of scan files, each of which contains the wave height data points from a single scan of all sixty-four wires on the "circular harp." In the sample data run, for example, five-hundred twenty such files are generated, and each file represents a scan taken a twentieth of a second apart. The "sw_auto.c" program begins reading in one scan file at a time and obtains 1) header information such as the geometric dimensions of the probe locations, and 2) post-processed wave height data for that scan. For each scan, the program calculates the wave height products between all combinations of probe pairs ($Prod_{1,1}$, $Prod_{1,2}$, ..., $Prod_{64,64}$). The subscripts are indices for probe locations going counter-clockwise. Because there are many redundant products (e.g. $Prod_{1,2}$ is the exact same as $Prod_{2,1}$), the autocorrelation space has quadrant symmetries. Furthermore, the averages of certain correlation product values need to be found because there are multiple products for identical spatial lags. For instance, $Prod_{1,2}$ and $Prod_{34,33}$ represent the same spatial lag and eventually the equivalent autocorrelation. Therefore, those

two products (and all those in similar relationships) need to be averaged. Of particular note are the zero-lag correlation products. There are sixty-four of these products, which represent the same autocorrelation, and they are consequently averaged. After every relevant average correlation product is found for each scan in the ensemble, then an ensemble average across all scans is performed to obtain the autocorrelation values corresponding to the known set of spatial lags. The x- and y- components of these spatial lags are calculated knowing the geometry of each correlation pair. The behavior of the sea surface is, of course, assumed to be a random process stationary in time and homogeneous in space such that the wave height statistics are functions only of relative time differences and spatial lags.

Finally, the autocorrelation values and their associated spatial lags in two dimensions are printed to a number of output files. Most importantly, one output file is to be used as an input to "dfsum.f", which computes the directional spectrum, and another file is configured as a data file for TECPLOT, a graphical package.

The second program, "dfsum.f", first convolves the autocorrelation vector space with a smoothing window. Then, the program proceeds to calculate the directional spectrum by finding the optimal (least squares) solution vector to an overdetermined set of linear equations, $Ax = b$. In this system, b is the autocorrelation vector (found from "sw_auto.c"); A is a matrix containing all combinations of two-dimensional Fourier components (sinusoidal waveforms with specified "k_xx-type" and "k_yy-type" arguments); and x is the solution vector containing the Fourier coefficients (amplitudes) of those various Fourier components. Values in the A-matrix are known for given k_x and k_y (i.e. the columns yield the wavenumbers of interest) and given x and y (i.e. the rows yield the appropriate spatial lag values). Each

equation in this linear set of equations thus represents a two-dimensional Fourier sum of all possible wavenumber terms. The number of equations is set by the size of the autocorrelation vector space. Each autocorrelation value corresponding to a known spatial lag provides one independent equation representing a linear combination of Fourier terms with not-yet determined coefficients. The system of equations, moreover, is overdetermined because the number of independent equations (known autocorrelation values) exceeds the number of unknowns (Fourier coefficients). Thus, by finding the least squares solution to the system, the optimum solution vector for the spectrum can be found. After the solution vector is computed in "dfsum.f", the autocorrelation is reconstructed using this solution. An output file containing the reconstructed autocorrelation is generated so that the integrity of the solution may be checked. In addition, the solution vector is scaled by the appropriate factors to yield the directional spectrum of the data set, which is also written to a data file. One final check in the program is a comparison of R(0), the zero-lag autocorrelation (or mean-square wave height), to the sum of the spectral coefficients (or the area under the spectrum). These two values should be close in value.

4. Evaluation of system performance

4.1. Characterization of the freshwater wave gauges

4.1.1. Linearity

To evaluate the linearity of the freshwater wave gauges, DC calibrations are performed. A DC calibration consists of measuring a set of output voltages for a known set of calibration heights. For the short-wire gauges, these calibration heights are determined by placing blocks of known thicknesses under the two ends of a wooden beam on which the wave gauges are mounted. This beam rests across the laboratory wave tank, and the gauges are positioned so that the mean water level is roughly in the middle region of the active probe. The high-pass filters are turned off so that DC levels can be measured.

DC calibrations for the long-wire gauges are performed in more or less the same way. Instead of using blocks for calibration, however, the central rod of the long-wire wave gauge is clamped to a ring stand placed on the rim of the wave tank, and the gauge can be shifted up and down for calibration purposes.

4.1.2. Repeatability

To observe the stability of these calibrations over time, multiple data sets are taken over several days. Each set of measurements is performed with the same settings (gain,

frequency response, switch settings, etc.), and the probe wires are carefully cleaned before each data set. In such a way, the repeatability of the calibration measurements can be determined.

4.1.3. Evaluation of the effectiveness of the sunken probe

To study how effectively the fully submerged probe compensates for changes in water conductivity, one set of DC calibrations is performed for gauges instrumented with a sunken probe, and another set of calibrations is performed for gauges instrumented with a fixed 620Ω resistor in place of the sunken probe. Both sets of calibrations are performed on two separate days, a few days apart. The calibrations for the "wet" sunken probes are then compared to those for the "dry" sunken probes to observe any differences in performance stability.

4.1.4. Frequency response curves

In addition to evaluating the linearity of the gauges, it is important to examine their frequency responses. There are two ways in which the frequency responses of the gauges are measured. First, the frequency response characteristics of various filter sections can be obtained by first disconnecting those sections from their surrounding circuitry and then measuring the output signals produced by those sections, given various input signals from a signal generator. Ratios of output amplitude to input amplitude can be found for a set of

signals at known frequencies, and the frequency responses of those sections can then be plotted.

The other frequency response measurement technique is to generate water waves of various frequencies in the MIT Towing Tank Facility and to examine the voltage output of the long-wire freshwater gauge with all its filters operating. For each frequency of interest, peak-to-peak amplitudes are measured for both the output voltages and the actual water wave heights. The output voltage amplitude is normalized to the input wave height amplitude, and a set of those ratios is then plotted for a range of frequencies to yield the instrument's frequency response.

4.1.5. Sensitivity and signal-to-noise ratio

The sensitivity of the wave gauges depends largely on the gain settings of the circuit. In other words, for a circuit with a high amount of amplification, there is higher sensitivity in the sense that the output can reflect smaller wave amplitudes. The ultimate limits on the instrument's sensitivity are "noise floors" and meniscus effects. First of all, under the assumption that there is no noise whatsoever, there is a physical limit on the smallest wave amplitude to which the probe wires can be sensitive. Because of the adhesive nature of water, there is some small amount of "clinging" to the probe wire. Because of these meniscus effects, very small changes in wave heights are not sensed by the probe wires.

Perhaps a more practical issue is the limitation on sensitivity caused by noise. An examination of the noise levels present in the output signal combined with knowledge of the

DC calibration slope (in volts per inch) yields a rough estimate on the sensitivity limit due to noise. If the noise levels translate into wave heights that exceed the levels affected by meniscus behavior, then the system's sensitivity becomes noise-limited.

4.1.6. Wave tests and waveform descriptions

The performance of both sets of freshwater wave gauges is ultimately evaluated in terms of their operation in the field. The short-wire gauges are mounted and tested in the wave tank facility of the Marine Instrumentation and Computation Laboratory, whereas the long-wire gauges are tested at MIT's Towing Tank. Water waves of various known frequencies and amplitudes are generated in each of these facilities, and the corresponding output voltage waveforms generated by the wave gauges are examined. Oscilloscope traces are recorded in the short-wire case for descriptive purposes.

4.2. Characterization of the saltwater wave gauges

4.2.1. Characterization of the voltage along a probe wire

Because the behavior of the saltwater gauge depends largely on how effectively the submerged portion of the probe wire is grounded in the water, it is useful to characterize how voltage levels vary along the probe wire. Peak-to-peak voltages of an attenuated driving

oscillator signal are measured along known heights on the probe wire, both above and below the water line. Finally, a plot of voltage against height on the probe wire is made.

4.2.2. Dependence on water salinity

It is also important to examine the dependency of the saltwater wave gauge's behavior on water salinity. That is, how and to what extent do the calibration curves for a gauge change for varying salinities? To measure the salinity dependence, DC calibrations are performed in water samples of nine different salinities, ranging from 0.3 parts per thousand to 27.4 parts per thousand.

4.2.3. Linearity

Linearity of the saltwater gauges is evaluated in exactly the same way as mentioned for the freshwater gauges. For tests in a bucket, DC calibrations are performed by clamping the central rod of the "circular harp" to the platform of a motor-driven oscillator and measuring output voltages for known displacements of the platform. For tests in the wave tank, DC calibrations are performed by resting the "circular harp" on a vertically movable grid and measuring output voltages for known grid displacements.

4.2.4. Repeatability

The repeatability of measurements for saltwater gauges is just as important as that for freshwater gauges. By repeating DC calibration measurements on multiple days and by comparing those results, a good measure of the system's repeatability can be achieved.

4.2.5. Frequency response

The frequency response characteristics of the filters can be found by exactly the same means as that of the freshwater gauges. The procedure applied to sixty-four channels would be rather tedious, however, and thus a more efficient way of evaluating and comparing the respective frequency responses of sixty-four channels is utilized. By measuring the output response of the saltwater gauge to a step input, the frequency response (or transfer function) of the system can be calculated. The transfer function (in the frequency domain) is simply the Fourier transform of the time-domain output response divided by the Fourier transform of the step input (see Eqn. 4.1).

$$H(\omega) = \frac{Y(\omega)}{X(\omega)} \qquad [4.1]$$

where

$$Y(\omega) = \int_{-\infty}^{\infty} y(t)e^{-j\omega t}dt \text{ and}$$
$$X(\omega) = \int_{-\infty}^{\infty} x(t)e^{-j\omega t}dt$$

The former Fourier transform (Y(ω)) is calculated using a Fast Fourier Transform algorithm, while the latter transform (X(ω)) is commonly known (see Eqn. 4.2).

for x(t) = u(t) = unit step, $$X(\omega) = \frac{1}{j\omega} \qquad [4.2]$$

Had the system been evaluated purely in the time-domain, the convolution integral of the time-domain transfer function with the step input would have yielded the output response in the time domain, but this calculation is much more complicated and is thus avoided. In the end, the frequency response is given by Equation 4.3.

$$H(\omega) = j\omega \times Y(\omega) \qquad [4.3]$$

where Y(ω) is determined experimentally
by performing an FFT of a sampled y(t)

Each response can then be normalized to one by dividing all the magnitudes throughout the frequency range by the largest magnitude. Finally, a comparison of the similarity of responses for multiple channels is achieved by superimposing the normalized frequency response curves on one graph.

4.2.6. Sensitivity

Like the freshwater gauges, the sensitivity of the saltwater gauges is constrained by both meniscus effects and noise, and similarly, a rough estimate of the sensitivity of the gauges

can be made by knowing DC calibration slopes and output noise levels. In the case of the saltwater instrument, however, noise is much more of a concern simply because the saltwater instrument is multi-channeled.

4.2.7. Crosstalk and interference

Crosstalk and interference are problems which are greatly dependent on cabling techniques. The problem of crosstalk arises when signal wires are densely packed and unshielded from one another. There is a degree of electromagnetic coupling between signal wires so that a strong signal on one wire, for instance, will show up on a neighboring wire in some attenuated form. To obtain a rough estimate of how much coupling occurs in the system, several kinds of tests can be performed. The first method is to compare DC output voltages on neighboring channels, with all high pass filters inactive. The output voltage on one channel can be changed by a known amount by shorting a portion of its probe wire, and the resulting changes in voltages on its neighboring channels can be measured. Another way of measuring crosstalk is to oscillate the "circular harp" up and down in a bucket of saltwater and then to examine the output signal for a channel whose input is grounded. Finally, a direct measurement of crosstalk and interference can be made simply by observing the outputs carefully on an oscilloscope.

Crosstalk and interference can be problems in several forms. First of all, there is potential crosstalk among the signals of individual channels. In particular, the sixteen channels of each board are particularly sensitive to each other because their signal wires are grouped

together in a single cable. Secondly, the 10 kHz driving signal can potentially appear as noise on other signal lines such as the output lines. Finally, there may be high-frequency interference like radio-frequency interference which is "picked up" by the cables acting as antennas.

4.2.8. Bucket tests using a mechanical oscillator

The first set of saltwater instrument tests is performed by using a mechanical oscillator to move the entire "circular harp" up and down in a bucket of salt water. The central stainless steel rod of the "circular harp" is clamped tightly in two places to a vertical platform whose oscillations are driven by a motor. The motor's frequency can be adjusted to provide oscillations of a fixed amplitude at various frequencies. Figure 4.1 provides a rough diagram of the oscillator setup.

The oscillator provides a very controlled way of examining the behavior of the saltwater instrument. The "circular harp" is moved up and down at a known frequency and amplitude, and thus all the channels are fed the exact same input. The response of the instrument in terms of output voltages is expected to be identical for each channel. By performing a Fast Fourier Transform (FFT) on each of the outputs, spectral plots can be made for each channel. A comparison of peak frequencies and amplitudes provides one indicator for how well the saltwater instrument is operating. An examination of the output waveforms provides yet another more qualitative indicator of the instrument's performance. At the very

least, the output waveforms are expected to appear sinusoidal, and all the waveforms should be in phase.

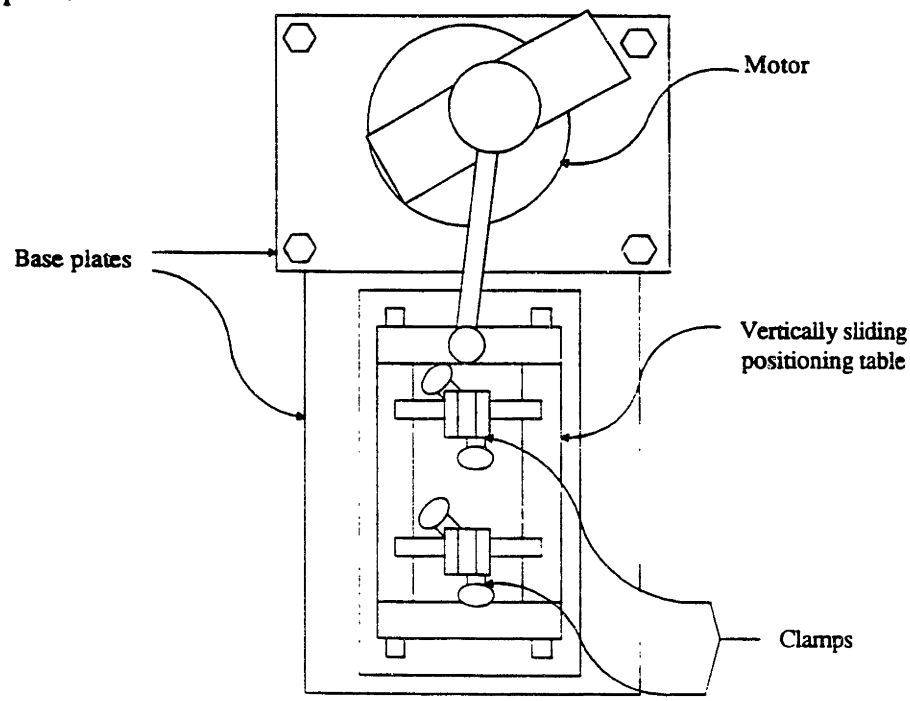

Figure 4.1 : Mechanical Oscillator

4.2.9. Wave tank tests using a wavemaker

The ultimate in-laboratory tests for the saltwater wave gauge are those performed in a wave tank full of salt water. Such tests can provide data not only on how well the instrument measures wave frequencies and amplitudes but also on how well it determines directionality. By scanning the outputs of all sixty-four channels and creating an ensemble of output scans, the two-dimensional directional spectrum can be constructed. Water waves of various frequencies and amplitudes are generated in a given direction, and the "circular harp" is placed

in a known orientation with respect to the incoming wave fronts. The instrument's output data is then collected and analyzed.

Like the analysis done for the bucket test, a time/frequency FFT analysis is performed on each channel. In addition, the short-wave directional spectrum is calculated using the autocorrelation information gathered.

5. Data Measurements and Analysis

5.1. Freshwater wave gauge analysis

5.1.1. Linearity

Figure 5.1 (parts a through d) contains the plots of calibration curves for each of four short-wire freshwater wave gauge channels. Each plot shows data taken at six different instances over a period of three days. The data for each curve is fit to a line using a least squares method. From the plots, it is apparent that all the curves are extremely linear; the variances from the fits are mostly on the order of 10^{-4} cm^2, and the maximum deviations are mostly on the order of 10^{-2} cm. The slopes from the curve fits can be found easily to yield all the necessary conversion factors.

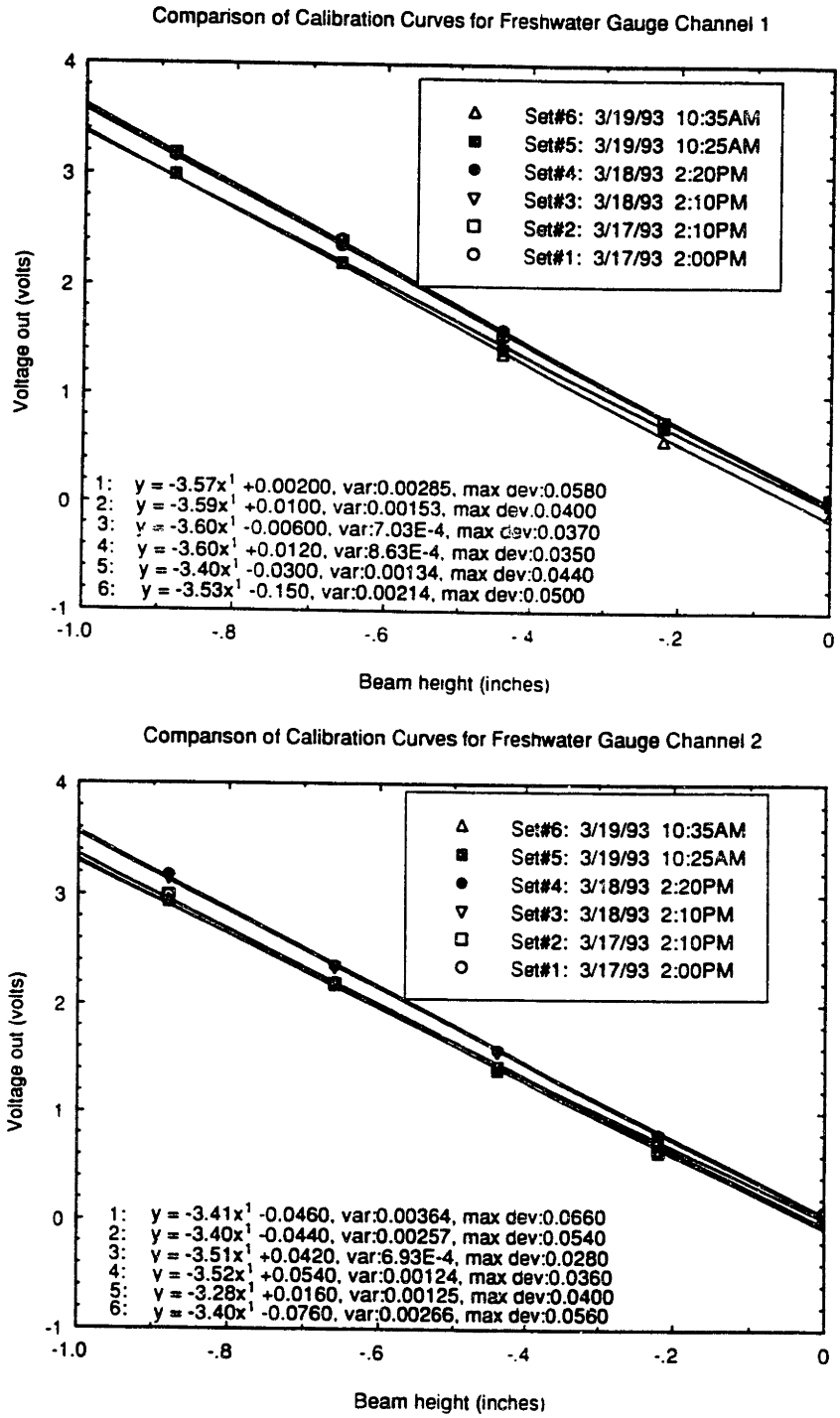

Figure 5.1 (parts a and b): Calibration Curves for Short-wire Freshwater Wave Gauges

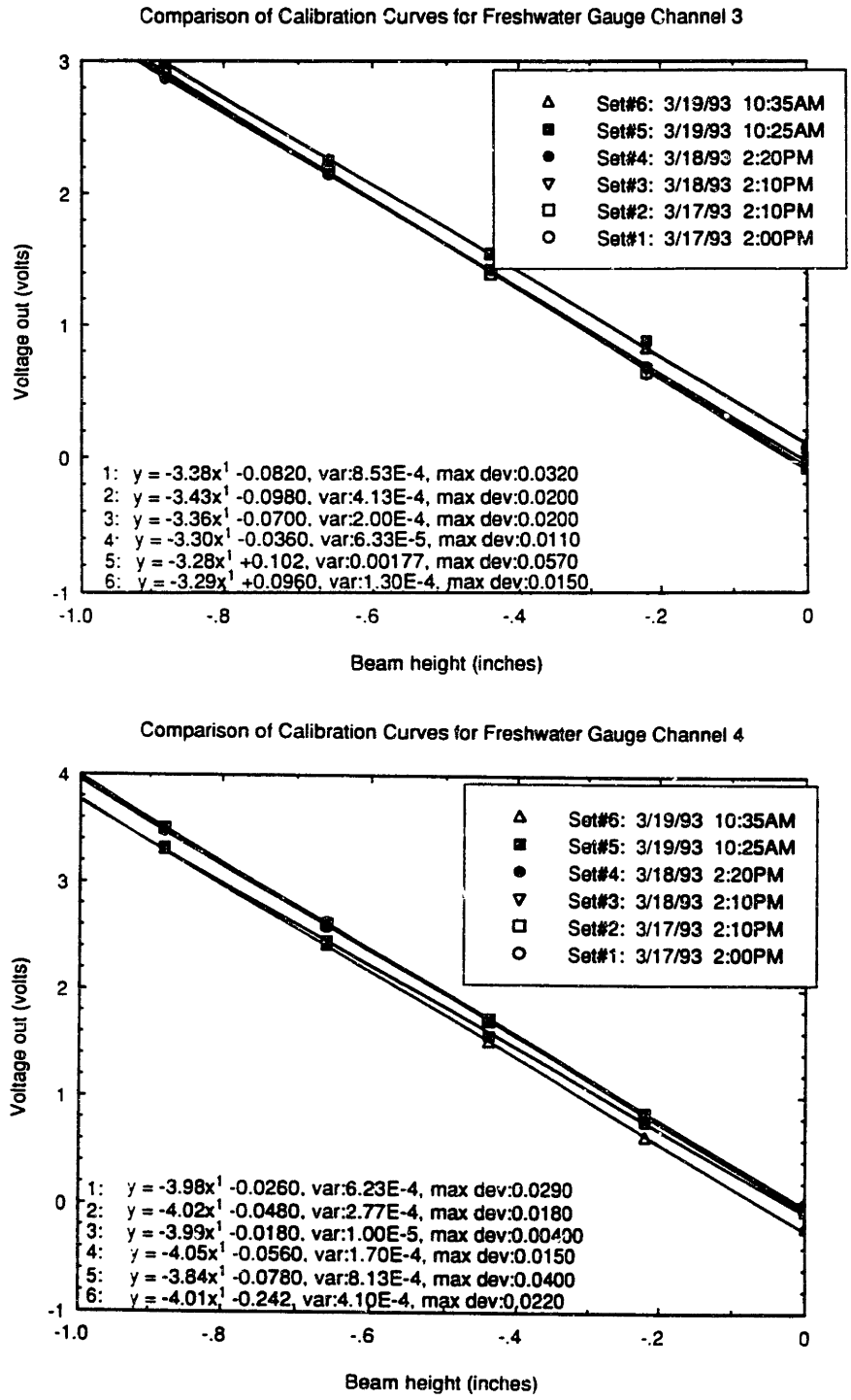

Figure 5.1 (parts c and d): Calibration Curves for Short-wire Freshwater Wave Gauges

To check that there is linearity for the longer wire freshwater wave gauges, DC calibration curves have also been plotted for a greater range of heights. The gains of the circuits are reduced for the long wires so that the measurement readings will not go off-scale. Figure 5.2a shows two calibration curves for a medium length calibration (six inches), and Figure 5.2b shows the calibration curve for a long calibration (sixteen inches). In both cases, the results remain extremely linear.

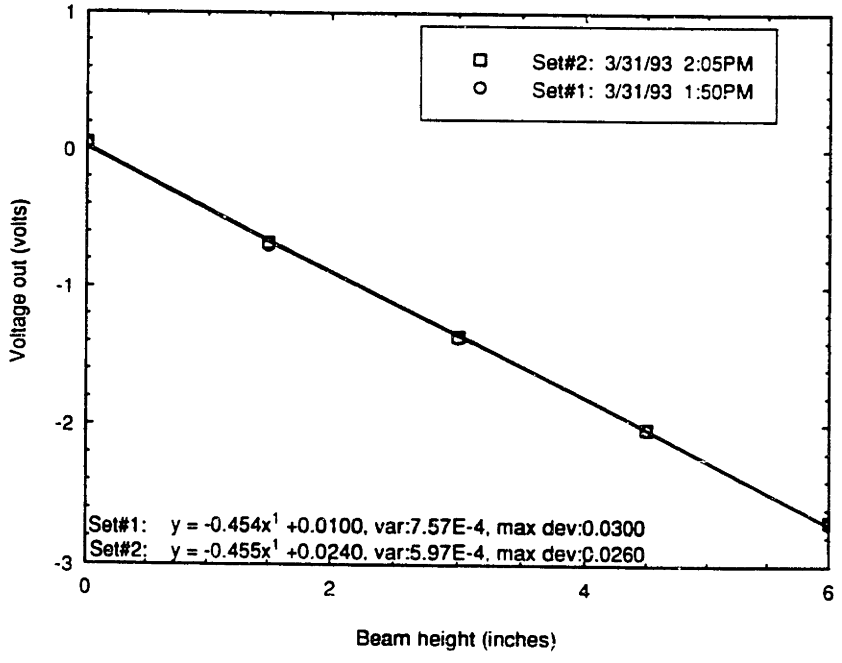

Figure 5.2: a) Medium-length Calibrations

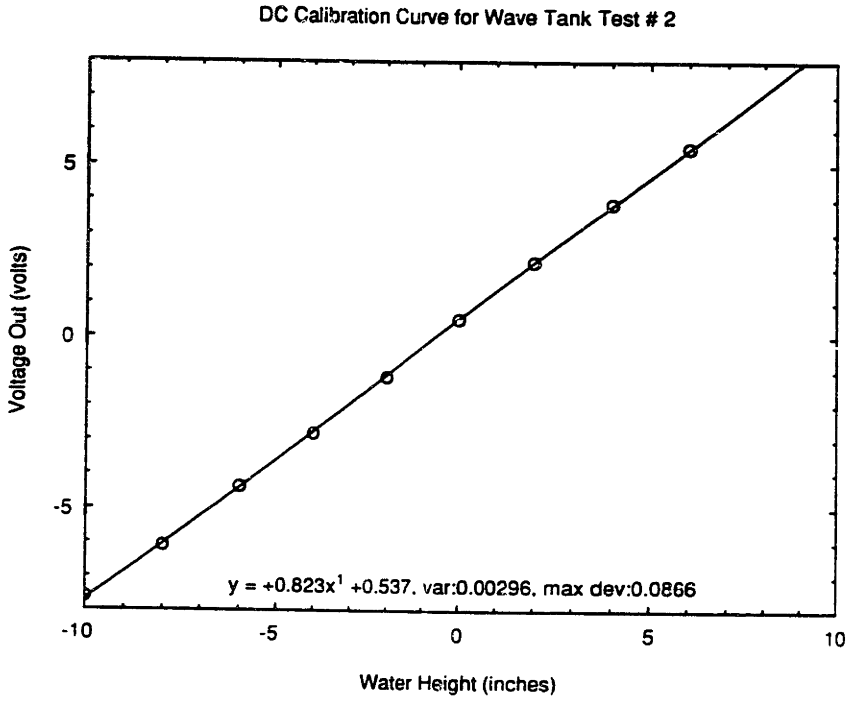

Figure 5.2: b) Long Calibration

5.1.2. Repeatability

Figures 5.1 and 5.2a provide information not only on linearity but also on repeatability. Repeating the exact same calibrations at various times allows for the analysis of the behavior of the analog front-end circuitry over time. In particular, the gauge's stability in performance can be evaluated in terms of changes in slope and changes in DC offset.

The data for the short-wire freshwater gauges seems to indicate that over time, calibrations remain relatively stable in slope and shift only slightly in offset. Slope stability is much more important than offset stability, primarily because it is the calibration slope that sets

the output conversion factor. Furthermore, any shift in DC offset can be easily removed, if desired, by adjusting the appropriate trim offset potentiometer in the analog front-end. Table 5.1 shows the calibration slope values for all four channels at six different measurement times.

Slopes of Curve Fits: (in V/in)

		Ch.1	Ch.2	Ch.3	Ch.4
March 17	2:00PM	-3.57	-3.41	-3.38	-3.98
March 17	2:10PM	-3.59	-3.40	-3.43	-4.02
March 18	2:10PM	-3.60	-3.51	-3.36	-3.99
March 18	2:20PM	-3.60	-3.52	-3.30	-4.05
March 19	10:25AM	-3.40	-3.28	-3.28	-3.84
March 19	10:35AM	-3.53	-3.40	-3.29	-4.01

Table 5.1: Short-wire Calibration Slopes Over Several Days

The results indicate that the slopes of a given channel vary at most by five percent over three days. For calibrations performed within ten minutes of each other, slope variations amount only to one or two percent. Thus, there is good repeatability in the wave gauge measurements.

5.1.3. The effectiveness of the sunken probe

DC calibration measurements can also be used to analyze the effectiveness of the sunken probe in terms of improving the freshwater gauge's stability over time. Figure 5.3 contains the "wet" calibration curve for one wave gauge channel, and Figure 5.4 contains the corresponding "dry" calibration curve. The "wet" system describes the use of a sunken probe, and the "dry" system describes the use of a fixed resistor in place of the sunken probe. It is evident that the slopes of the calibration curves for the "dry" system shift by a significant amount, whereas, in the case of the "wet" system, the curves remain fairly constant in slope for the exact same time period. Appendix E contains the "dry" and "wet" calibration curves for the three remaining channels tested. The results are consistent for all of the channels tested.

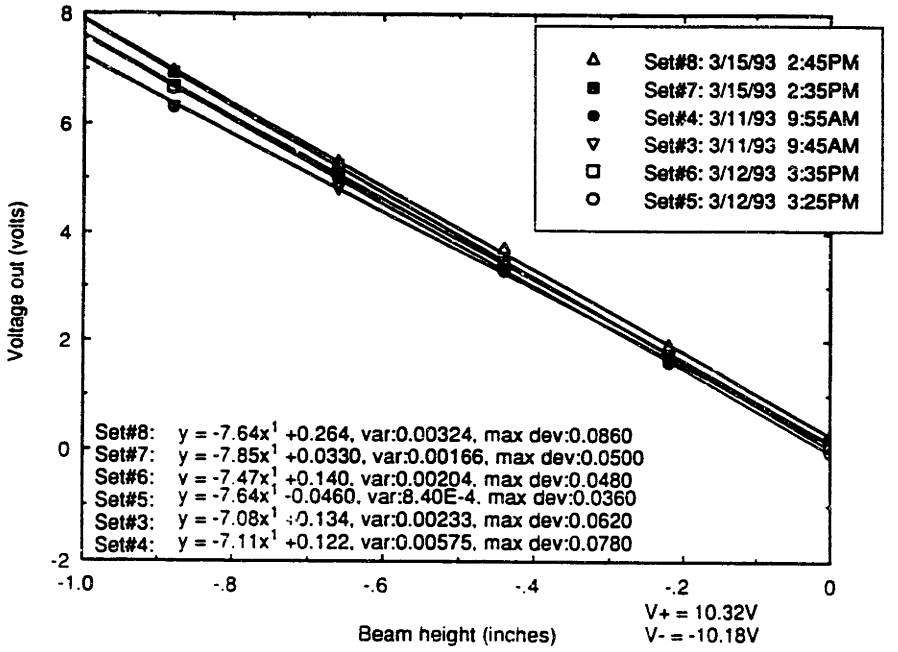

Figure 5.3: "Wet" Calibration Curves for Freshwater Wave Gauge Channel #1

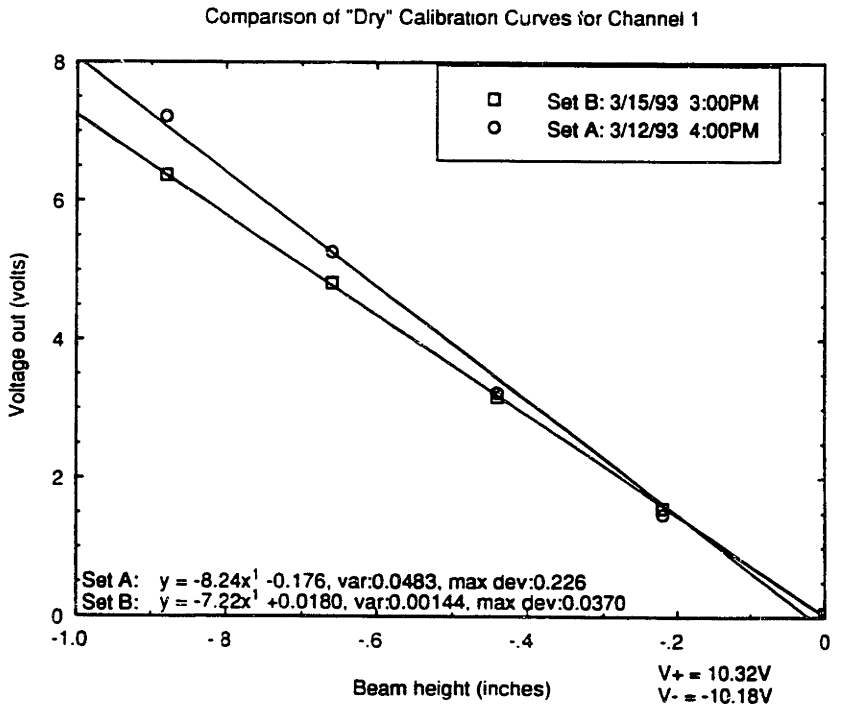

Figure 5.4: "Dry" Calibration Curves for Freshwater Wave Gauge Channel #1

Table 5.2 presents for all channels the slopes of the linear curve fits for the "wet" and "dry" systems at two times.

	"Dry" slopes (V/in)		"Wet" slopes (V/in)	
	March 12	March 15	March 12	March 15
Channel 1	-8.24	-7.22	-7.47	-7.64
Channel 2	-7.30	-6.61	-6.51	-6.46
Channel 3	-8.33	-7.38	-5.40	-5.55
Channel 4	-8.08	-7.13	-6.22	-6.32

Table 5.2: Comparing "Dry" Calibration Curves to "Wet" Calibration Curves

It is clear that with the sunken probes, the variation in calibration slopes over the three days is much less. The "dry" slopes vary by almost 1 volt/inch on all channels, whereas the "wet" slopes vary by approximately 0.1 volts/inch on all channels. Thus, the utilization of a completely submerged probe for the freshwater instruments seems essential to the repeatability of measurements over a few days.

5.1.4. Frequency response curves

The frequency responses of the various filter sections of the short-wire freshwater gauges are pictured in Figure 5.5. These are from direct laboratory measurements. Figure

5.5a shows a typical fourth-order Butterworth low-pass filter frequency response. For this particular figure, the cutoff frequency was set at roughly 19.5 Hz. The response represents the response given by the last two low-pass filter sections cascaded together.

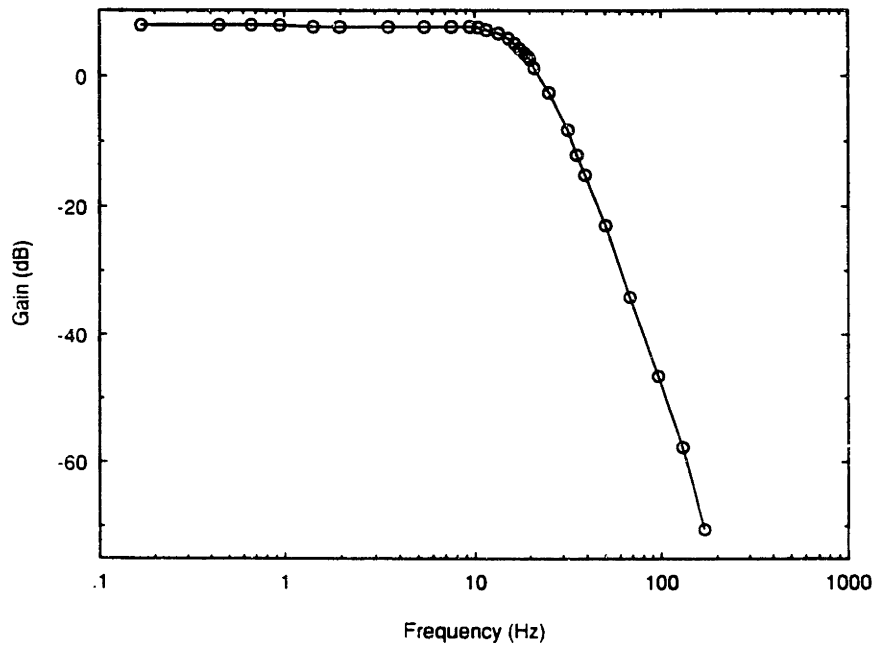

Figure 5.5 (a): Typical Fourth-order Butterworth Low-pass Filter Frequency Response

Similarly, Figure 5.5b shows a typical second-order Butterworth high-pass filter frequency response with a cutoff frequency at 0.34 Hz. There are two curves shown in this plot, and they represent the responses for two cases: one in which the high-pass filter switch is closed (i.e. filtering off) and the other in which the high-pass filter switch is open (i.e. filtering on). It is important to notice that the passband gain of the filter section is preserved when the filtering is turned off; if the gain were to change during switching, then the gauge's dynamic range during DC calibrations would be different from that during AC operation.

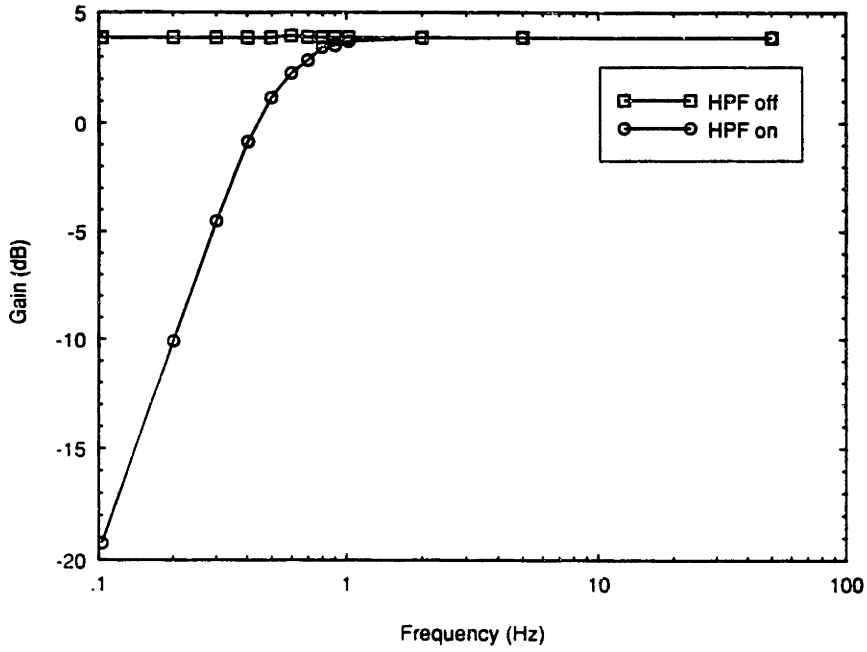

Figure 5.5 (b): Second-order High-pass Filter Frequency Response with Switching

The response characteristics for both the low-pass filters and the high-pass filters are consistent with what is expected in theory. The curves are maximally flat in the passband as is expected for Butterworth filters. Also as expected, the filter "fall-off" rates are all -20 dB per decade per pole (or -6 dB per octave per pole). For instance, the fourth-order low-pass filter response drops off by 80 dB in one decade of frequency. Finally, the actual breakpoint frequencies (3-dB points) do correspond to the frequencies set by the chosen resistor and capacitor values.

The frequency response for the long-wire freshwater gauge is given in Figure 5.6. The response curve represents the total filter response of all the filter sections cascaded together.

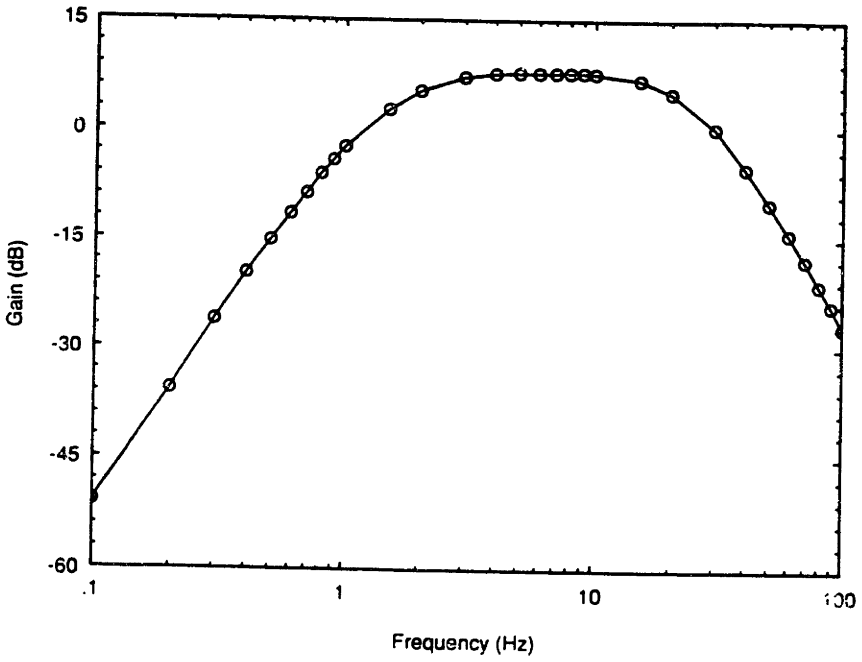

Figure 5.6: Complete Filter Response of the Long-wire Freshwater Gauge

The frequency response of the long-wire gauge is also determined by using the gauge to measure waves of known frequencies and amplitudes generated in the MIT Towing Tank. The results of these measurements are shown in Figure 5.7.

The gain of the system, determined by normalizing the peak-to-peak output voltage to the actual wave height, is plotted for a range of wave frequencies. The plot confirms qualitatively the behavior of the high-pass portion of the frequency response. Quantitatively, the plot is also consistent; that is, for three poles of high-pass filtering, the "drop-off" rate is roughly 18 dB per octave, as expected.

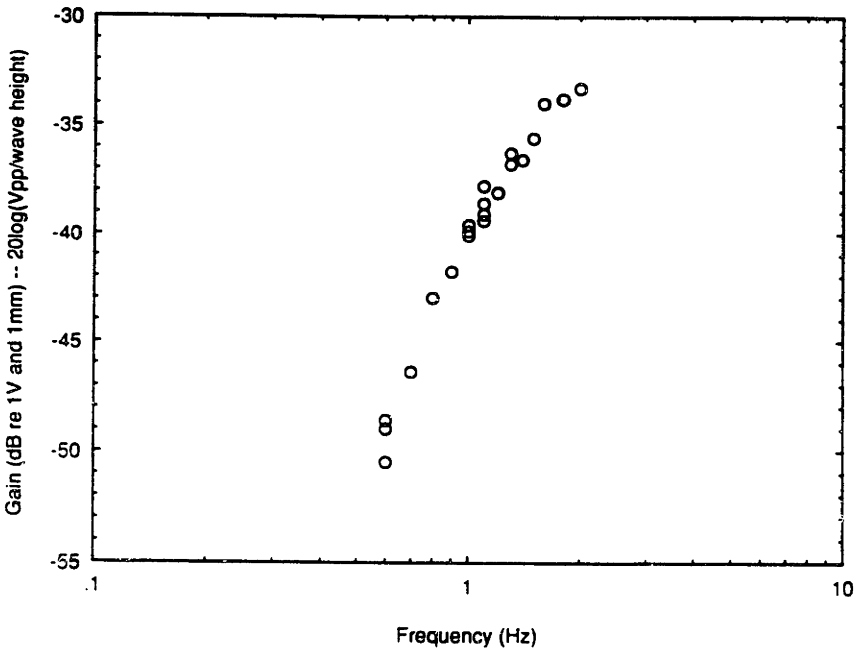

Figure 5.7: Frequency Response of the Long-wire Gauge in the Towing Tank

5.1.5. Sensitivity and signal-to-noise ratio

For 36 AWG nichrome wire, it is observed that waves whose amplitudes measure on the order of a tenth of a millimeter are subject to meniscus effects. With regard to sensitivity limitations due to noise levels, a rough estimate can be given by measuring noise levels on the output. Typically, for the freshwater gauges, up to fifty millivolts of noise (peak-to-peak) can be seen on the output signal lines. Given a DC calibration slope of say, 3.5 volts per inch, this noise level translates roughly into a peak-to-peak wave height measuring one third of a

millimeter. Because the limit from noise effects is roughly the same as that from meniscus effects, the amount of noise is tolerable from an operation point of view.

In essence, the freshwater wave gauges should in most circumstances be able to measure wave heights to within a fraction of a millimeter.

5.1.6. Wave tests and waveform descriptions

Figure 5.8 contains some sample oscilloscope traces detailing the operation of the short-wire freshwater gauges in the wave tank. The traces show the time histories of the gauge's output voltages for waves generated at three frequencies: 2 Hz, 5 Hz, and 9 Hz. In each picture, the bottom trace (channel 2) represents the output of the short-wire freshwater wave gauge. The top trace represents the output of an older set of wave gauges, the ones to be replaced.

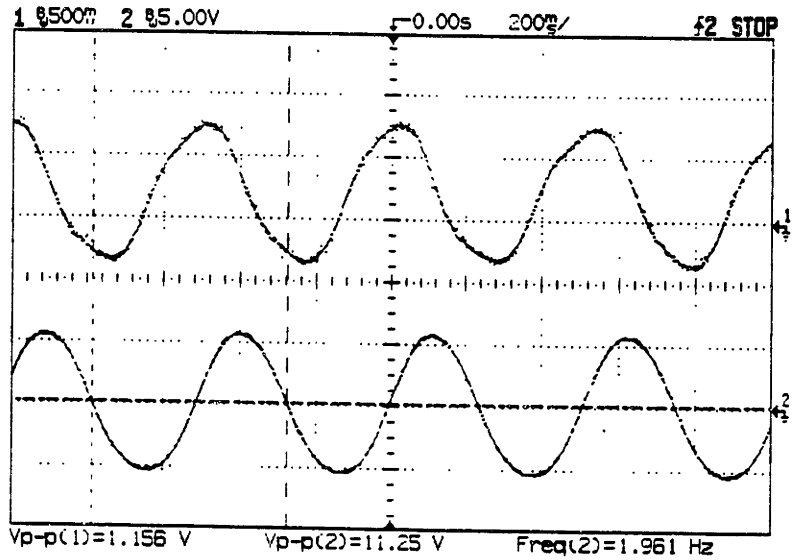

Figure 5.8: (a) 2-Hz Waveforms

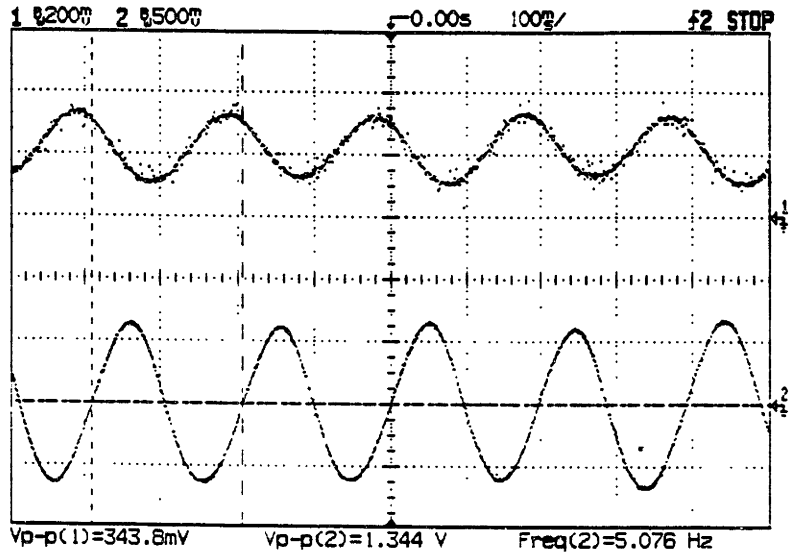

Figure 5.8: (b) 5-Hz Waveforms

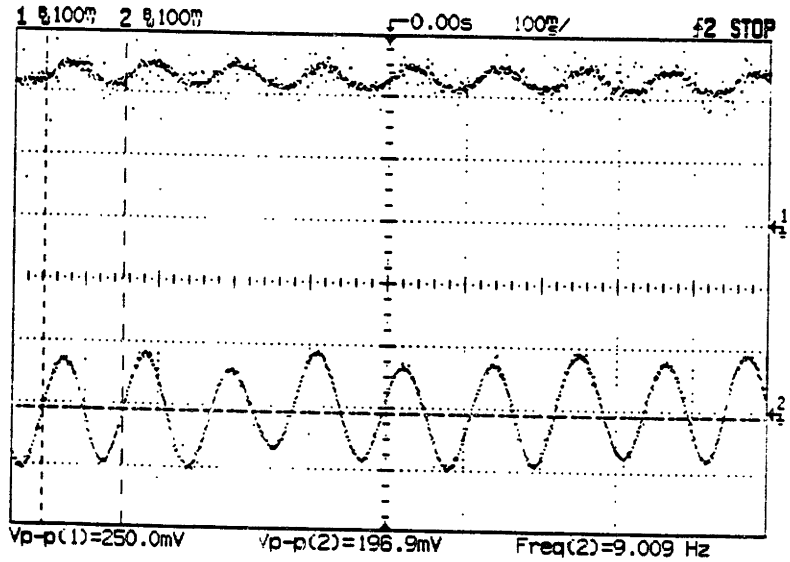

Figure 5.8: (c) 9-Hz Waveforms

All the "new" waveforms are indeed sinusoidal and represent correctly their associated wave frequencies. The "new" gauges also perform much better in terms of signal-to-noise ratio, a fact which is especially apparent at higher frequencies and lower amplitudes. To insure that these differences in performance are indeed attributable solely to the electronics (and not to the probe wires), the probes are reversed for the two sets of electronics. The results show in a consistent fashion that the worse performance is associated with the old electronics.

The new freshwater wave gauge design thus meets its design constraints and performs suitably in laboratory wave tank tests.

5.2. Saltwater wave gauge analysis

5.2.1. Evaluation of the voltage along a probe wire

Figure 5.9 contains a graph describing how voltage levels vary along the length of a saltwater probe wire.

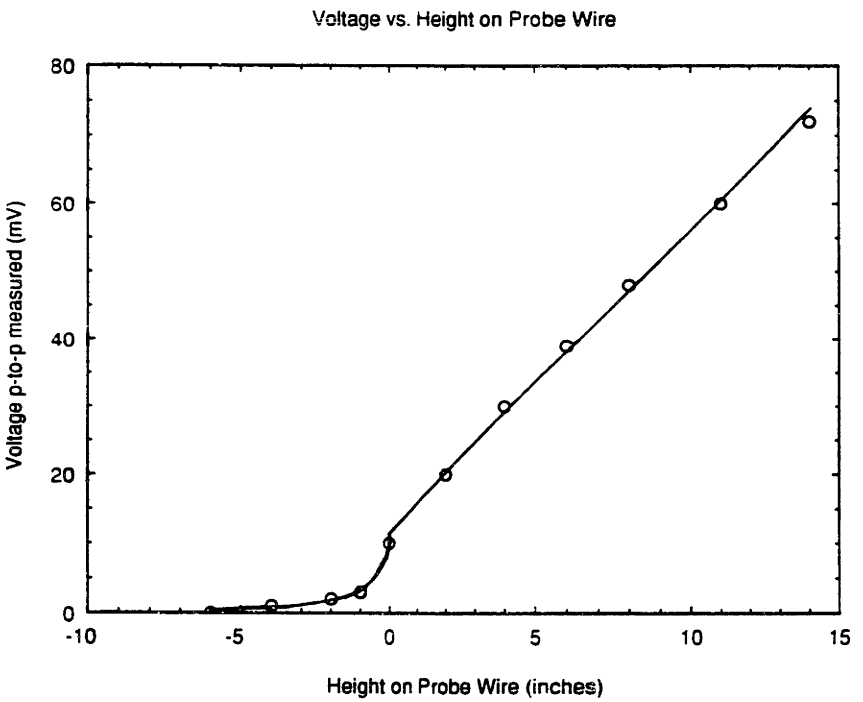

Figure 5.9: Voltages along a Saltwater Probe Wire

The behavior of the voltage can be examined in two sections: 1) the section of probe wire above the water line, and 2) the section of probe wire below the water line. Voltages in the

"dry" section vary linearly with height along the probe wire. This result is, of course, expected for a probe wire of uniform resistance. The voltages in the "wet" section appear to drop off in the manner of exponential decay. This result is important because it indicates that the voltage at the water line does not fall immediately to zero; rather, the voltage drops off gradually to zero over several inches. Thus, to prevent "artificially" grounding the wire too close to the water line, it is necessary to have at least six inches of probe wire before the electrical ground. Otherwise, the path to ground is more through the probe wire than through the water, thus causing insensitivity to water level changes.

In other words, if the submerged length of probe wire is small, then the intrinsic resistance of the "wet" portion of wire is much smaller than the effective resistance of the path to ground through the water; thus, when viewing the two possible paths as resistors in parallel, it is apparent that the path through the wire is the dominant path to ground. On the other hand, if the submerged length of probe wire is large, then the effective resistance of the path to ground through the water is smaller than the intrinsic resistance of the "wet" portion of wire; in this case, the water path is the dominant path to ground. For example, for a submerged length of one inch, the intrinsic wire resistance is roughly 2Ω (assuming 27Ω / ft for 36 AWG nichrome wire), and the effective resistance of the water path is given by Equation 2.1 as 15Ω (assuming $\sigma = 0.035$ mhos/cm, $r = 0.0056$ cm, and $R = 20$ cm). Similarly, for a submerged length of twelve inches, the intrinsic wire resistance is now roughly 27Ω, and the effective resistance of the water path is 1Ω. These predictions seem to be consistent with the behavior observed from Figure 5.9. A more rigorous theoretical derivation of the electrical behavior of this "ground wire" can be found in Appendix F. Both

this theory and the experimental measurements confirm that for the saltwater wave gauge to be effective, it is necessary to have at least six inches of probe wire between the electrical grounding point at the bottom and the water level at all times.

5.2.2. Dependence on water salinity

Figure 5.10 illustrates how the saltwater gauge's DC calibration curves depend on the salinity of the water.

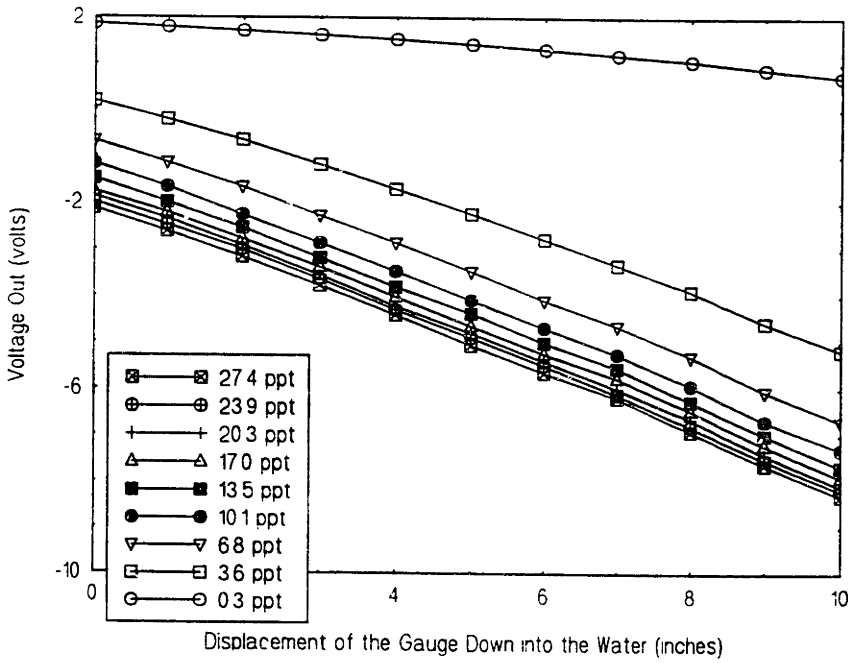

Figure 5.10: Salinity Dependence of the DC Calibration Curves

Identical DC calibrations are performed in water samples of varying salinities. For increasing salinities, the curves resemble each other more and more. The slopes definitely approach the same value, and even the amounts of DC offset become less and less. The similarity in calibration curves for the "saltier" samples can be explained by the fact that as the water becomes more saline, any changes in the effective resistance of the water path due to salinity differences become negligible in comparison with resistance changes in the "dry" probe section due to surface elevation changes. From the graph in Figure 5.10, it is evident that to test accurately the behavior of the saltwater gauge, a water salinity of about ten parts per thousand would be sufficient. Calibration slopes would be identical, and offsets could be eliminated through trim offset adjustments, if needed.

5.2.3. Linearity

The linearity of the saltwater wave gauge is evaluated in the same manner as that of the freshwater wave gauge. Figure 5.11a presents the DC calibration curves for one channel of the saltwater gauge at six different times. In all instances, there is a very linear relationship between the output voltage of the gauge and the gauge height out of the water.

Of great practical importance, however, is the noticeable effect of salt "build-up" on the probe wires. The linearity of the salt water wave gauges depends on the cleanliness of their probe wires. Figure 5.11b illustrates how the calibration curves can become quite non-linear when uncleaned two-day old wire is used.

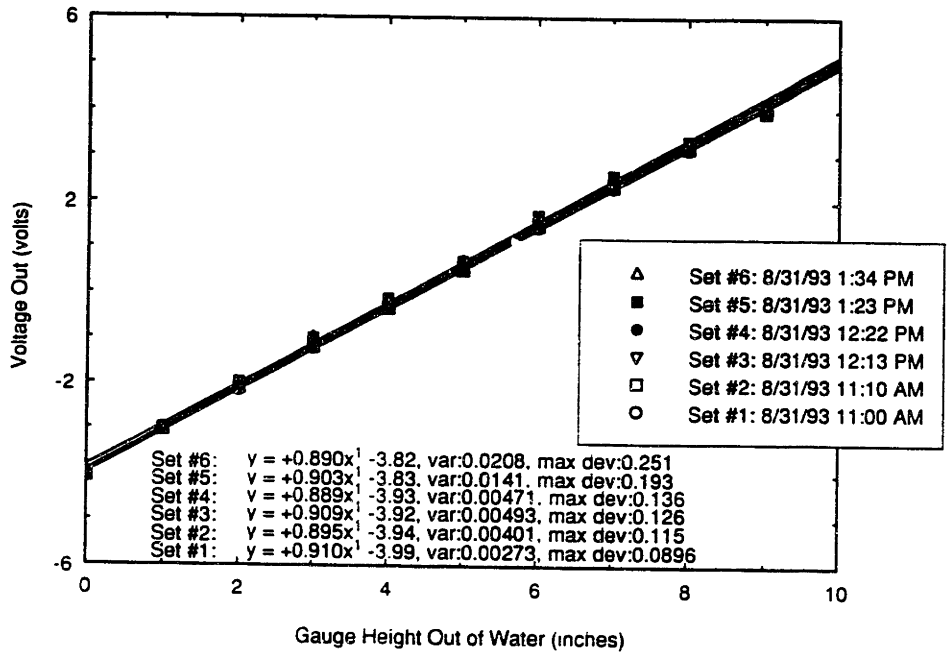

Figure 5.11: (a) Saltwater Wave Gauge DC Calibration Curves

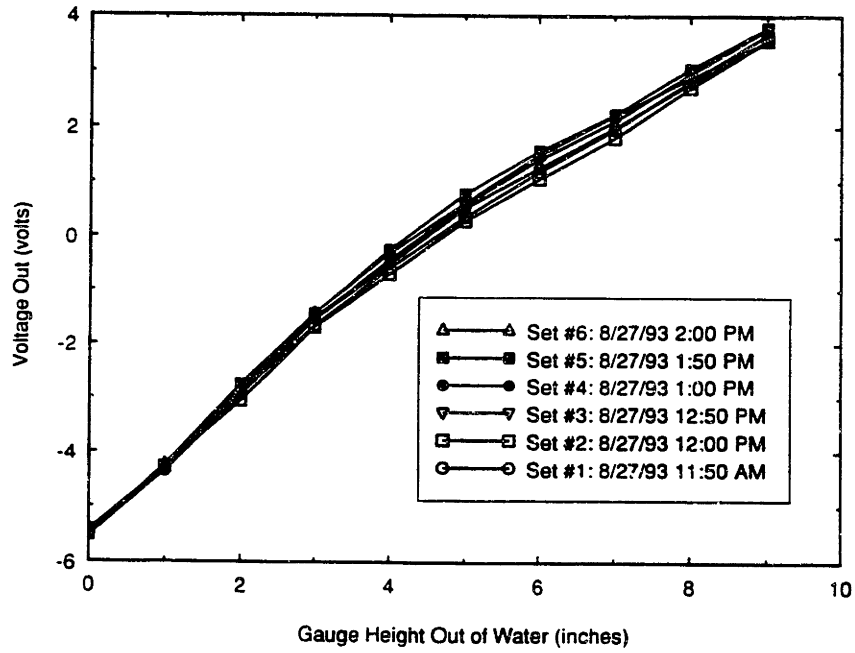

Figure 5.11: (b) Saltwater Wave Gauge Calibration Curves for "Dirty" Probe Wires

5.2.4. Repeatability

Figure 5.11 shows not only the linearity of the gauges but also the repeatability of the gauges over time. There is only a ± 1% change in the calibration slopes over the course of two and a half hours.

5.2.5. Frequency response

Because the saltwater gauge is a multi-channel instrument, it is important to insure that the frequency responses for each channel are the same. Figure 5.12 shows a frequency response curve comparison for two saltwater channels whose filter circuitry consists of 1% tolerance components (both resistors and capacitors). The response curves are essentially identical.

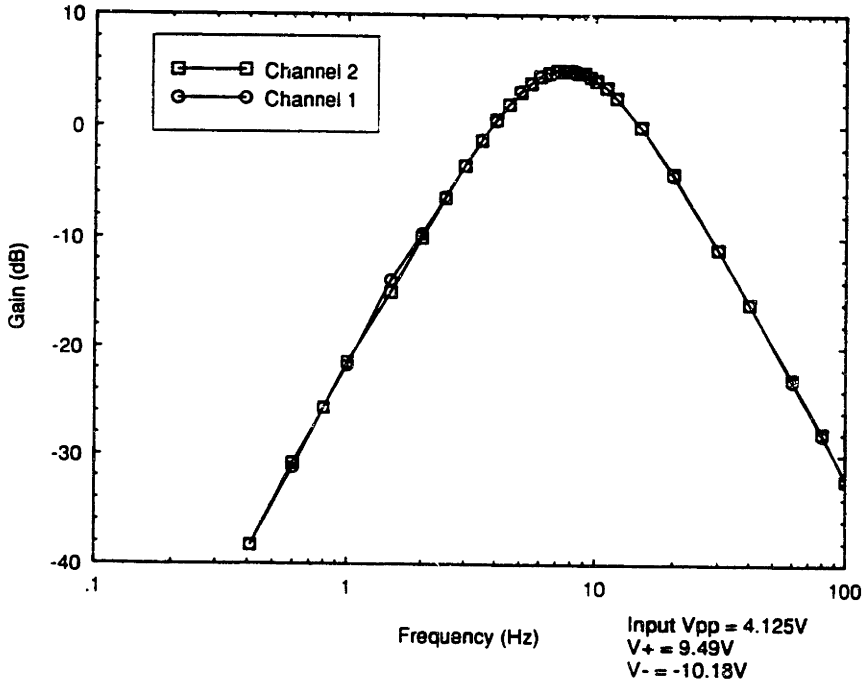

Figure 5.12: Comparing Saltwater Wave Gauge Circuitry with 1% Components

In the case of the sixteen-channel printed circuit boards, the filter components consist of 1% tolerance resistors and 5% tolerance capacitors. To measure the similarity of those frequency responses, the step response of the saltwater circuitry is recorded for each of the sixteen channels. Figure 5.13 shows the computed normalized frequency response curves.

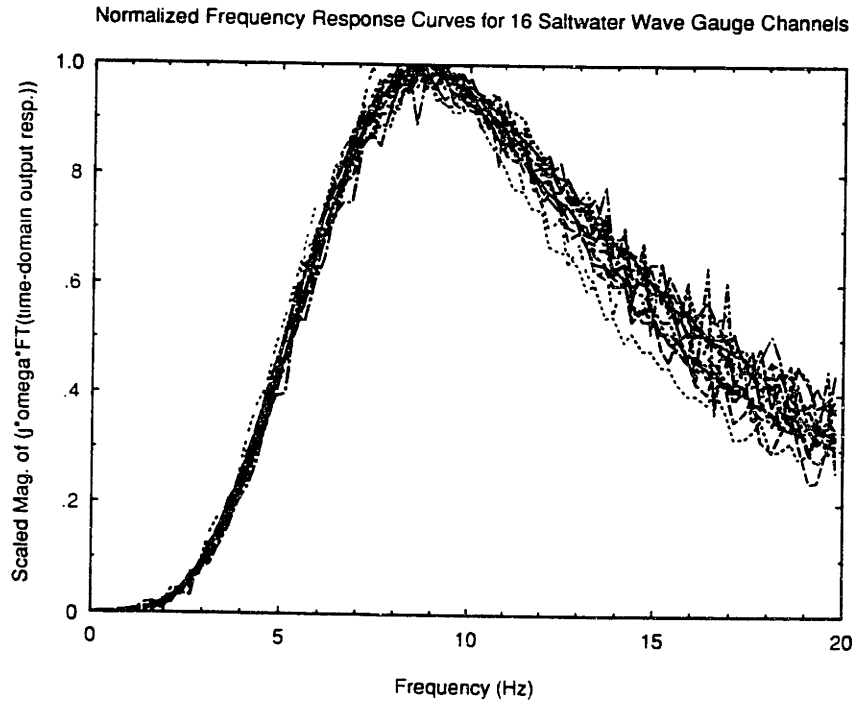

Figure 5.13: Normalized Frequency Response Curves for Sixteen Saltwater Channels

For the frequency range of interest, 1 to 10 Hz, the curves are quite similar. The higher frequency ripples present in the curves are directly related to some of the noise present on the output voltage lines. This noise is apparent upon examining the time-domain output response to a step input into the saltwater circuit (see Figure 5.14). The noise was generated by a DC-DC converter present on the printed circuit board during these tests; the converter is no longer used to regulate power, so this particular noise problem is no longer an issue.

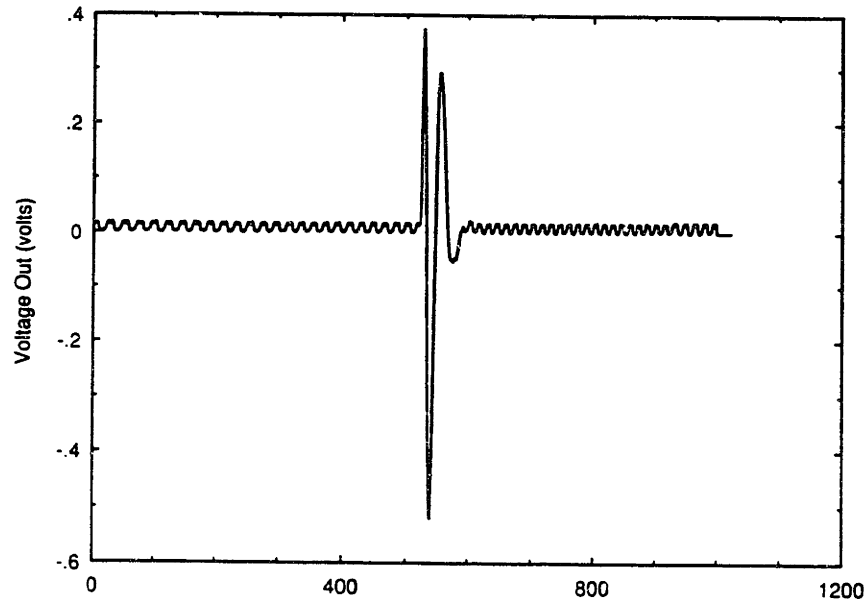

Figure 5.14: Time-domain output response to a step input

Finally, Figure 5.15 describes the time-domain input step used as the excitation.

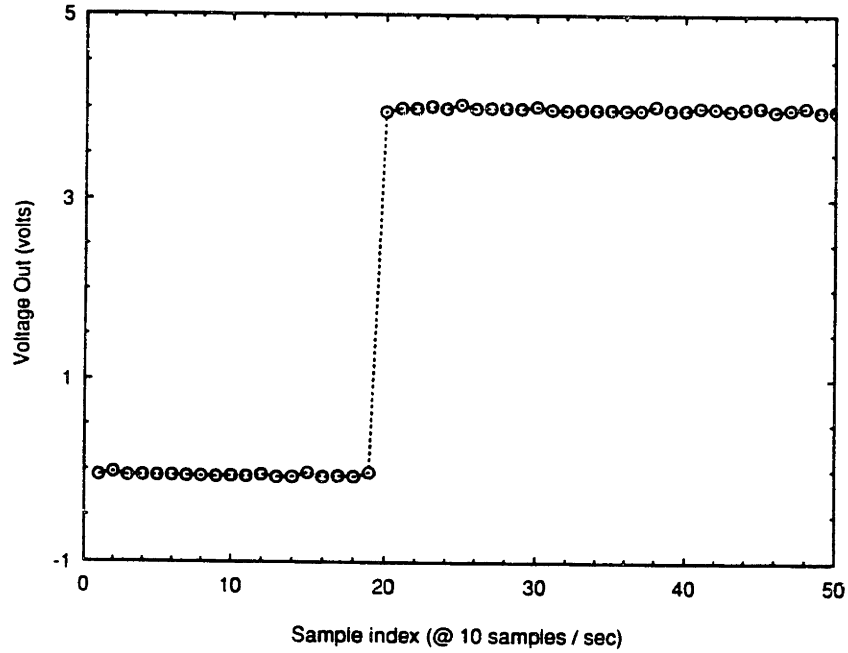

Figure 5.15: Time-domain input step excitation

In any case, the filter responses are sufficiently similar to each other and to what is expected for there to be confidence in this aspect of the saltwater gauge's operation.

5.2.6. Sensitivity

The sensitivity of the saltwater gauge can be estimated by translating the noise level on the output into a wave height through some calibration slope. In the case of the gauges, assuming an output noise level of 100 mV peak-to-peak and a calibration slope of 2 volts/in, the sensitivity of the gauge is on the order of half a millimeter in wave amplitude.

Alternatively, the sensitivity can be found by examining the noise floor level in a given frequency spectrum. This estimate is perhaps more accurate because it considers the fact that the noise energy is spread over a range of frequencies. The results of such measurements show that individual noise components are only on the order of a tenth of a millimeter.

5.2.7. Crosstalk and interference

5.2.7.1. Intra-cable crosstalk

Intra-cable crosstalk describes the crosstalk that occurs between individual wires of a single multi-conductor cable. For instance, two adjacent conductors in a ribbon cable may be prone to such crosstalk. The effects of such crosstalk would be apparent upon examination of

the behavior of output voltages in response to differing input signals on adjacent lines. To test the levels of such crosstalk, a controlled test is performed.

The gains of the sixteen channels on a single printed circuit board are all set such that their DC calibration slope values are at roughly 0.5 volts/inch. The "circular harp" is left out of the water so that the probe resistances for these channels are simply the wire resistances along the entire length of the "harp." The output voltages of the sixteen channels are all adjusted to be around one volt by using the trim potentiometers. Now, by shorting a two-inch section of one of the probe wires, the output voltage on one of the channels is forced to roughly two volts. The output voltages of the two nearest channels are also affected; they shift by roughly a tenth of a volt. The other more distant channels are negligibly affected. Thus, there appears to be a 1:10 ratio of crosstalk between channels, which have signal wires that run close together and that are unshielded from each other. When the output of one channel is forced near saturation (at eleven volts), the neighboring channels show shifts of roughly one volt in their outputs. Thus, the ratio of crosstalk seems fairly constant.

This seemingly significant problem is actually quite tolerable when actual wave steepnesses are considered. Assuming a maximum value of 0.2 for wave steepness, the maximum amount of height difference between adjacent probe wires spaced one centimeter apart is two millimeters. The worst-case crosstalk associated with a 2-mm height difference would be a signal that corresponds to a height of 0.2 mm, a value which is on the order of the noise limit. This scenario, of course, assumes that the signal wires for adjacent probe wires are run next to each other, like in a ribbon cable. For signal wires that run near each other but represent probe wires that are spaced a distance apart, the crosstalk problems are less easily

predictable. Ultimately, in any worst-case situation, there is a 20-dB signal-to-noise ratio. Minimizing this crosstalk through individual wire shielding or twisted pairs is one of the major components in the continuing goal to improve the performance of the multi-channel wave gauge.

5.2.7.2. Inter-cable crosstalk

Unlike intra-cable crosstalk, inter-cable crosstalk occurs between the signal wires of different cables. For instance, by examining the output signals very closely on an oscilloscope, it is seen that a primary constituent of the noise on the output line is a trace of the 10.0 kHz probe amplifier excitation signal. Most likely, this crosstalk results from the close proximity of the data acquisition ribbon cables to the printed circuit board ribbon cables, especially in the area of the interface board. The printed circuit board ribbon cables carry the relatively high-frequency excitation signals, which apparently show up as noise on the output voltage lines going toward the data acquisition boards. These noise levels can grow to as large as 100 mV. This high frequency noise is undesirable because it is aliased into what appears as low frequency noise when the output voltages are sampled at twenty samples per second. Two kinds of solutions are possible: 1) low-pass filtering these output signals right before data acquisition, and 2) using shielded ribbon cable.

5.2.7.3. Interference

Interference is essentially any noise other than crosstalk that is "picked up" by the instrument cabling or power lines. For instance, some sources may be radio-frequency interference or 60-Hz type interference from power lines. These types of noise sources are particularly apparent in situations where cables act as antennas or where electrical grounding is not handled well. By filtering heavily, insuring good ground paths, and regulating supply voltages, these problems of interference can be addressed effectively.

5.2.8. Bucket tests using a mechanical oscillator

The first test of the entire instrument operating in saltwater is performed by using a mechanical oscillator to move the "circular harp" up and down in a 30-gallon bucket of saltwater. The results of this set of tests provide important information about how effectively the instrument works. In particular, the effects of crosstalk and noise can be examined.

Figure 5.16 contains the processed graph of a sample of waveforms acquired while running the oscillator. The graph is processed in the sense that each output data value for a given channel has been scaled by that channel's calibration slope and is thus given in inches. The slopes are estimated using a linear least squares algorithm on the calibration data. Appendix C1 contains plots of these calibration curves. At the time of these bucket tests, only fifty-four out of the sixty-four wave gauge channels were fully operational; thus, there has only been data recorded for those active channels.

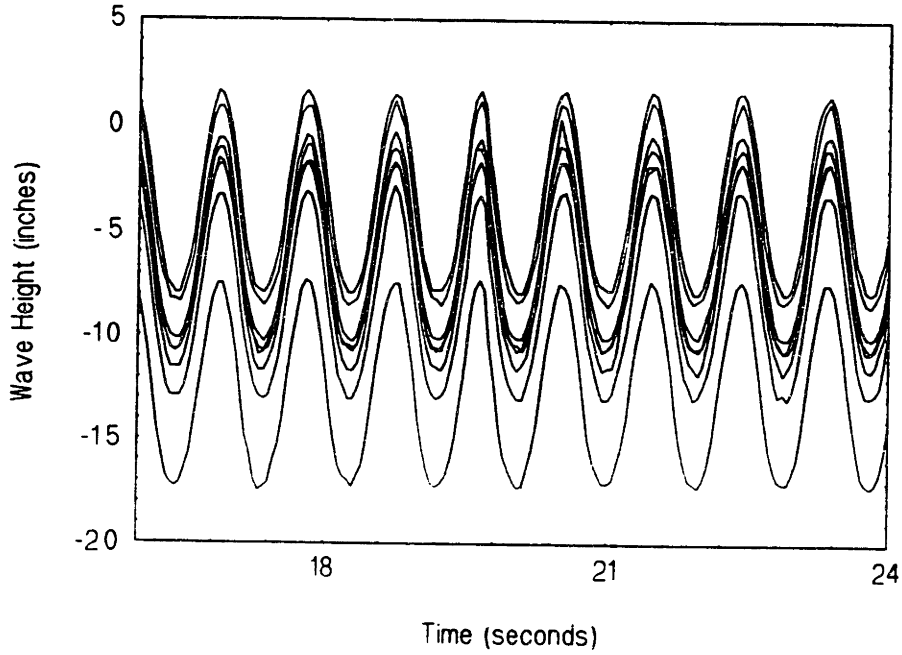

Figure 5.16: Acquired Waveforms for 1.1 Hz Water Waves

The graph contains the acquired output waveforms of eight of the sixty-four channels. For each channel, a data point sample is taken every twentieth of a second; that is, the data sampling rate is twenty Hertz. First, it is evident from the graph that the waveforms are all perfectly in phase as they should be for a uniformly moving "circular harp." Second, the amplitudes of all of the waveforms are more or less the same as they should be for a constant amount of travel displacement. Furthermore, the amplitudes of these waveforms match the actual displacement amplitude, 0.47 inches. Third, all the waveform frequencies match the water wave frequency of 1.1 Hertz. Finally, it is clear that there is a certain amount of noise present on each of the signals. The noise is apparently high-frequency noise which is undersampled during data acquisition.

To analyze the data further, a series of fast Fourier transforms has been performed to obtain spectral information. Figure 5.17 contains some sample spectrum plots for data taken on one of the saltwater wave gauge channels (channel 37). Each plot represents the frequency distribution for the output taken when the "circular harp" is oscillated at a particular frequency. For oscillation frequencies higher than four Hertz, the dynamics become increasingly unstable because a relatively large load is being moved back and forth at sufficiently high speeds to shake the holding apparatus. One further source of interference at those frequencies are the waves that are generated in the bucket. Data is collected for oscillation frequencies ranging from 0.24 Hertz to 3.85 Hertz.

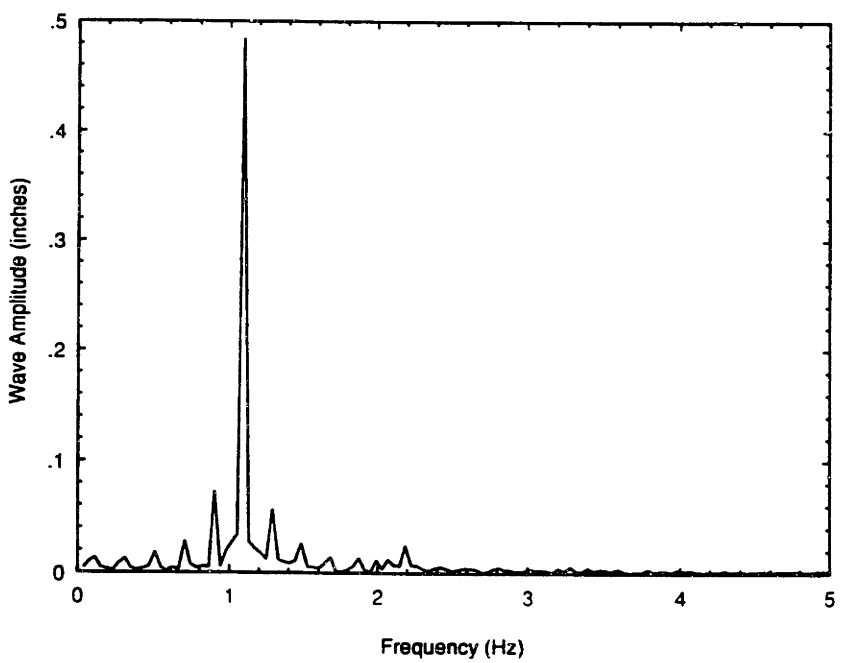

(a)

Figure 5.17: Frequency Spectrum Plots for a Single Saltwater Channel (a) measurement of 1.1 Hz oscillations

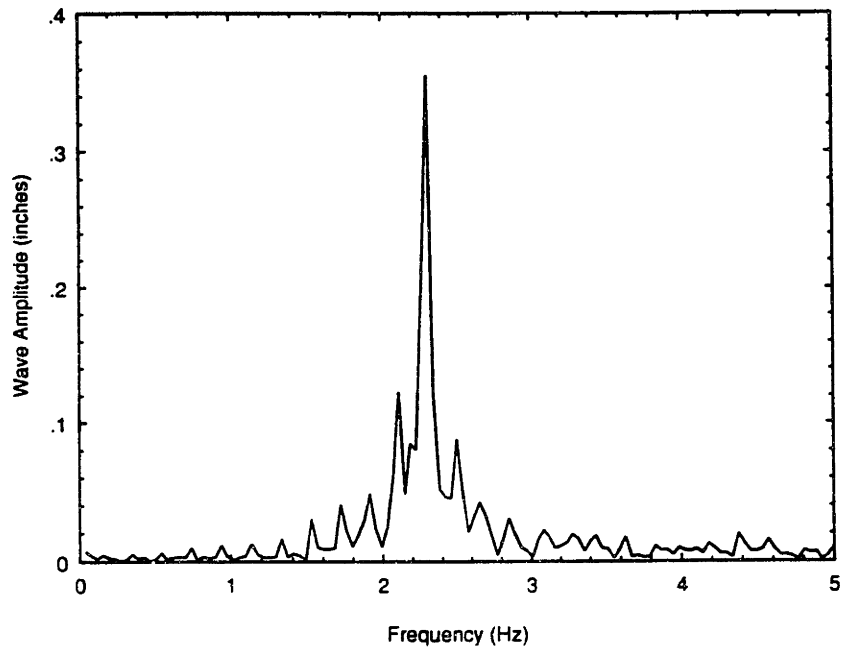

(b)

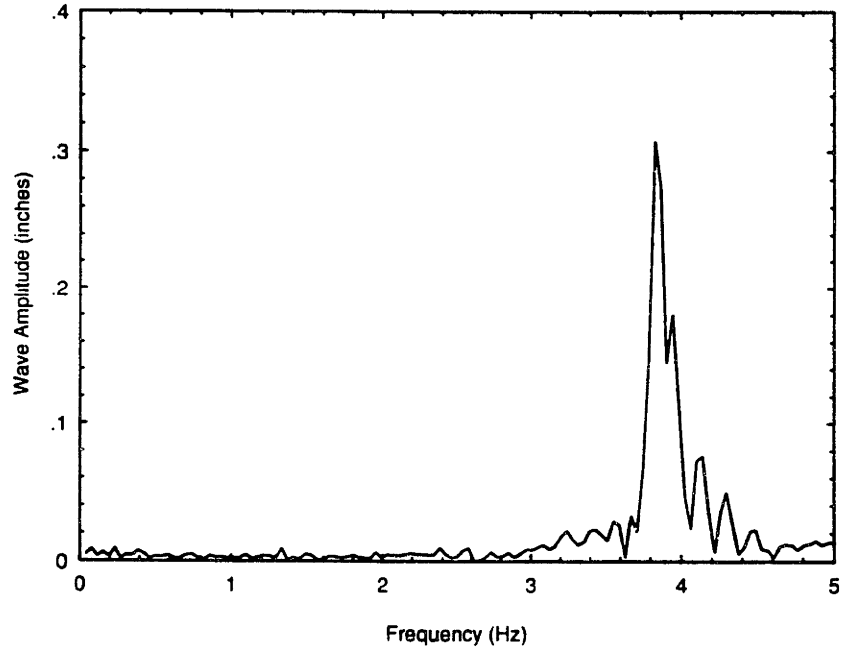

(c)

Figure 5.17: Frequency Spectrum Plots for a Single Saltwater Channel (b) measurement of 2.2 Hz oscillations, (c) measurement of 3.8 Hz oscillations

The spectrum plots are consistent with what is expected. In all cases, the peak frequency of the plot matches the oscillation frequency of the corresponding data run (see Table 5.3).

Actual Oscillation Frequency (Hz)	Calculated Peak Frequency (Hz)
0.24	0.234
0.56	0.586
0.92	0.938
1.06	1.09
1.35	1.37
1.69	1.72
2.22	2.30
2.90	2.93
3.17	3.20
3.85	3.83

Table 5.3: A Comparison of Calculated Peak Frequencies with Actual Oscillation Frequencies

There is some evidence, however, of "leakage effects"; that is, because the samples do not encompass a perfect number of periodic cycles of the main frequency, small evenly spaced spikes occur around the central spectral peak. These spikes are not a major problem simply because they are small and clearly evident.

More importantly, the amplitude of the oscillation can be predicted by integrating the power (or variance) spectral density curve over a narrow bandwidth around the peak frequency. Appendix C2 organizes the results of the processed data. Column 1 of each data set contains the calculated wave amplitude (in inches) for each channel. This amplitude is calculated by first summing all the squared amplitudes within three frequency bins each way

around the peak frequency; the square root of this sum then yields an estimate of the wave amplitude at the peak frequency. Column 2 contains the frequency of the largest wave amplitude, or in other words, the frequency of the largest Fourier component from the FFT. Column 3 contains the actual value of the largest Fourier component. Finally, columns 4 and 5 give the values of the two neighboring components of the peak.

Overall, the results of these calculations are relatively uniform across all the wave gauge channels. For example, for the data set in which the oscillation frequency is 0.24 Hertz and the oscillation amplitude is 0.47 inches, the average amplitude estimate given by the spectral analysis is 0.473 inches, and the standard deviation of the estimates is 0.0253 inches. These statistics provide a means of evaluating both the precision and the accuracy of the measurements across all channels. A comparison of the average estimated value of the amplitude with the actual displacement amplitude gives a good indication of the **accuracy** of the measurements. In the case of the example, 0.473 inches is a very good match to 0.47 inches. The **precision** of the measurements, on the other hand, can be evaluated by examining the standard deviation of the predictions by all the channels. Again, in the case of the example, there is a standard deviation of 0.0253 inches, which amounts to about a five percent error about the average. Contributions to this five percent error are most likely attributable to small errors in the DC calibration slope values. Small water level motions in the bucket may also contribute to a degree of error. An overall error of around five percent, is not discouraging at all, however. Table 5.4 tabulates these statistics for a range of oscillation frequencies.

Oscillation Frequency (Hz)	Average Estimated Amplitude (in)	Standard Deviation of Estimates (in)	Percent Error about the Average (%)
0.24	0.473418	0.025325	5.3
0.56	0.470631	0.019706	4.2
0.92	0.467869	0.016634	3.6
1.06	0.461091	0.014030	3.0
1.35	0.581466	0.109609	18.9
1.69	0.448036	0.015299	3.4
2.22	0.418061	0.015998	3.8
2.90	0.392967	0.012940	3.3
3.17	0.398901	0.016529	4.1
3.85	0.462724	0.027995	6.1

Note: The actual oscillation amplitude in all cases is 0.47 inches.

Table 5.4: Statistics of the Amplitude Estimates from the Bucket Tests

In most cases, the results are fairly precise; the variance among channel estimates typically does not exceed five percent of the average estimate. The one exception is the result for the oscillation frequency of 1.35 Hz. This data set is clearly inconsistent with the rest of the data sets. Both the average and the standard deviation for this frequency are much too high. The cause for this deviation in behavior probably relates to the existence of a large wave mode in the bucket. In terms of the accuracy of the measurements, however, there is an apparent trend in the estimated amplitude values. As the oscillation frequencies increase, the estimated amplitudes tend to decrease. One possible reason for this behavior may be the fact that at higher frequencies, the mechanical oscillator cannot cover the full 0.94 inches of travel. An alternate explanation may be that at higher frequencies, a net amount of wave motion may affect the amount of distance the shifting water level actually covers on the probe wires. In any case, for the more controlled lower frequency oscillations, the results are quite good, both in accuracy and precision.

5.2.9. Wave tank tests and directional spectrum analysis

Although the bucket tests provide a lot of important information about the performance of the saltwater wave gauge instrument, wave tank tests are necessary to evaluate the directional capabilities of the gauge. By orienting the "circular harp" in a known direction and generating waves in a known direction, it is possible to test how well the saltwater instrument resolves directionality, wavenumber, and amplitude. Appendix D contains some of the relevant numerical data associated with chosen examples of the wave tank experiments.

Figure 5.18 contains some sample frequency spectrum plots corresponding to the time-varying output signals of an individual wave gauge channel (channel #22).

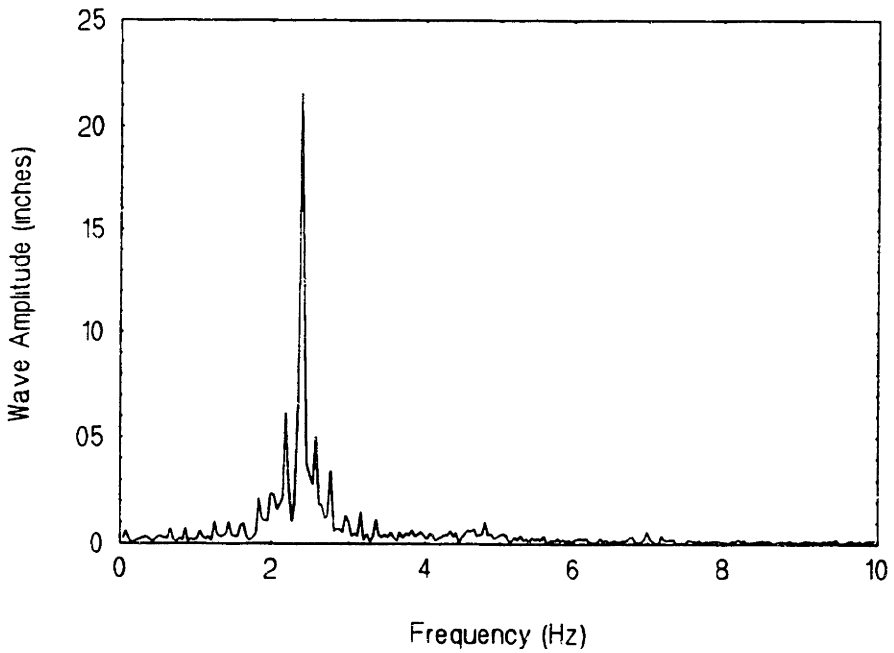

(a)

Figure 5.18: Frequency Spectrum Plots for a Single Saltwater Channel
(a) measurement of 2.3 Hz water waves

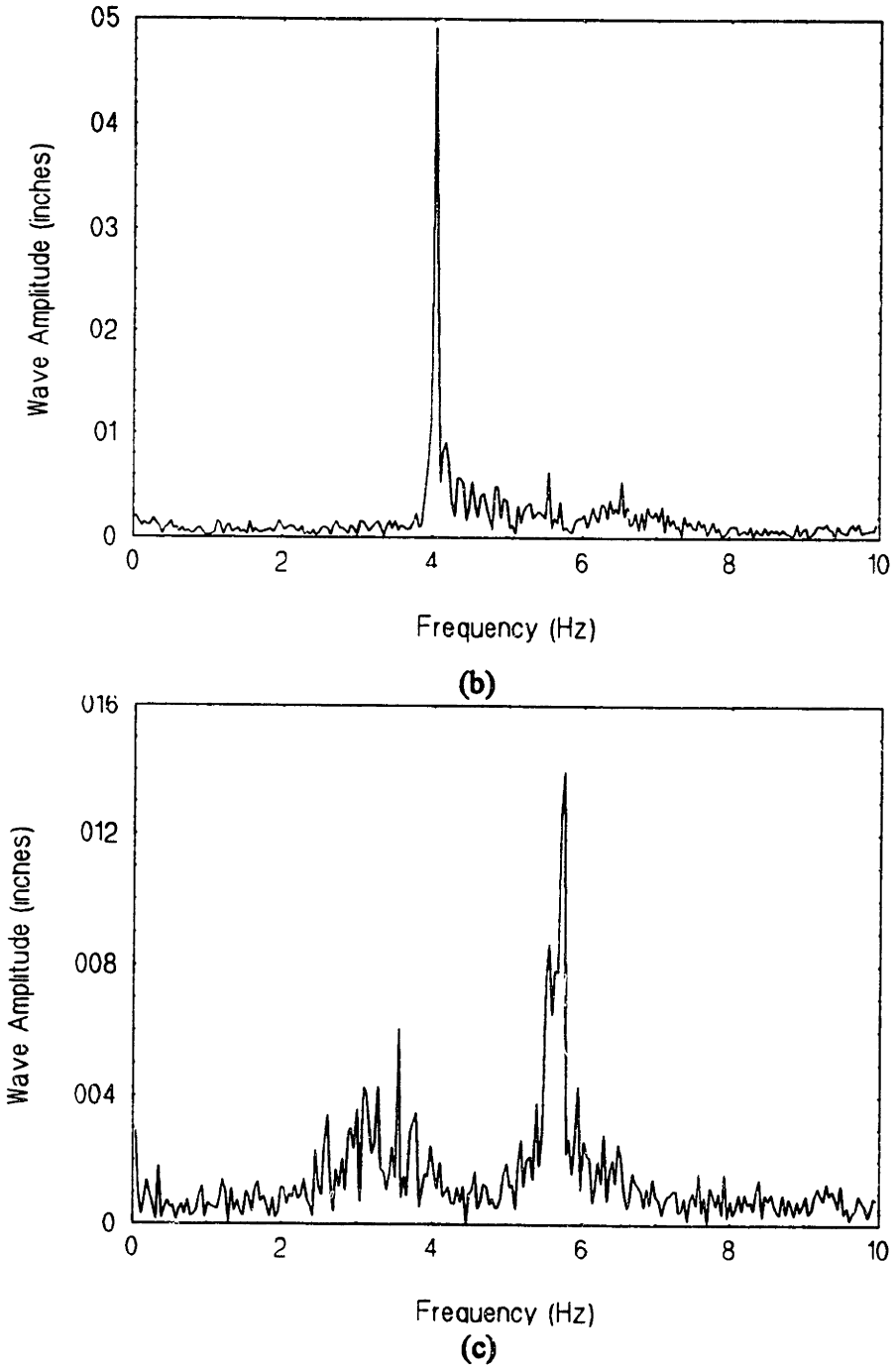

Figure 5.18: Frequency Spectrum Plots for a Single Saltwater Channel (b) measurement of 4.1 Hz water waves, (c) measurement of 5.5 Hz water waves

A comparison of these plots to those in Figure 5.17 reveals the consistency in gauge behavior whether testing occurs in a bucket or in a wave tank. The only major difference between the two sets of plots is the difference in signal-to-noise ratios. For the bucket tests, a strong signal is generated; that is, the wave wires travel nearly one full inch from peak to trough. In the wave tank tests, however, the largest waves generated are less than half an inch in peak-to-peak amplitude. These contrasts are evident when examining the respective ratios of peak levels to noise floor levels. For wave oscillations of roughly 2.25 Hertz, there is roughly a peak-to-floor ratio of 36 for the bucket test and a peak-to-floor ratio of 22 for the wave tank test. Even with the reduced signals for the wave tank tests, it is clear that the expected frequencies and amplitudes can be isolated in the outputs. Tables 5.5 and 5.6 contain the summaries of the frequency and amplitude results of the wave tank tests.

Actual Wave Frequency (Hz)	Calculated Peak Frequency (Hz)
1.9	1.99
2.3	2.38
2.9	3.01
3.4	3.52
4.1	4.02
5.0	5.04
5.5	5.74
6.0	6.13

Table 5.5: A Comparison of Calculated Peak Frequencies with Actual Wave Frequencies

Wave Frequency (Hz)	Independent Amplitude Estimate (in)	Average Estimated Amplitude (in)	Standard Deviation of Estimates (in)
1.9	0.12	0.095	0.016
2.3	0.14	0.14	0.025
2.3	0.28	0.21	0.021
2.9	0.14	0.10	0.018
3.4	0.08	0.075	0.013
4.1	0.05	0.050	0.008
5.0	0.06	0.071	0.015
5.5	0.04	0.020	0.004
6.0	0.01	0.0084	0.0018

Table 5.6: Statistics of the Amplitude Estimates from the Wave Tank Tests

Given the lower signal-to-noise ratios of the wave tank tests, especially at the higher wave frequencies, the frequency and amplitude results are quite reasonable. The estimated amplitudes are generally fairly close to those from an independent wave gauge measurement, and the variances in the mean estimates across channels are sufficiently low to supply confidence about the estimated wave amplitudes. The performance of the saltwater instrument in the wave tank is consistent with its performance in the bucket.

More importantly, directional information can be gathered from the wave tank tests. Figure 5.19 contains a contour plot of the processed data for 4.02 Hz waves propagating only in the x-direction. The vertical axis of the plot represents wavenumbers in the x-direction, and the horizontal axis represents wavenumbers in the y-direction. The shaded contours within the wavenumber grid represent varying levels of spectral intensities, with darker shades representing higher levels.

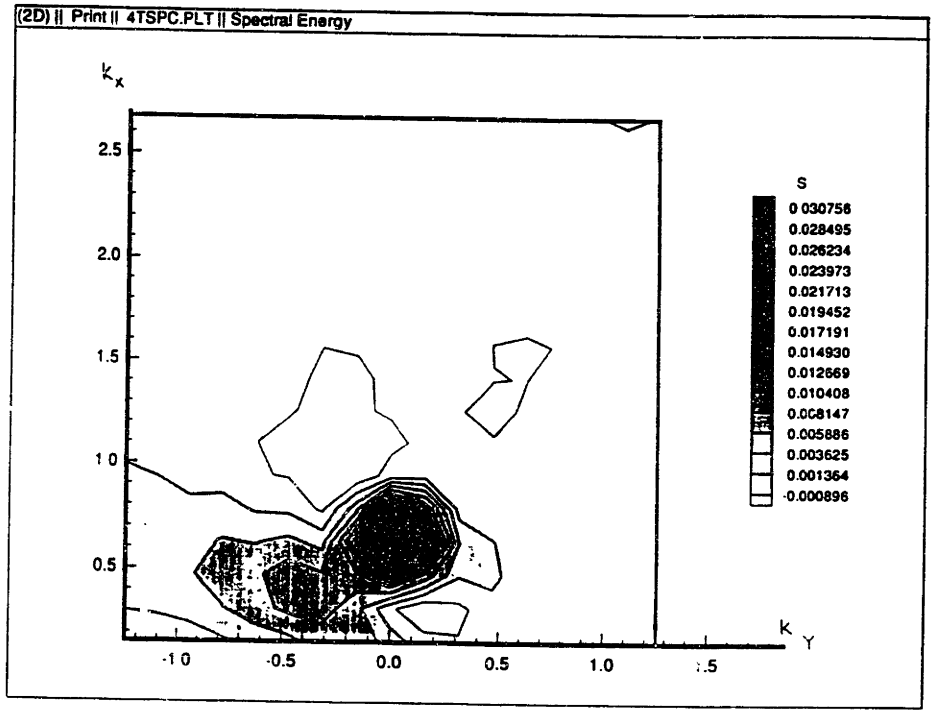

Figure 5.19: Wavenumber Contour Plot for a Single 4-Hz Wave in the X-direction

These contour plots may be slightly misleading in the sense that they show more resolution than what actually exists. In other words, many contour lines are based on points of interpolation. The actual resolution in wavenumber space is roughly 0.157 cm^{-1}, or $\pi/20$ cm^{-1}. The size of this increment is constrained by the geometry of the wave wire circle. Given that the diameter of the wave wire circle is 20 cm, the largest separation length in the constructed two-dimensional autocorrelation space corresponds to a wavelength of 40 cm. Accordingly, in spectral wavenumber space, there is a resolution limit of $2\pi/\lambda$, where λ is 40 cm. Figure 5.20 contains the spectral plots of three k_y slices through the equivalent contour

plot in Figure 5.19. These line plots convey more clearly the true resolution and information contained in the signal analysis.

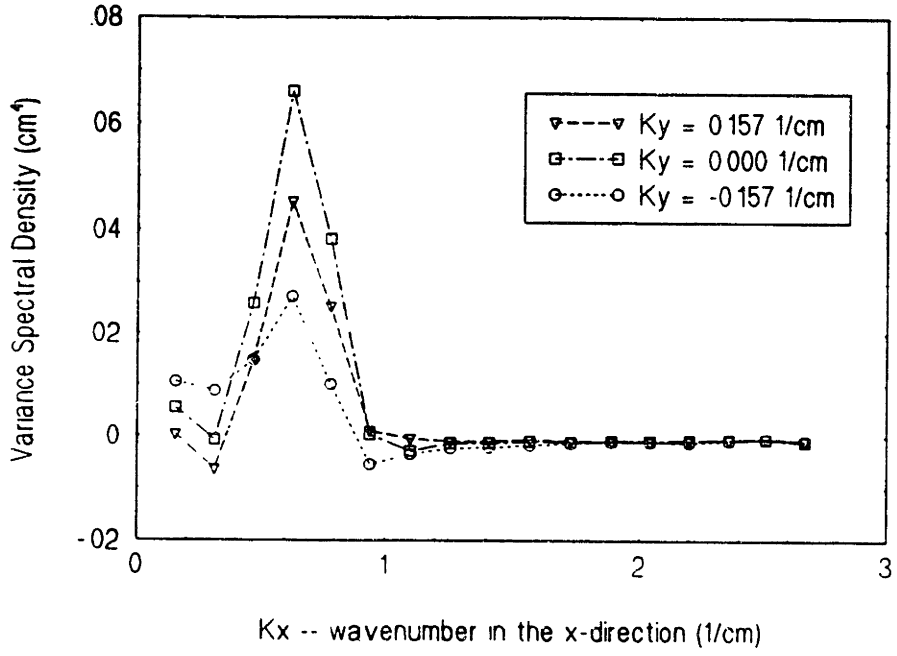

Figure 5.20: Three Slices of the Contour Plot for an X-directed 4-Hz Wave

To compare frequency spectra to wavenumber spectra, it is necessary to know how the two characteristics are related. Equation 5.1 contains the dispersion relationship between frequency and wavenumber for deep water waves (i.e. depth >> wavelength).

$$k = \frac{\omega^2}{g} \qquad \text{Eqn. 5.1}$$

where k is the wavenumber, ω (= $2\pi f$) is the circular wave frequency, and g is the gravitational acceleration

Thus, for example, a 4.02 Hz wave translates into a wavenumber of **0.65** 1/cm. This value corresponds very closely to the k_x value of the peak on the spectrum plot in Figure 5.19. The k_y value of the peak in that plot is also consistent. That is, the value is close to zero, which means that there is very little frequency content in the transverse direction.

Figure 5.21 contains another contour plot.

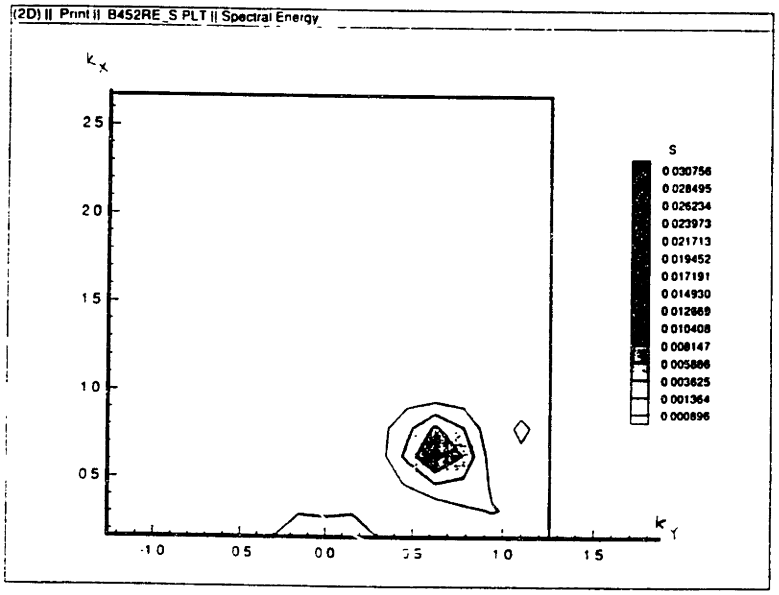

Figure 5.21: Wavenumber Contour Plot for a 4.88-Hz Wave at Forty-Five Degrees

In this case, 4.88 Hz waves propagate at a forty-five degree angle with respect to the gauge orientation. A 4.88 Hz wave corresponds to a wavenumber of **0.96** 1/cm. In terms of the spectrum plot, there are consistent results. The peak occurs at a k_x = 0.65 1/cm and a k_y = 0.65 1/cm. The magnitude of the **k**-vector is thus 0.92 1/cm, and the angle of the **k**-vector is forty-five degrees. Thus, the spectrum plot reflects very accurately what is given as a controlled input. Most importantly, this spectrum plot confirms that the saltwater wave gauge instrument is capable of discerning directionality accurately.

Finally, contour plots are made for multiple-frequency randomly-generated waves. Figure 5.22 contains the time-domain and corresponding frequency domain plots for a hand-generated set of waves in the x-direction. These plots are the acquired results for a single wave gauge channel.

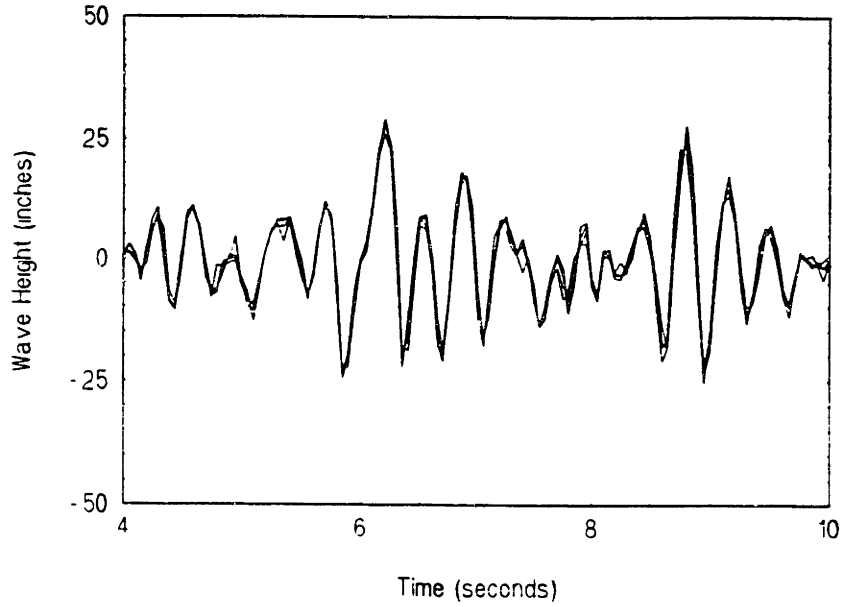

(a) Time-domain plot

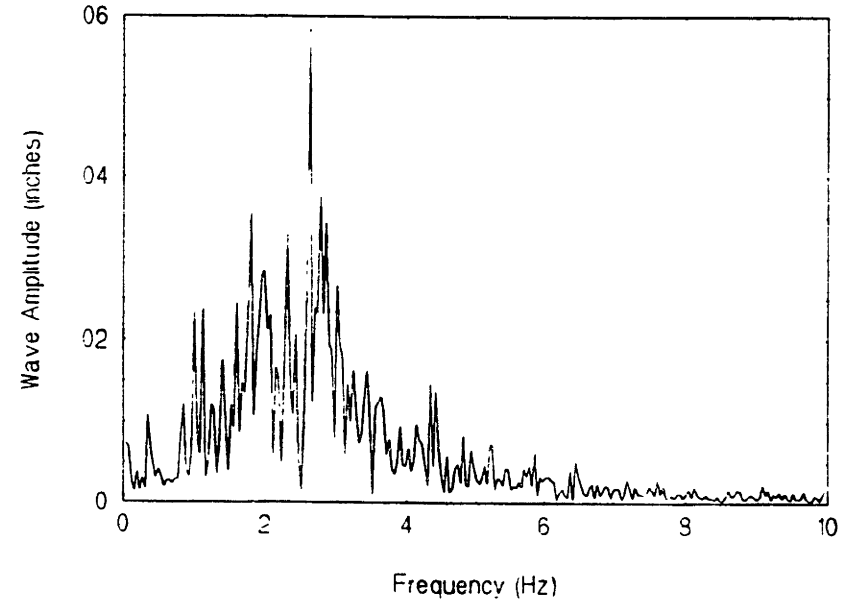

(b) Frequency-domain plot

Figure 5.22: Multiple-frequency, Randomly Generated Wave Input in the X-direction (a) Time-domain data for four channels, (b) Frequency-domain data for one channel

Figure 5.23 contains the directional contour plot associated with this x-directed set of waves.

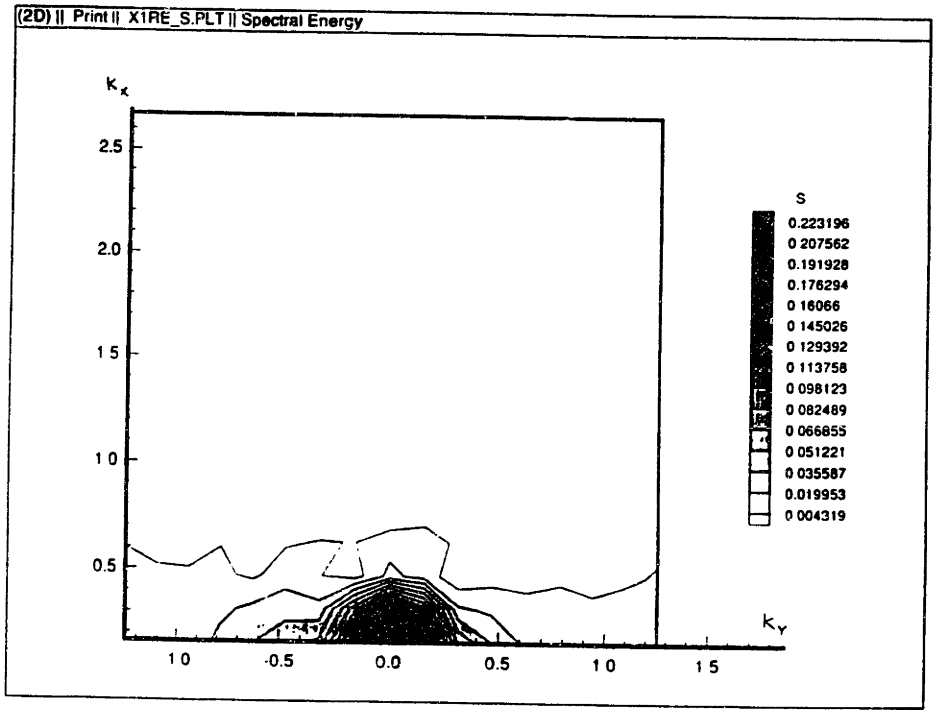

Figure 5.23: Wavenumber Contour Plot for a Random X-directed Set of Waves

From this contour plot and the frequency plot in Figure 5.22b, it is evident that the frequency spread of the wave set is not sufficiently large to exceed the first few wavenumber bins along the x-direction. Unfortunately, the resolution limit of 0.157 1/cm constrains most of the "interesting" data to the first few bins, where most of the wave energy is located. Figure 5.24 contains three slices of the contour plot in Figure 5.23 and gives a more accurate picture of the data. The expected smearing of wavenumbers is difficult to perceive, given both the limitation in resolution and the limitation in frequency range from hand-generated waves.

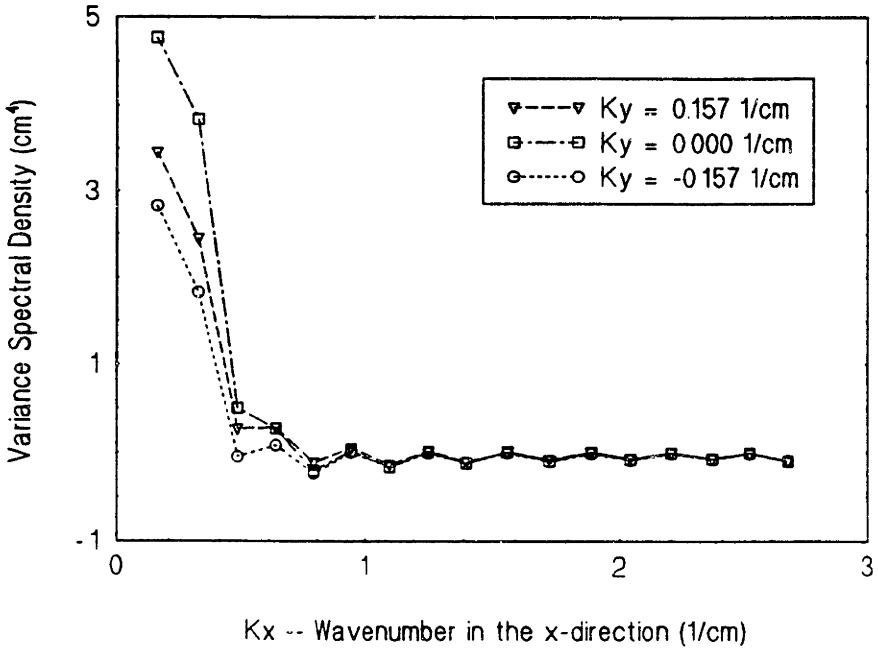

Figure 5.24: Three Slices of the Contour Plot for a Random X-directed Set of Waves

Figure 5.25 contains the contour plot associated with a hand-generated set of waves at forty-five degrees.

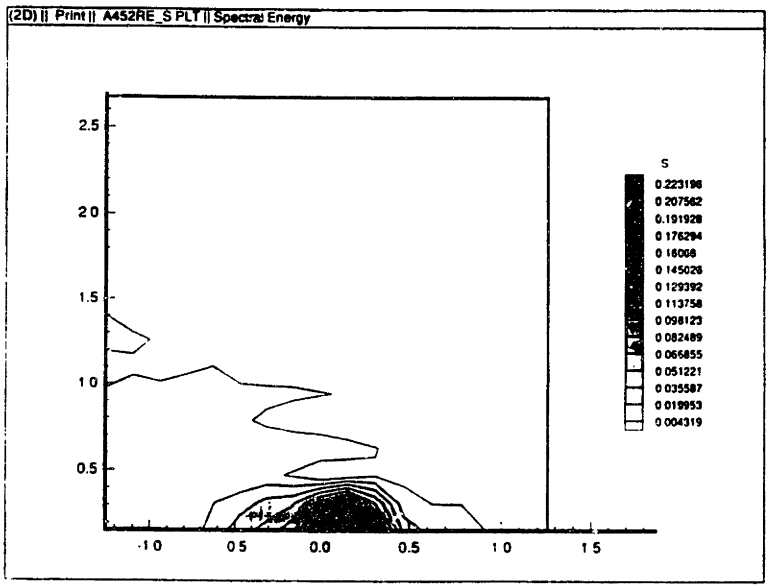

Figure 5.25: Wavenumber Contour Plot for a Random Set of Waves at Forty-Five Degrees

Like Figure 5.23, most of the wave energy is bundled together in the lower wavenumber bins. Upon careful inspection, the directionality of the spreading at forty-five degrees is observable. Figure 5.26 contains the time-domain and corresponding frequency domain plots for the hand-generated waves at forty-five degrees.

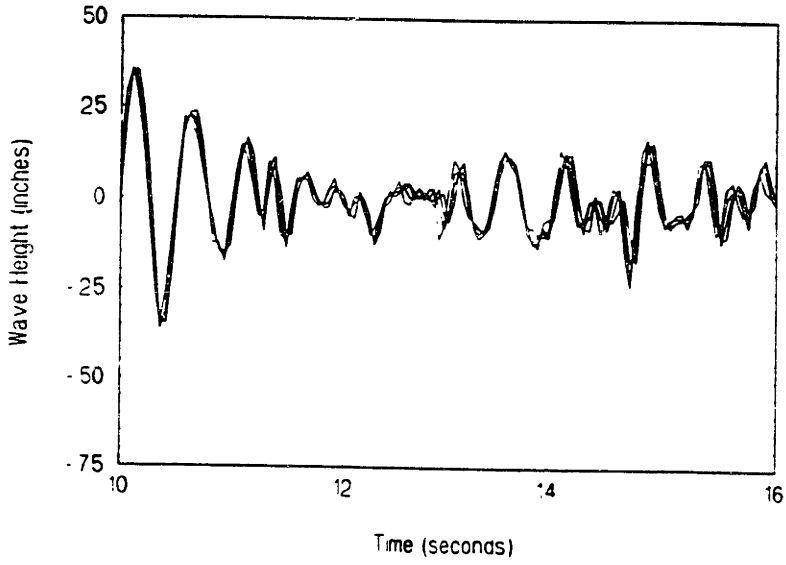

(a) Time-domain plot

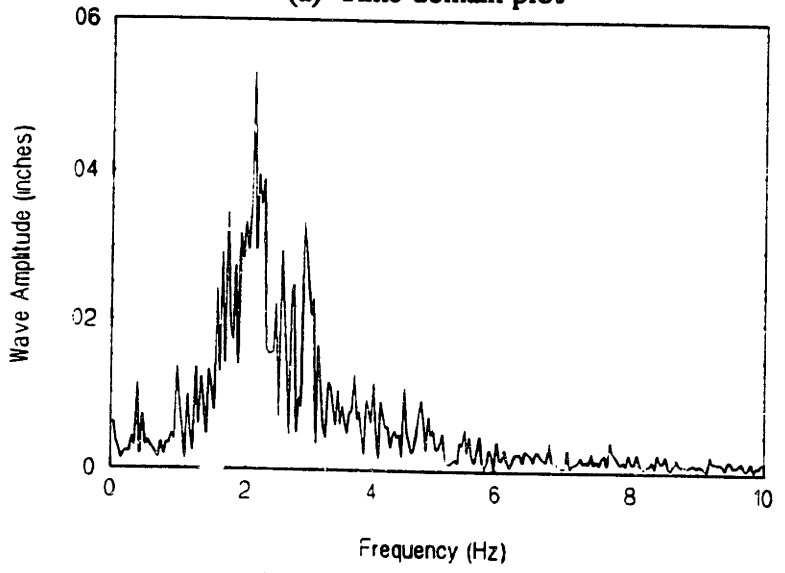

(b) Frequency-domain plot

Figure 5.26: Multiple-frequency, Randomly Generated Wave Input at Forty-Five Degrees (a) Time-domain data for four channels, (b) Frequency-domain data for one channel

The frequency plot is very similar to that in Figure 5.22b; the time-domain plots, however, illustrate how in the forty-five degree case, there is more phase spreading between the first four channels of the instrument. Because the first four channels are oriented at a forty-five degree angle from the incoming wave fronts, there are greater time lags between their responses. In the x-directed case, the first four channels are pointed more directly at the incoming waves, so their responses are nearly identical. In any case, the wavenumber plots in both of the hand-generated wave sets appear to be consistent with what is seen in their respective frequency and time plots.

The results of all of these spectrum plots not only indicate that useful wave height data can be collected on all sixty-four channels, but they also show that the short-wave directional spectrum can be reconstructed through the post-processing of that data. All in all, the instrument seems to work quite effectively in obtaining sea wave directional spectra.

6. Conclusions

The resistive/conductive wave gauge designs have proven to be effective designs for the measurement of water waves which range in amplitude from fractions of a millimeter to fractions of a meter and range in frequency from zero to ten Hertz. Implementations of these designs have been thoroughly tested in both saltwater and freshwater laboratory environments, and their performances have been carefully characterized. All the instruments demonstrate very good linearity, sensitivity, and repeatability. In addition, it has been shown that the frequency response characteristics of the gauges can be easily and effectively tailored

to the particular needs of an experimental application. Furthermore, in the special case of the saltwater instrument, the directionality of the wave components can be readily obtained from post-processing.

6.1. System limitations

Even though the gauges produce good results, it is still desirable to reduce existing noise levels wherever possible. Signals acquired by the saltwater instrument, in particular, can at times be degraded by high levels of noise and inter-cable interference. These noise-related concerns, however, can be remedied by a better cabling scheme and possible filtering. Current noise levels, during satisfactory operation, vary from 50 mV to 100 mV. Reducing these levels will increase wave gauge sensitivity and improve the accuracy of spectrum analyses. High-frequency noise both from the environment and from signal wire interference is potentially bothersome primarily because of aliasing effects; that is, frequency components which are above the Nyquist frequency of 10 Hz are undersampled and thus could appear as lower frequency waveforms in the digitized spectrum. Currently, however, any noise and interference problems are alleviated by carefully arranging the cables to minimize interference effects. In the long-term, a better cabling scheme will insure that noise and interference will always be at a minimum during operation.

Another set of limitations, with respect to the saltwater instrument in particular, relates to practical problems such as ruggedness and the flexibility for making changes. Given that the wave-measuring instrument is based on a system of probe wires, it is somewhat

susceptible to damage. The thin nichrome wires can easily be broken or pulled loose. Thus, it is convenient to be able to change and replace wires quickly and easily. Currently, because the wires are tied to the bottom plate and soldered to electrical connections at the top, it is fairly troublesome to replace wires. Furthermore, the existing interface electronics board is a hand-wired board which is not placed in an enclosure. Thus, it must be handled delicately so that wires do not come loose during jostling. One final source of inconvenience can be found in the chassis used to mount the four analog front-end printed circuit boards. Ideally, it is desirable to have the boards mounted rigidly during use and also to have them slide in and out easily for modifications. Currently, the printed circuit board guides within the chassis hold the four circuit boards so tightly that they cannot slide in and out. Consequently, to make changes on the boards, it is necessary to dismantle the entire setup and then reassemble it after the modifications are performed.

Finally, for experiments to be performed "at sea," sufficient waterproofing needs to be done on all the connectors and enclosures to ensure that saltwater does not cause any unwanted short circuits.

6.2. Recommendations

Potential improvements can be made first to reduce the saltwater instrument's susceptibility to noise and second to increase its ruggedness.

A number of modifications can be made to the saltwater instrument to alleviate problems relating to noise, crosstalk, and interference. First, stronger low-pass filtering right

before data acquisition will greatly help high-frequency noise reduction and thus prevent unwanted aliasing. Second, better electrical cables can potentially reduce existing crosstalk and interference problems. Albeit expensive, ribbon cables and multi-conductor cables which contain individually shielded twisted pairs in addition to overall shielding are the most recommended. Individual coaxial cables are yet another alternative. Furthermore, currently unshielded ribbon cables can be replaced with shielded equivalents to reduce the instrument's susceptibility to noise and inter-cable interference. Yet another way to minimize interference effects is to shorten the existing ribbon cable lengths as much as possible. At one extreme, the interface board can perhaps be integrated with the analog front-end boards, so that current inter-board ribbon cables will not be needed. Finally, the existing wire connections to the DAS-16 data acquisition board need to be shielded.

In addition to these noise-improvement modifications, there are changes which can potentially improve the ruggedness of the instrument and ease the usage of the instrument. First, the printed circuit board guides within the chassis can be changed to guides which allow the boards to slide in and out when necessary. Second, an enclosure for the existing interface board should be made so that all interconnections will be more rugged and reliable. Finally, the "circular harp" should be modified so that there is a better attachment scheme for the nichrome wave probe wires. The current scheme of tying the bottoms of the probe wires directly to the bottom plate and using nylon strings to connect the probe wires to springs at the top makes wire changes very inconvenient. A quicker and easier way to replace wires would greatly improve the ease of usage.

Other possible design changes to the instrument include 1) the utilization of four-layer (rather than two-layer) printed circuit boards to minimize crosstalk on the boards, and 2) the use of a low-noise external signal generator rather than signal-generator integrated circuits to provide a driving oscillation frequency. The signal generator integrated circuits currently being used (ICL8038 chips) seem to be very susceptible to electrical noise. Finally, if it is desirable to have a sharper resolution in wavenumber, the overall diameter of the wave wire circle can be increased preferably by adding more wires to maintain the same wire spacing. Remember that wire spacing is what determines the highest wave frequency measurable.

The recommendations mentioned so far vary greatly in their difficulty for implementation. It is useful to remember at this point that the existing wave gauge instruments do still work effectively without any of these changes. The most common problems encountered so far in the usage of these gauges have been easy to solve without fundamental modifications. That is, the problems associated with 1) using old and dirty probe wires, 2) cable mismanagement, 3) electrical ground loops, and 4) power line noise are what most typically cause performance degradation of the wave gauges. Assuming proper usage, conductive/resistive wave gauges have proven to be a very effective way of measuring wave heights in the water. With improvements, moreover, the gauges can become even more reliable in their ability to measure waves.

Appendix A: Estimating the Effective Resistance Between Probes in Water

Refer to Figure 2.1....

Let the current density $J = \sigma E_r$ where σ is the conductivity of water and E_r is the radial electric field

It is also known that $J = \frac{I}{2\pi r l}$

Thus, $E_r = \frac{I}{2\pi r l \sigma}$ In addition, $E_r = -\nabla\Phi = -\frac{\partial\Phi}{\partial r}$

In general, a line integration along the radius yields

$$\int_{r_{ref}}^{\tilde{r}} \nabla\Phi \bullet dr = \Phi(\tilde{r}) - \Phi(r_{ref})$$

so, in this case, for a known voltage V on the central probe conductor,

$$\int_r^R -E_r(r') \bullet dr' = 0 - V$$

$$V = \int_r^R E_r(r') \bullet dr' = \frac{I}{2\pi l\sigma}(\ln R - \ln r)$$

$$V = \frac{I}{2\pi l\sigma} \ln\left(\frac{R}{r}\right)$$

Finally, the effective resistance is $Res = \frac{V}{I} = \frac{1}{2\pi\sigma l} \ln\left(\frac{R}{r}\right)$

Appendix B: Wave Gauge Schematics

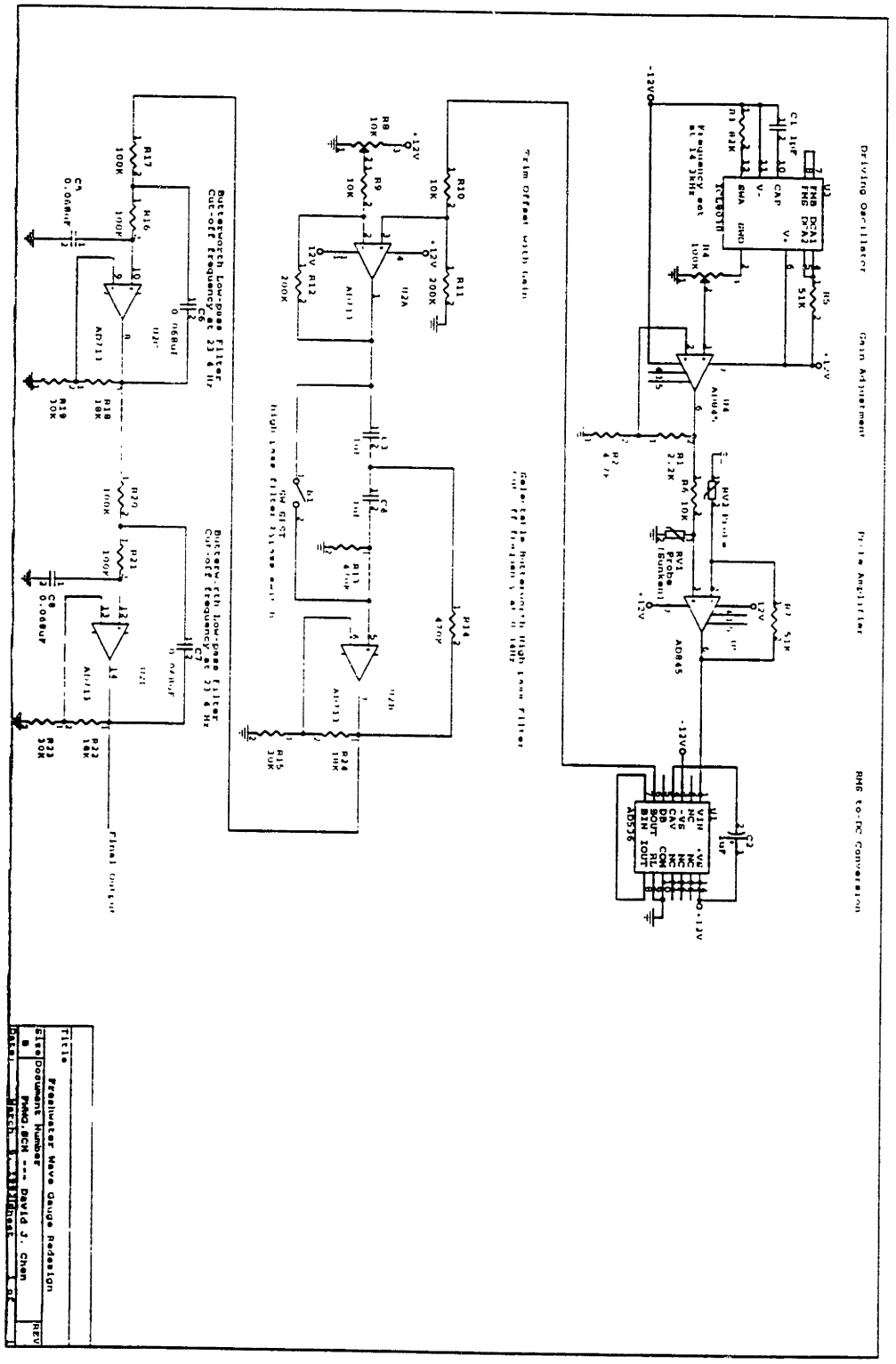

Short-wire Freshwater Wave Gauge Schematic

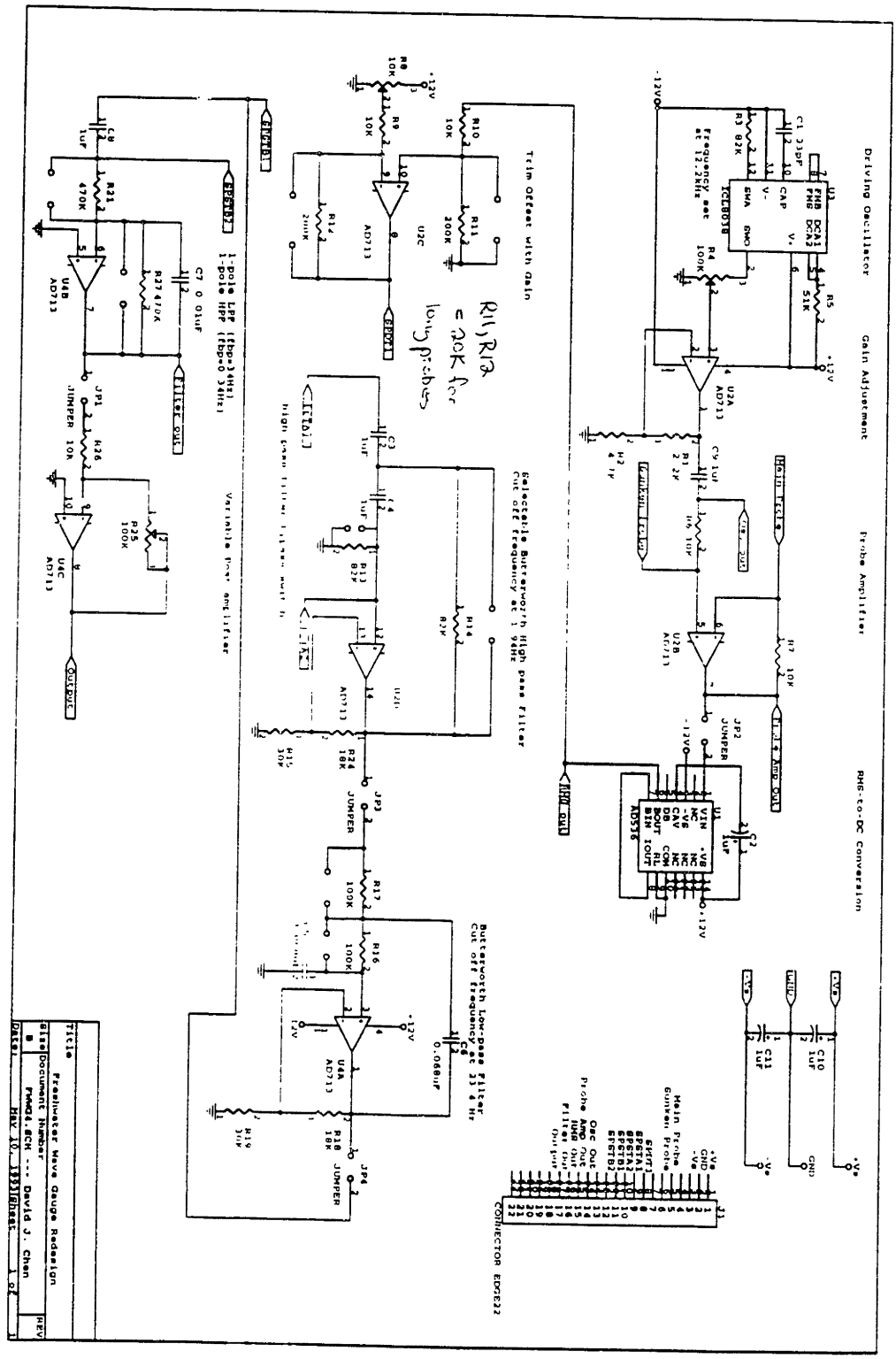

Long-wire Freshwater Wave Gauge Schematic

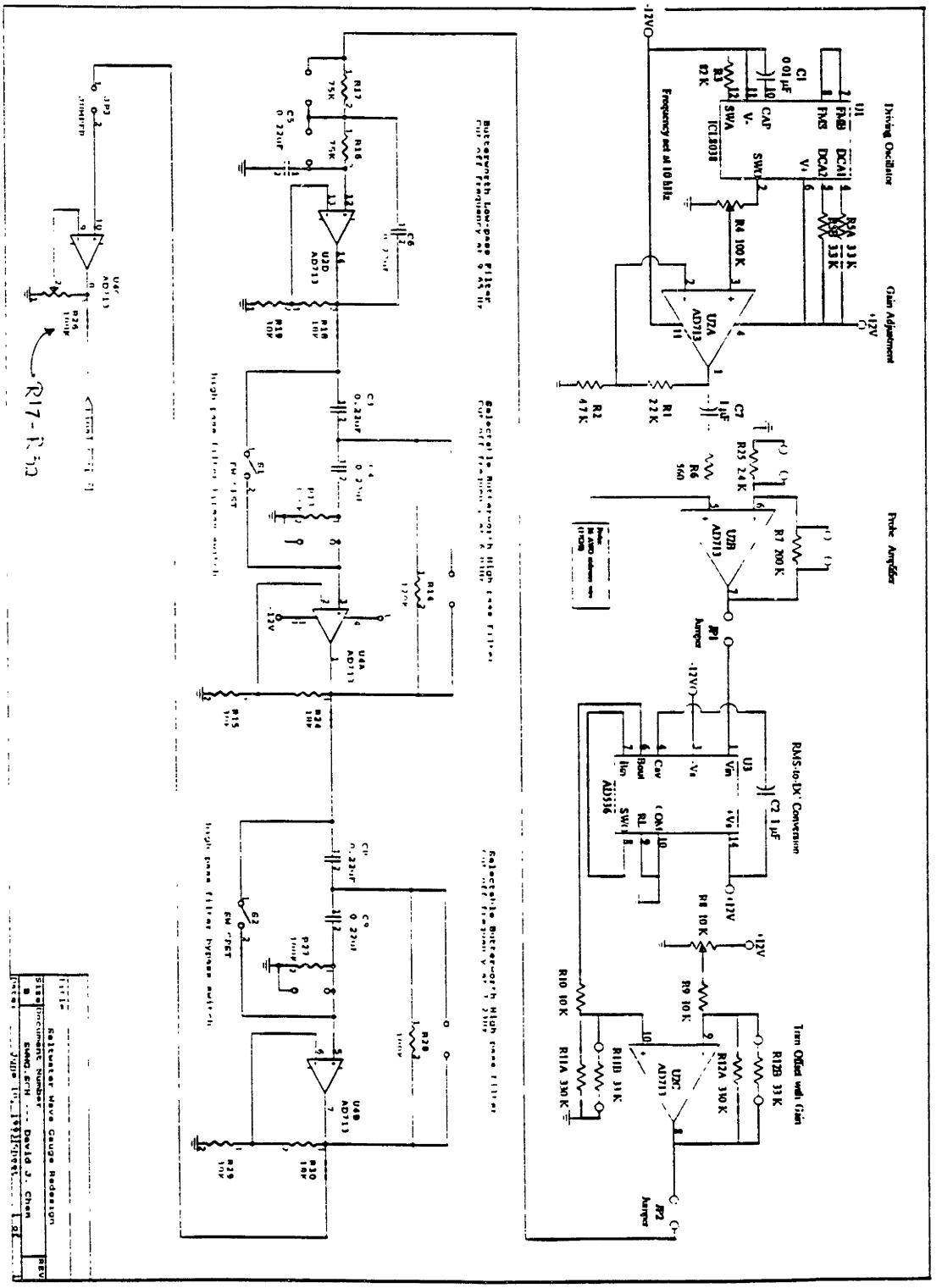

Saltwater Wave Gauge Schematic

Appendix C: Bucket Test Data

Appendix C1: Calibration Curves

DC Calibration Curves for 13 Operating Channels on Saltwater Board #1

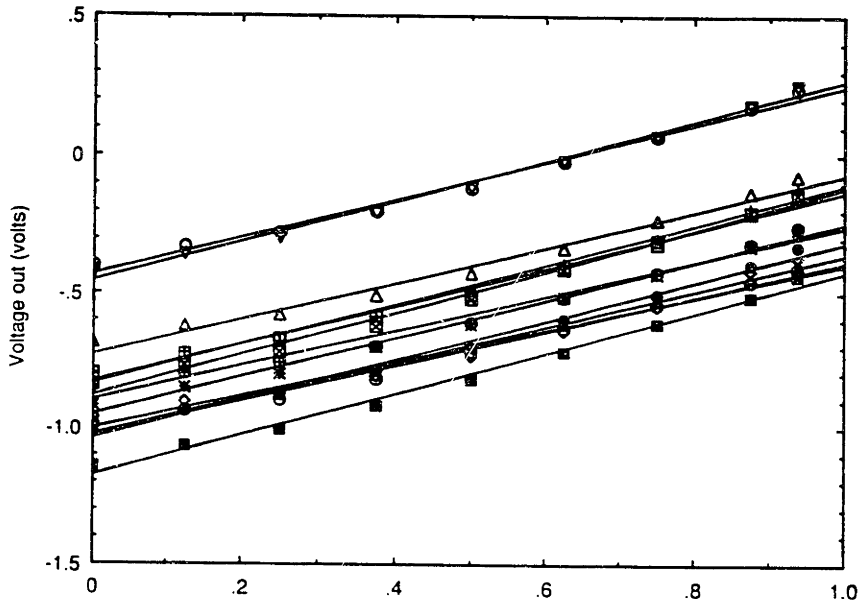

DC Calibration Curves for 14 Operating Channels on Saltwater Board #2

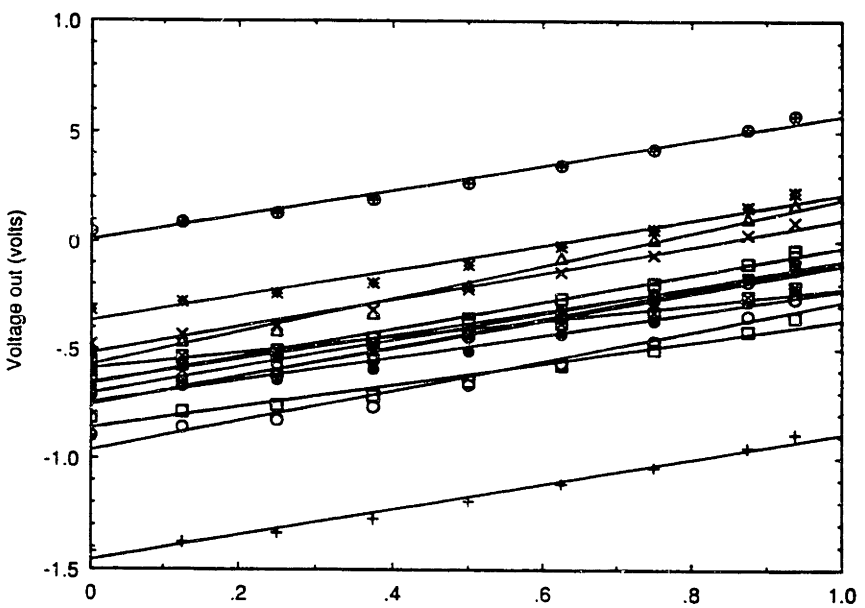

DC Calibration Curves for 13 Operating Channels on Saltwater Board #3

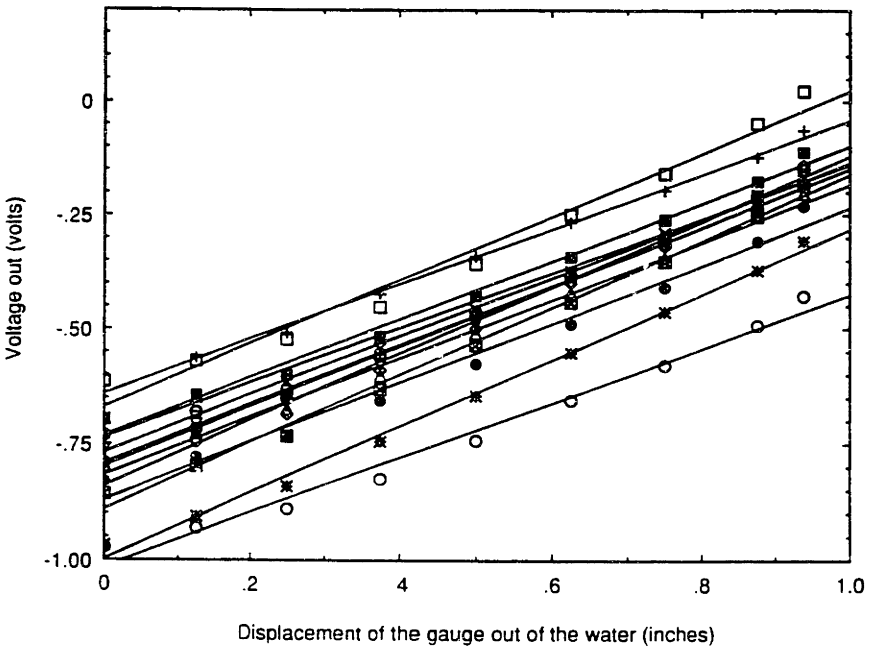

DC Calibration Curves for 14 Operating Channels on Saltwater Board #4

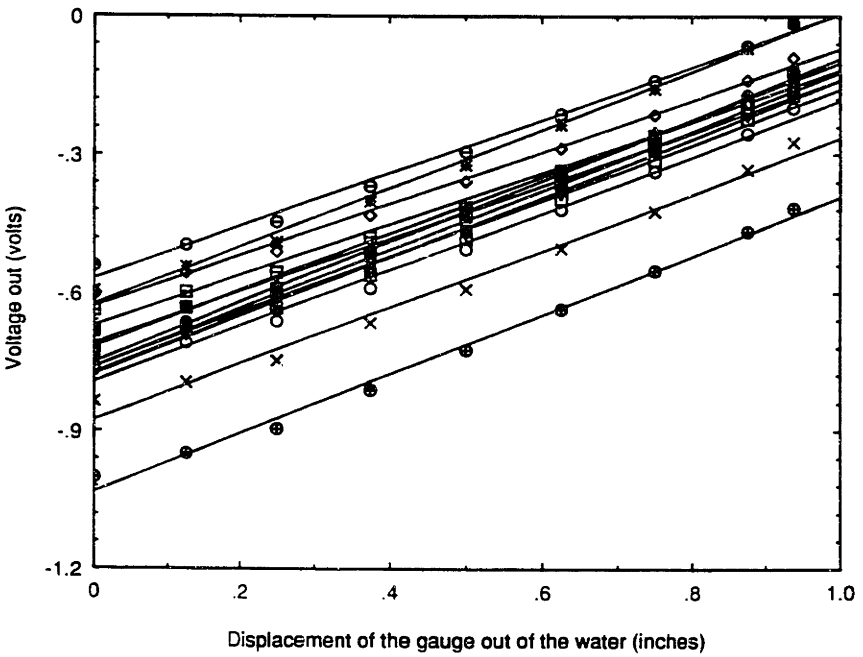

Appendix C2: Processed Frequency Data

	Amp, freq_max, qmax, left, right :				
1	.44365410	1.09375000	.44031470	.02976056	.02368283
2	.44363200	1.09375000	.44036380	.02876252	.02413895
3	.45888580	1.09375000	.45518530	.03278182	.02581656
4	.46093510	1.09375000	.45715020	.03133673	.02722306
5	.44332280	1.09375000	.44002500	.02998208	.02415333
6	.44431770	1.09375000	.44051840	.03106387	.02530610
7	.45883690	1.09375000	.45520340	.03141352	.02443600
8	.44388530	1.09375000	.44036870	.03109007	.02729693
9	.44280920	1.09375000	.43907690	.03195433	.02487874
10	.44447320	1.09375000	.44088270	.03103083	.02565517
11	.42738580	1.09375000	.42407820	.02930116	.02386985
12	.44062070	1.09375000	.43709740	.03151136	.02484875
13	.44098890	1.09375000	.43729170	.03089627	.02574371
14	.45372320	1.09375000	.45003320	.03083076	.02513785
15	.45716320	1.09375000	.45343250	.03247704	.02561749
16	.45966710	1.09375000	.45592330	.03162738	.02522792
17	.45519380	1.09375000	.45157520	.03143650	.02482662
18	.44763240	1.09375000	.44397840	.03168365	.02380927
19	.46406570	1.09375000	.46031750	.03144988	.02618142
20	.46954690	1.09375000	.46576670	.03378594	.02495246
21	.46254980	1.09375000	.45879250	.03080731	.02613977
22	.47695540	1.09375000	.47314380	.03449133	.02504577
23	.43668110	1.09375000	.43323380	.02931513	.02415024
24	.46089210	1.09375000	.45713530	.03150592	.02553155
25	.44714920	1.09375000	.44361990	.02932882	.02495879
26	.47050380	1.09375000	.46672470	.03193033	.02682378
27	.48128660	1.09375000	.47736740	.03420134	.02633543
28	.48997040	1.09375000	.48608580	.03308605	.02799647
29	.46418850	1.09375000	.46035640	.03224120	.02628627
30	.48810750	1.09375000	.48423590	.03373145	.02761918
31	.48402150	1.09375000	.48015640	.03391235	.02666775
32	.47661270	1.09375000	.47292860	.03216050	.02663476
33	.48275350	1.09375000	.47880910	.03331585	.02686286
34	.48851750	1.09375000	.48466180	.03340167	.02784433
35	.47922820	1.09375000	.47534430	.03283524	.02604767
36	.47004280	1.09375000	.46631730	.03198523	.02583987
37	.45915940	1.09375000	.45541920	.03277949	.02541778
38	.47014750	1.09375000	.46638520	.03206971	.02582786
39	.46852630	1.09375000	.46481640	.03332139	.02551258
40	.46444550	1.09375000	.46067510	.03160119	.02637951
41	.46057120	1.09375000	.45692780	.03211297	.02579579
42	.46768060	1.09375000	.46391230	.03203220	.02560206
43	.46052270	1.09375000	.45689800	.03179114	.02544636
44	.47086050	1.09375000	.46714890	.03342815	.02525711
45	.45705140	1.09375000	.45336040	.03008703	.02669841
46	.47368590	1.09375000	.46993800	.03438529	.02593464
47	.45231070	1.09375000	.44872390	.03028975	.02558187
48	.45672420	1.09375000	.45300050	.03214253	.02604456
49	.46232900	1.09375000	.45864270	.03242052	.02625471
50	.46092510	1.09375000	.45718200	.03104730	.02567024
51	.46953140	1.09375000	.46583860	.03303656	.02564685
52	.46493790	1.09375000	.46121620	.03145183	.02627472
53	.46227950	1.09375000	.45844170	.03363072	.02618969
54	.45701940	1.09375000	.45338920	.03166215	.02554527

Frequency of oscillation = 1.1 Hz

	Amp, freq_max, qmax, left, right :				
1	.39239730	2.30468800	.30951600	.18177050	.10428110
2	.38931910	2.30468800	.30681240	.18143610	.10545610
3	.40540420	2.30468800	.31972250	.18792100	.10887330
4	.41098850	2.30468800	.32570380	.18926080	.10799600
5	.39374130	2.30468800	.31146980	.18278180	.10317620
6	.40185440	2.30468800	.31796590	.18583080	.10552140
7	.41696810	2.30468800	.32775870	.19520360	.11183240
8	.40652980	2.30468800	.32055800	.18749320	.10930270
9	.40709600	2.30468800	.32256640	.18851470	.10890810
10	.40776970	2.30468800	.32227150	.18711170	.11054790
11	.39629570	2.30468800	.31374430	.18155010	.10601090
12	.40763180	2.30468800	.32051910	.18920160	.11052790
13	.41107760	2.30468800	.32437870	.19081330	.10937410
14	.43416970	2.30468800	.34223160	.20140280	.11698410
15	.42958760	2.30468800	.33870600	.19923630	.11543270
16	.43197010	2.30468800	.34085540	.20051920	.11546970
17	.43000820	2.30468800	.33906080	.19988190	.11467000
18	.42063580	2.30468800	.33182220	.19488870	.11231470
19	.42756190	2.30468800	.33690070	.19857010	.11494960
20	.43473360	2.30468800	.34275950	.20163180	.11581690
21	.42895210	2.30468800	.33855390	.19874270	.11515120
22	.43954870	2.30468800	.34638350	.20407460	.11705100
23	.43018310	2.30468800	.33940180	.19986340	.11414390
24	.42289430	2.30468800	.33269210	.19657350	.11399350
25	.41603420	2.30468800	.32822220	.19374910	.11000760
26	.42886200	2.30468800	.33827640	.19892820	.11459460
27	.43615530	2.30468800	.34319760	.20334100	.11612110
28	.43743390	2.30468800	.34525550	.20224100	.11672340
9	.43158530	2.30468800	.33994260	.20062140	.11556370
0	.45055600	2.30468800	.35553790	.20811790	.12190140
31	.44532530	2.30468800	.35101350	.20715770	.11902250
32	.44397650	2.30468800	.34995510	.20588550	.11926520
33	.44348720	2.30468800	.34958960	.20529760	.11957830
34	.44773480	2.30468800	.35317060	.20775050	.11988690
35	.43782490	2.30468800	.34542540	.20220620	.11864250
36	.42745720	2.30468800	.33689290	.19874080	.11428370
37	.41615210	2.30468800	.32810350	.19297420	.11148450
38	.42221050	2.30468800	.33256700	.19617420	.11365310
39	.42218670	2.30468800	.33318840	.19533430	.11291420
40	.41965180	2.30468800	.33013730	.19504080	.11436560
41	.40866310	2.30468800	.32208410	.18972800	.10969210
42	.41528790	2.30468800	.32692020	.19311580	.11284000
43	.41016370	2.30468800	.32308840	.19047690	.11040700
44	.41125480	2.30468800	.32360570	.19107510	.11156750
45	.39589300	2.30468800	.31164190	.18381740	.10781160
46	.41326090	2.30468800	.32479040	.19303450	.11246060
47	.39781870	2.30468800	.31352990	.18473840	.10767570
48	.39916960	2.30468800	.31438060	.18469050	.10893930
49	.40467480	2.30468800	.31862310	.18813280	.10920340
50	.40008420	2.30468800	.31505710	.18567190	.10918960
51	.41103960	2.30468800	.32354440	.19174220	.10957480
52	.40425320	2.30468800	.31847940	.18776010	.10935990
53	.40238610	2.30468800	.31715590	.18758810	.10696030
54	.39737910	2.30468800	.31294480	.18530330	.10611370

Frequency of oscillation = 2.2 Hz

	Amp, freq_max, qmax, left, right :				
1	.45606790	3.82812500	.27575830	.13998250	.24820200
2	.44331450	3.82812500	.27053670	.13550440	.23923900
3	.45369100	3.82812500	.27734400	.13465890	.24670120
4	.45904190	3.82812500	.28070970	.13587400	.24897370
5	.43848870	3.82812500	.26896100	.13377130	.23737220
6	.44624730	3.82812500	.27318960	.13725440	.24258400
7	.43812550	3.82812500	.27245670	.12781360	.24121450
8	.42669650	3.82812500	.26843000	.12370670	.23440730
9	.42342040	3.82812500	.26782680	.12103530	.23248290
10	.42461480	3.82812500	.26703180	.12132370	.23003210
11	.44703240	3.82812500	.28001620	.12457720	.24378160
12	.42709620	3.82812500	.26630640	.12374540	.22929440
13	.43507130	3.82812500	.26937500	.12225590	.23615900
14	.49141410	3.82812500	.30449870	.13315530	.27001620
15	.49628120	3.82812500	.30816630	.13366730	.27009570
16	.48648810	3.82812500	.29913630	.13514660	.26705380
17	.49717010	3.82812500	.30446490	.14141270	.27039320
18	.49464130	3.82812500	.30464880	.13996560	.26792930
19	.47331690	3.82812500	.29175490	.13188590	.25813810
20	.50467660	3.82812500	.31539580	.14075570	.27084670
21	.49708350	3.82812500	.31006150	.13929450	.26761340
22	.54087580	3.82812500	.34580170	.14609300	.28220140
23	.50404260	3.82812500	.32214220	.13040930	.26818050
24	.47816420	3.82812500	.30721890	.12156310	.25570120
25	.48297040	3.82812500	.30973460	.12391730	.26076080
26	.50038090	3.82812500	.31869690	.13078720	.27458920
27	.49631690	3.82812500	.31105770	.13918090	.27439320
28	.49848870	3.82812500	.30814550	.14315160	.27569130
29	.49779290	3.82812500	.30512290	.14021430	.27531300
30	.50029860	3.82812500	.30767500	.14663150	.27498980
31	.48934590	3.82812500	.30418110	.14072380	.26633640
32	.48643330	3.82812500	.30220820	.13772570	.26563540
33	.47921230	3.82812500	.29906370	.13496380	.26117210
34	.47301640	3.82812500	.29639120	.13160500	.25922910
35	.46524700	3.82812500	.29244600	.13045470	.25341110
36	.46414210	3.82812500	.29297560	.13168680	.25011580
37	.44823250	3.82812500	.28233610	.12831990	.23985840
38	.45690610	3.82812500	.28895070	.13064390	.24421370
39	.46450720	3.82812500	.29266860	.13239200	.24968240
40	.46125100	3.82812500	.29185980	.13116680	.24860780
41	.45438790	3.82812500	.28724490	.12950600	.24554310
42	.45231140	3.82812500	.28550060	.13105870	.24378340
43	.44818930	3.82812500	.28300070	.12806440	.24117060
44	.43987230	3.82812500	.27689650	.12492830	.23827970
45	.43374480	3.82812500	.27287010	.12393390	.23368280
46	.43862810	3.82812500	.27599700	.12427810	.23734730
47	.43009560	3.82812500	.27100240	.12114640	.23254840
48	.43213820	3.82812500	.27192570	.12122550	.23282390
49	.42883180	3.82812500	.26850040	.12259700	.23432630
50	.43305640	3.82812500	.26957490	.12411200	.23734710
51	.44561790	3.82812500	.27591210	.12791150	.24358450
52	.42778030	3.82812500	.26356150	.12300100	.23516120
53	.43844290	3.82812500	.26939230	.12826660	.23950140
54	.43640540	3.82812500	.26750450	.13058400	.23894650

Frequency of oscillation = 3.8 Hz

Appendix D: Wave Tank Test Data

Calibration Curves for Wave Tank Test #1:

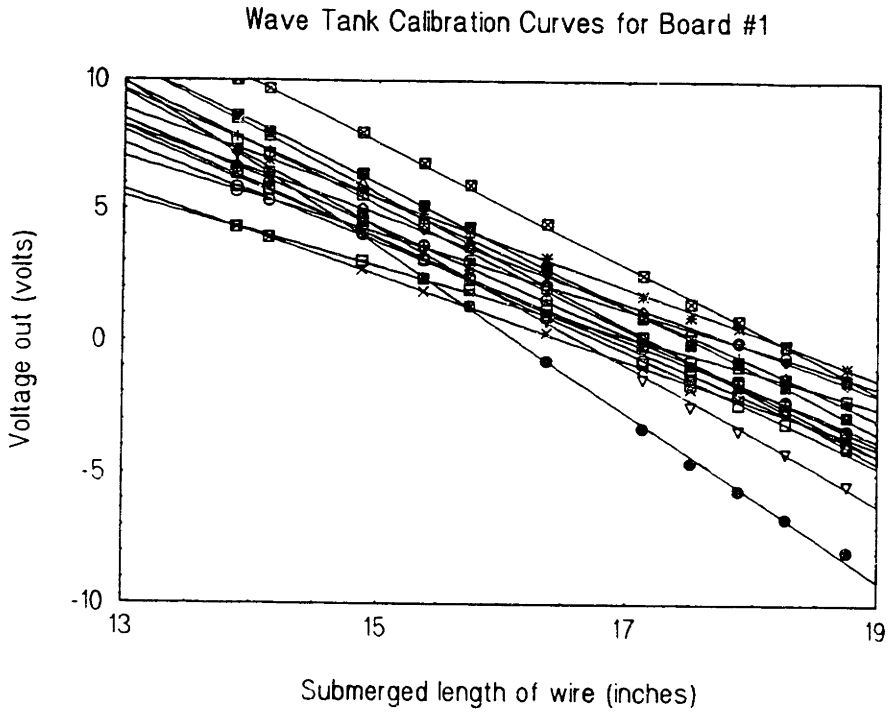

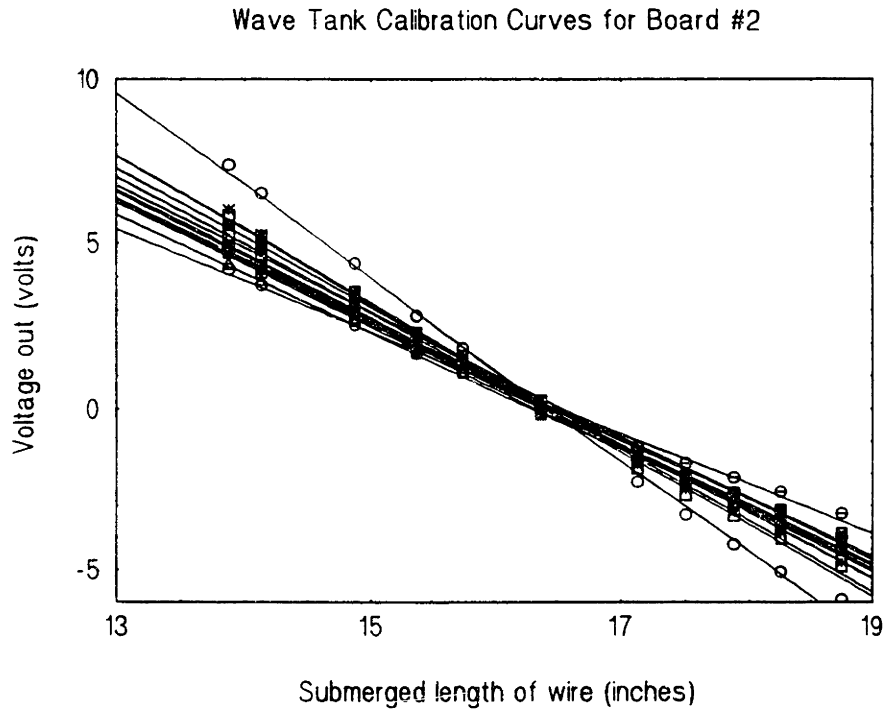

Wave Tank Calibration Curves for Board #3

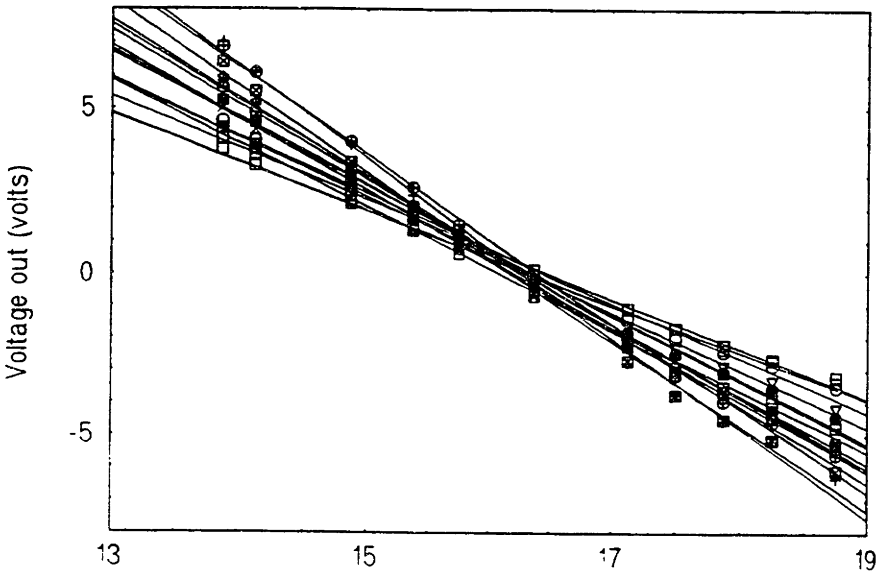

Wave Tank Calibration Curves for Board #4

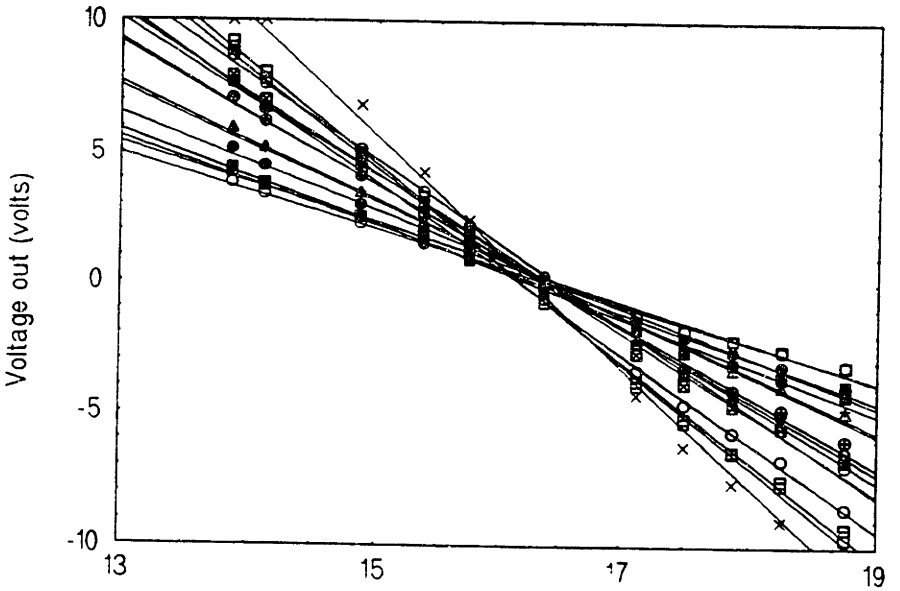

Calibration Curves for Wave Tank Test #2:

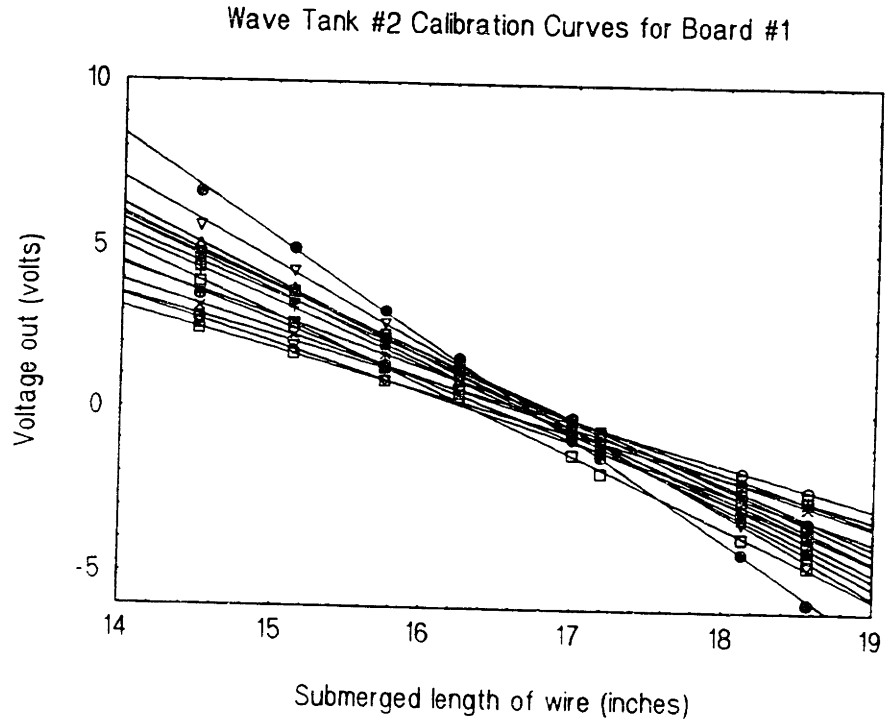

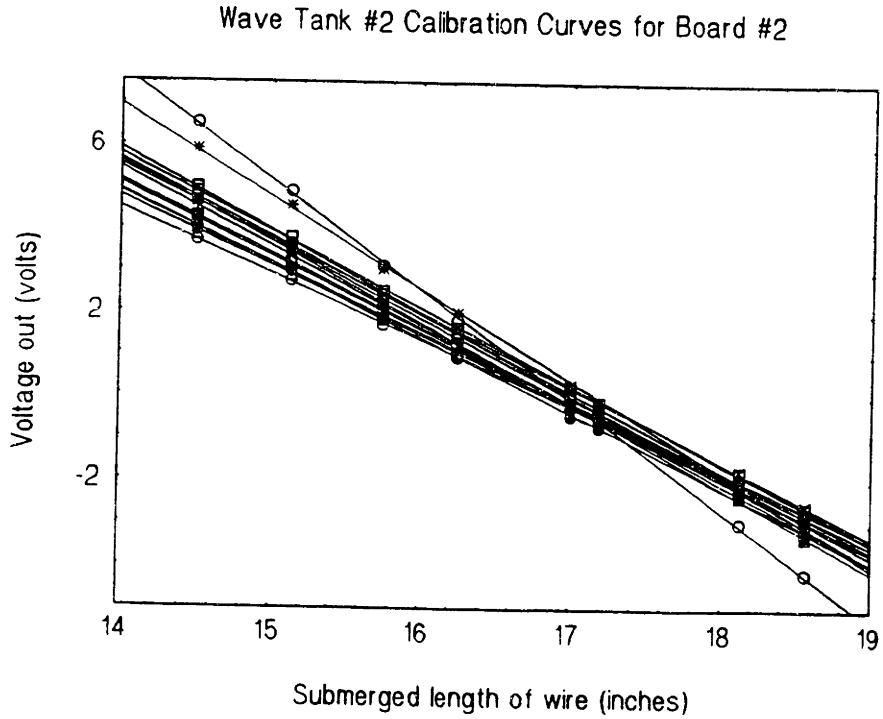

Wave Tank #2 Calibration Curves for Board #3

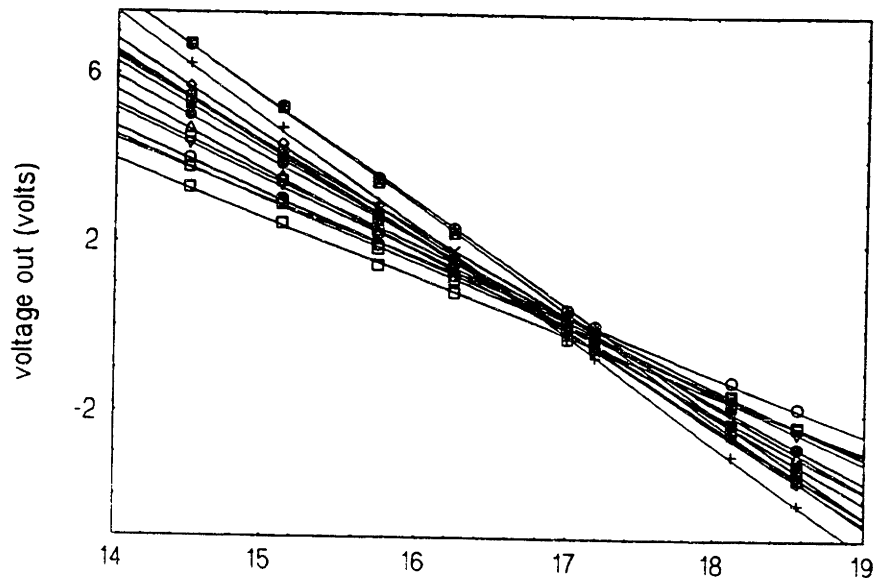

Wave Tank #2 Calibration Curves for Board #4

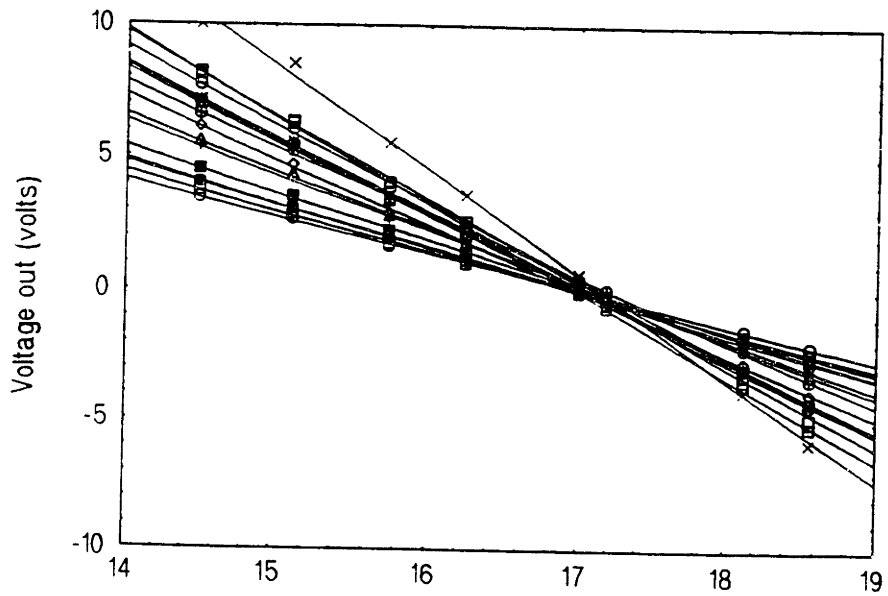

Data Files for the Cited Wave Tank Examples:

Note: The values tabulated in these charts are twice as large in value than those drawn in the contour plots. The values listed here are the correct ones; those in the plots are for qualitative purposes only.

FC4Z.TAB

Ky \ Kx	0.1571	0.314	0.471	0.628	0.785	0.943	1.100	1.257	1.414	1.571	1.728
-1.257	2.973E-04	2.956E-03	5.347E-03	6.227E-03	5.788E-03	3.570E-03	1.066E-03	-8.774E-04	-1.428E-03	-1.056E-03	-3.367E-05
-1.100	-1.392E-04	3.507E-03	6.193E-03	6.075E-03	5.226E-03	2.545E-03	-1.038E-04	-1.490E-03	-1.182E-03	-4.062E-04	3.742E-04
-0.943	6.002E-04	4.375E-03	6.844E-03	5.759E-03	3.802E-03	9.003E-04	-1.005E-03	-1.222E-03	-3.500E-04	-2.718E-05	6.970E-06
-0.785	2.027E-03	7.050E-03	9.186E-03	7.522E-03	4.307E-03	6.054E-04	-1.275E-03	-1.309E-03	-2.899E-04	-3.429E-04	-4.880E-04
-0.628	4.189E-03	1.005E-02	1.080E-02	6.859E-03	2.082E-03	-1.418E-03	-1.742E-03	-1.011E-03	-4.142E-04	-8.016E-04	-1.046E-03
-0.471	5.835E-03	1.283E-02	1.438E-02	8.326E-03	1.527E-03	-2.135E-03	-2.464E-03	-1.609E-03	-1.370E-03	-1.659E-03	-1.652E-03
-0.314	9.177E-03	1.417E-02	1.229E-02	5.534E-03	-2.768E-03	-4.215E-03	-2.642E-03	-2.384E-03	-2.099E-03	-1.771E-03	-1.498E-03
-0.157	1.064E-02	8.861E-03	1.487E-02	2.734E-02	1.011E-02	-5.345E-03	-3.418E-03	-2.257E-03	-2.187E-03	-1.612E-03	-1.318E-03
0.000	5.548E-03	-7.054E-04	2.588E-02	6.604E-02	3.825E-02	3.447E-04	-2.931E-03	-1.308E-03	-1.276E-03	-9.078E-04	-1.108E-03
0.157	3.769E-04	-6.314E-03	1.484E-02	4.531E-02	2.537E-02	1.077E-03	-5.034E-04	-8.975E-04	-8.842E-04	-5.787E-04	-9.894E-04
0.314	-1.450E-03	-2.913E-03	3.024E-03	7.406E-03	6.221E-04	-8.717E-04	-1.849E-04	-1.713E-03	-1.158E-03	-9.117E-04	-9.812E-04
0.471	-1.698E-03	7.132E-04	4.134E-03	2.926E-03	6.396E-04	5.769E-06	-1.644E-03	-2.250E-03	-1.765E-03	-1.835E-03	-1.342E-03
0.628	-9.426E-04	-7.433E-04	-8.609E-04	4.290E-04	1.808E-03	6.527E-04	-8.557E-04	-1.557E-03	-1.817E-03	-1.988E-03	-1.384E-03
0.785	-1.098E-03	-7.186E-04	-1.321E-03	-4.165E-04	1.577E-03	1.456E-03	4.068E-04	-8.271E-04	-1.224E-03	-1.716E-03	-1.493E-03
0.943	-1.456E-03	-1.207E-04	2.699E-04	-7.133E-04	-1.515E-04	4.795E-04	7.029E-04	9.327E-05	-3.694E-04	-1.104E-03	-1.157E-03
1.100	-4.488E-04	6.550E-04	7.244E-04	-3.693E-04	-3.049E-04	-1.045E-04	1.094E-04	-1.564E-04	-1.843E-04	-5.556E-04	-8.060E-04
1.257	-3.052E-04	7.539E-05	3.819E-04	2.958E-04	-5.044E-05	-8.265E-04	-1.102E-03	-9.570E-04	-4.844E-04	-5.188E-04	-6.118E-04

	1.885	2.042	2.199	2.356	2.513	2.670
	-2.619E-05	-7.719E-04	-8.500E-04	5.111E-05	-2.703E-04	-9.800E-04
	-2.287E-04	-1.135E-03	-9.661E-04	5.086E-04	4.044E-05	-1.156E-03
	-1.034E-03	-1.333E-03	-8.119E-04	2.883E-04	8.087E-05	-7.695E-04
	-1.294E-03	-1.292E-03	-8.383E-04	-4.302E-04	-4.459E-04	-6.633E-04
	-1.223E-03	-8.471E-04	-6.108E-04	-5.974E-04	-3.115E-04	-3.389E-04
	-1.482E-03	-1.051E-03	-9.725E-04	-7.692E-04	1.407E-04	4.244E-05
	-1.316E-03	-1.340E-03	-1.359E-03	-9.238E-04	9.028E-05	-1.023E-04
	-9.078E-04	-1.114E-03	-1.136E-03	-8.718E-04	-4.747E-04	-7.905E-04
	-8.046E-04	-8.774E-04	-6.680E-04	-5.285E-04	-5.485E-04	-1.028E-03
	-1.021E-03	-1.097E-03	-7.835E-04	-5.456E-04	-3.320E-04	-8.159E-04
	-1.162E-03	-1.284E-03	-1.079E-03	-7.193E-04	-1.907E-04	-5.559E-04
	-1.251E-03	-1.209E-03	-1.240E-03	-8.759E-04	-3.625E-04	-6.658E-04
	-1.192E-03	-1.008E-03	-1.118E-03	-6.815E-04	-4.392E-04	-8.629E-04
	-1.378E-03	-9.950E-04	-1.061E-03	-6.164E-04	-7.484E-04	-1.360E-03
	-1.324E-03	-1.042E-03	-1.138E-03	-5.235E-04	-8.192E-04	-1.642E-03
	-1.222E-03	-9.034E-04	-7.477E-04	-2.454E-04	-1.134E-03	-2.033E-03
	-7.944E-04	-4.320E-04	-2.612E-04	-2.648E-04	-1.181E-03	-1.696E-03

Contour Plot Data for the Case of an X-directed Four-Hertz Wave

B452FIN.TAB

Ky \ Kx	0.157	0.314	0.471	0.628	0.785	0.943	1.100	1.257	1.414	1.571	1.728
-1.257	3.316E-05	8.447E-04	1.684E-03	2.124E-03	1.658E-03	9.406E-04	5.898E-04	3.610E-04	1.902E-04	2.842E-04	4.911E-04
-1.100	1.679E-04	1.016E-03	1.747E-03	1.815E-03	1.101E-03	2.727E-04	1.378E-05	2.300E-05	-3.622E-05	8.252E-05	2.851E-04
-0.943	5.828E-04	1.135E-03	1.345E-03	9.938E-04	6.013E-04	1.310E-04	-3.023E-04	-2.024E-04	1.076E-04	1.578E-04	1.426E-04
-0.785	8.412E-04	1.101E-03	1.123E-03	7.918E-04	5.607E-04	2.380E-04	-1.594E-04	-1.350E-04	2.564E-04	1.252E-04	1.843E-05
-0.628	7.795E-04	9.038E-04	1.055E-03	6.417E-04	6.034E-05	-3.413E-04	-1.440E-05	2.390E-04	3.173E-04	-9.501E-05	-2.586E-04
-0.471	9.739E-04	1.451E-03	1.415E-03	5.173E-04	-1.274E-04	-2.904E-04	2.239E-04	3.749E-04	1.667E-05	-2.520E-04	-3.144E-04
-0.314	2.592E-03	2.335E-03	6.746E-04	-3.481E-04	-5.169E-04	1.533E-04	2.698E-04	1.545E-04	-4.574E-04	-4.053E-04	-3.460E-04
-0.157	4.724E-03	2.311E-03	-7.974E-04	-3.689E-04	-4.970E-04	3.196E-04	-1.548E-04	-2.720E-04	-7.211E-04	-3.864E-04	-3.317E-04
0.000	5.639E-03	1.765E-03	-1.804E-03	-3.514E-04	-8.054E-04	-1.621E-04	-4.317E-04	-5.764E-05	-4.462E-04	-1.156E-04	-2.181E-04
0.157	4.931E-03	2.353E-03	-4.522E-04	2.434E-04	8.372E-06	4.768E-04	2.332E-05	4.127E-04	-5.291E-05	3.731E-05	-1.638E-04
0.314	2.612E-03	1.775E-03	7.225E-04	1.204E-03	1.242E-03	1.562E-03	1.083E-03	6.358E-04	2.232E-04	1.994E-04	1.208E-05
0.471	-3.003E-04	-7.206E-04	3.185E-03	8.676E-03	6.074E-03	1.635E-03	1.173E-03	5.212E-04	2.102E-04	2.367E-04	1.482E-04
0.628	-1.425E-03	-9.014E-04	7.413E-03	**1.802E-02**	1.259E-02	2.316E-03	9.520E-04	6.946E-04	4.190E-04	2.911E-04	1.861E-04
0.785	3.655E-05	1.967E-03	6.192E-03	1.138E-02	7.397E-03	1.194E-03	7.879E-04	7.011E-04	5.640E-04	3.032E-04	1.885E-04
0.943	7.266E-04	2.953E-03	2.214E-03	1.747E-04	-9.929E-04	-4.644E-04	4.280E-04	5.567E-04	7.471E-04	5.835E-04	4.991E-04
1.100	8.514E-04	2.005E-03	8.241E-04	-1.547E-03	-2.054E-03	-1.285E-03	-8.790E-04	-3.388E-04	1.028E-04	2.463E-04	2.943E-04
1.257	8.587E-04	9.875E-04	1.874E-04	-6.651E-04	-1.203E-03	-1.601E-03	-1.656E-03	-1.243E-03	-9.273E-04	-5.936E-04	-4.065E-04

	1.885	2.042	2.199	2.356	2.513	2.670
	5.393E-04	2.560E-04	-7.415E-05	-1.614E-04	-9.163E-05	-5.395E-05
	2.789E-04	1.331E-05	-1.931E-04	-1.452E-04	-1.364E-04	-1.081E-04
	2.698E-05	-6.683E-05	-1.025E-04	-4.630E-05	-1.569E-04	-1.391E-04
	-6.021E-05	-1.197E-04	-1.842E-04	-1.764E-04	-1.888E-04	-1.548E-04
	-1.828E-04	-2.916E-04	-3.704E-04	-2.640E-04	-1.054E-04	-1.685E-04
	-1.243E-04	-2.695E-04	-2.910E-04	-1.675E-04	-5.910E-05	-2.658E-04
	-1.981E-04	-3.764E-04	-1.570E-04	-3.661E-05	-1.071E-04	-3.996E-04
	-2.106E-04	-4.435E-04	-1.496E-04	-1.353E-04	-2.408E-04	-4.297E-04
	-1.284E-04	-2.142E-04	7.793E-05	-1.088E-04	-1.984E-04	-2.935E-04
	-8.593E-05	-8.097E-06	2.396E-04	-5.980E-06	3.683E-05	-7.287E-05
	1.238E-04	7.665E-05	2.761E-05	-1.343E-04	1.785E-04	8.000E-05
	1.979E-04	1.812E-05	-1.130E-04	-1.757E-04	7.952E-05	1.325E-06
	9.275E-05	2.325E-06	1.098E-04	1.048E-04	-3.235E-05	-1.243E-04
	1.775E-04	2.026E-04	2.814E-04	2.757E-04	6.504E-05	1.757E-05
	4.936E-04	4.343E-04	2.821E-04	2.383E-04	3.178E-04	3.675E-04
	2.372E-04	2.668E-04	2.871E-04	2.439E-04	4.002E-04	4.723E-04
	-3.393E-04	-1.490E-04	7.077E-05	8.091E-05	1.301E-04	2.029E-04

Contour Plot Data for the Case of a 45°-directed Five-Hertz Wave

X1FIN.TAB

Ky \Kx	0.157	0.314	0.471	0.628	0.785	0.943	1.100	1.257	1.414	1.571	1.728
-1.257	2.755E-02	2.815E-02	1.302E-02	7.653E-03	3.088E-03	1.106E-03	-2.149E-03	-4.515E-03	-4.988E-03	-5.796E-03	-8.189E-03
-1.100	2.784E-02	2.569E-02	9.532E-03	6.577E-03	3.796E-04	-2.511E-03	-4.568E-03	-3.694E-03	-5.975E-03	-2.857E-03	-5.005E-03
-0.943	2.110E-02	1.713E-02	9.818E-03	4.612E-03	-3.231E-03	-7.962E-04	-4.849E-03	1.036E-03	-1.202E-03	1.085E-03	1.515E-03
-0.785	4.711E-02	3.257E-02	1.342E-02	7.664E-03	-4.402E-03	2.911E-03	1.358E-03	3.426E-03	4.056E-03	2.905E-03	2.990E-03
-0.628	7.019E-02	4.651E-02	3.520E-03	5.113E-03	3.527E-03	3.639E-03	5.846E-03	4.186E-03	3.597E-03	4.288E-03	2.316E-03
-0.471	8.376E-02	6.328E-02	2.288E-02	5.566E-03	4.184E-03	5.167E-03	-2.975E-04	2.660E-03	-3.339E-03	1.612E-03	-3.096E-03
-0.314	1.103E-01	5.044E-02	9.722E-03	9.783E-03	-9.951E-03	3.255E-03	-1.074E-02	8.644E-04	-8.547E-03	-3.098E-04	-7.743E-03
-0.157	2.825E-01	1.822E-01	-5.309E-03	8.024E-03	-2.428E-02	-4.819E-04	-1.707E-02	-7.500E-04	-1.163E-02	-8.050E-04	-1.023E-02
0.000	4.772E-01	3.844E-01	4.973E-02	2.639E-02	-2.124E-02	1.602E-03	-1.647E-02	3.134E-04	-1.206E-02	2.748E-04	-9.321E-03
0.157	3.464E-01	2.448E-01	2.657E-02	2.783E-02	-1.188E-02	4.820E-03	-1.361E-02	1.462E-03	-1.070E-02	1.380E-04	-8.392E-03
0.314	1.361E-01	4.732E-02	-1.321E-02	7.191E-04	-1.244E-02	1.566E-03	-1.130E-02	4.720E-04	-8.159E-03	4.167E-04	-7.001E-03
0.471	7.197E-02	3.452E-02	-1.953E-03	-1.019E-02	-1.090E-02	-6.434E-03	-9.440E-03	-3.680E-03	-6.936E-03	-1.661E-03	-6.278E-03
0.628	3.430E-02	2.113E-02	-1.975E-03	-3.730E-03	-9.808E-03	-9.331E-03	-7.799E-03	-7.868E-03	-6.356E-03	-4.167E-03	-4.623E-03
0.785	2.806E-02	1.834E-02	5.508E-03	2.403E-03	-6.503E-03	-2.501E-03	-8.084E-03	-8.252E-03	-7.361E-03	-6.863E-03	-5.677E-03
0.943	3.375E-02	1.724E-02	-2.590E-03	-4.947E-04	-8.655E-04	1.807E-03	-4.463E-03	-3.420E-03	-7.341E-03	-5.758E-03	-5.995E-03
1.100	2.952E-02	2.126E-02	4.113E-03	2.848E-03	-2.526E-03	5.070E-04	6.050E-04	-1.614E-03	-5.266E-03	-3.795E-03	-6.636E-03
1.257	1.641E-02	1.976E-02	1.140E-02	2.973E-03	-3.646E-03	-3.137E-04	-5.073E-04	-2.262E-03	-2.268E-03	-3.262E-03	-5.125E-03

	1.885	2.042	2.199	2.356	2.513	2.670
	-6.362E-03	-6.990E-03	-5.049E-03	-5.300E-03	-5.370E-03	-3.580E-03
	-2.140E-03	-1.814E-03	-5.053E-04	-1.886E-04	-1.440E-03	-4.762E-05
	2.714E-03	3.613E-03	2.731E-03	2.907E-03	2.721E-03	2.102E-03
	3.089E-03	2.684E-03	2.109E-03	3.912E-04	1.892E-03	-1.015E-03
	3.812E-03	1.352E-04	2.295E-03	-1.282E-03	1.449E-03	-4.272E-03
	1.486E-03	-4.779E-03	3.438E-04	-4.574E-03	-4.687E-04	-7.499E-03
	-5.482E-04	-6.603E-03	-7.413E-05	-6.148E-03	-1.002E-03	-8.271E-03
	-1.853E-03	-8.513E-03	-1.375E-03	-8.075E-03	-1.732E-03	-9.399E-03
	8.421E-05	-8.022E-03	-5.191E-04	-7.454E-03	-1.089E-03	-1.019E-02
	2.086E-04	-7.443E-03	-8.297E-04	-7.125E-03	-1.502E-03	-1.018E-02
	2.224E-04	-5.745E-03	5.875E-04	-5.760E-03	-7.958E-04	-8.732E-03
	-8.893E-04	-5.724E-03	-3.125E-04	-5.749E-03	-1.016E-03	-8.200E-03
	-2.148E-03	-4.552E-03	-1.249E-03	-3.976E-03	-1.398E-03	-7.792E-03
	-5.458E-03	-4.970E-03	-4.590E-03	-4.986E-03	-5.177E-03	-8.972E-03
	-5.846E-03	-4.880E-03	-6.162E-03	-4.206E-03	-5.911E-03	-7.760E-03
	-5.496E-03	-6.553E-03	-7.210E-03	-5.794E-03	-8.848E-03	-9.317E-03
	-4.275E-03	-6.237E-03	-6.513E-03	-7.460E-03	-9.462E-03	-9.235E-03

Contour Plot Data for the Case of a Random Set of X-directed Waves

Appendix E: "Wet" and "Dry" Calibration Curves for Short-wire Freshwater Gauges

Channels 2 through 4:

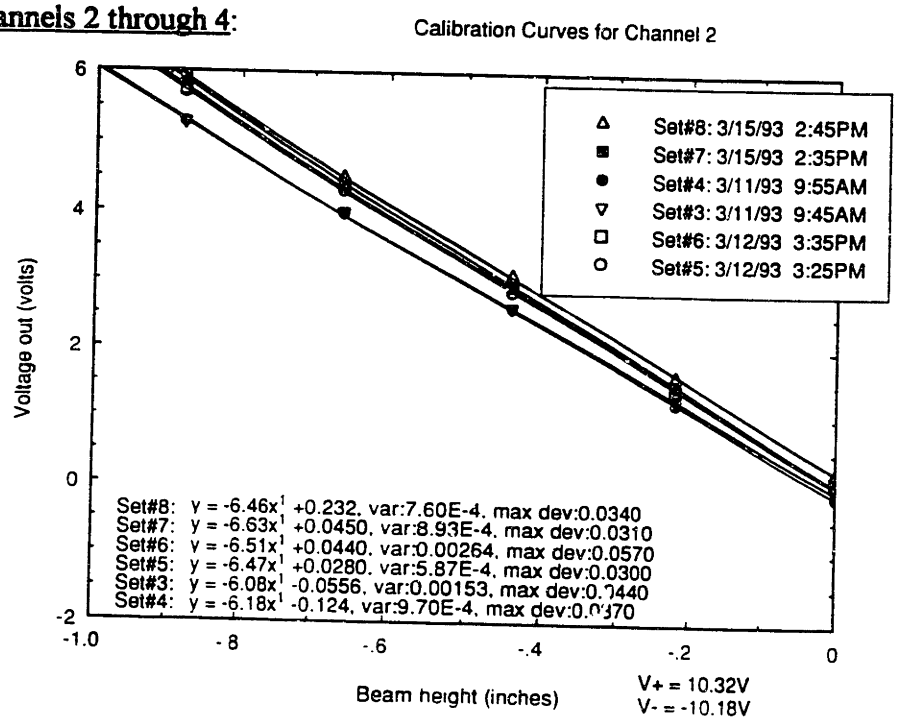

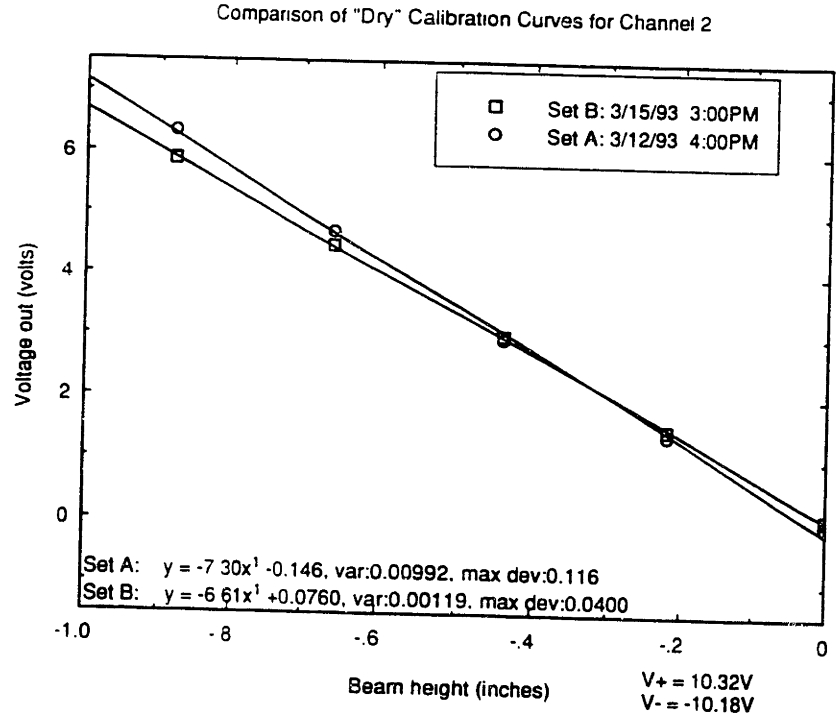

Channel 2 data

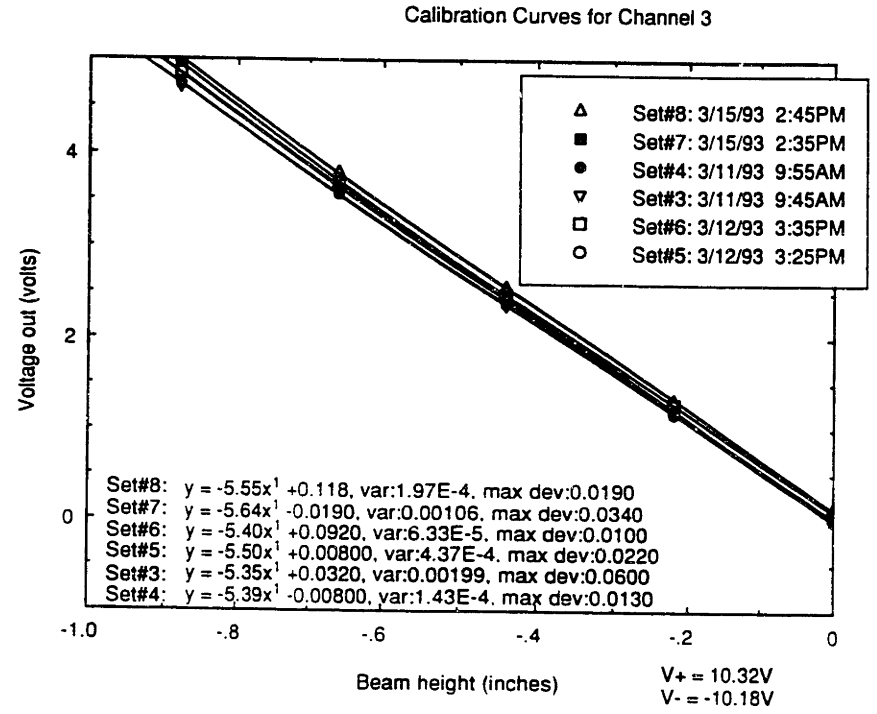

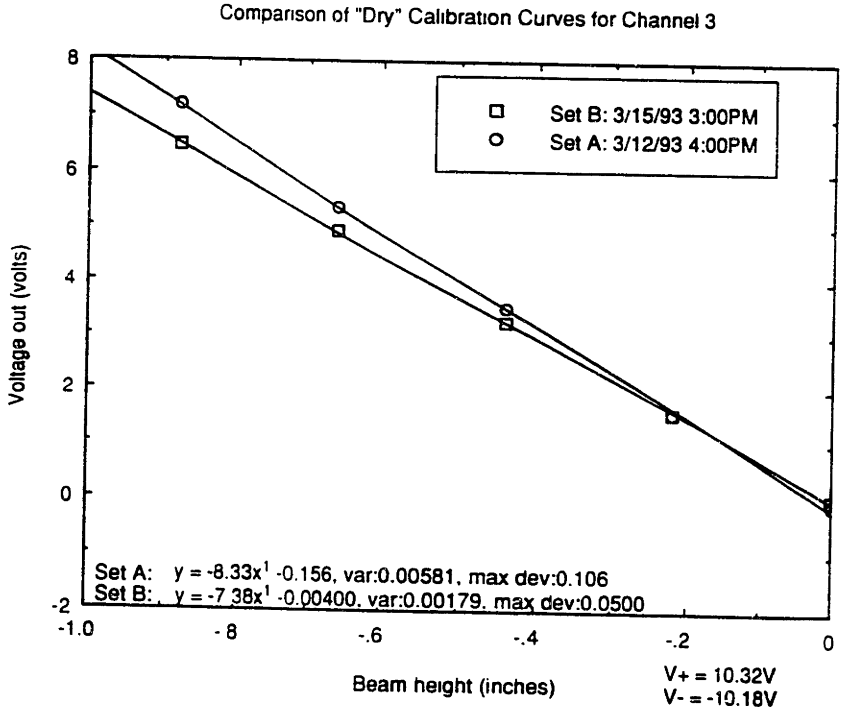

Channel 3 data

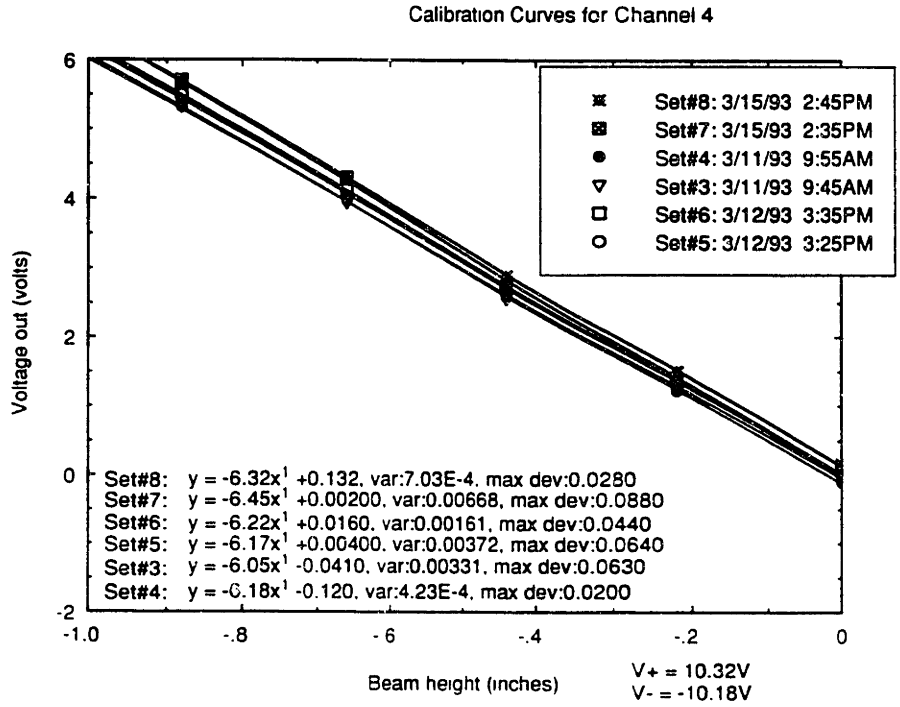

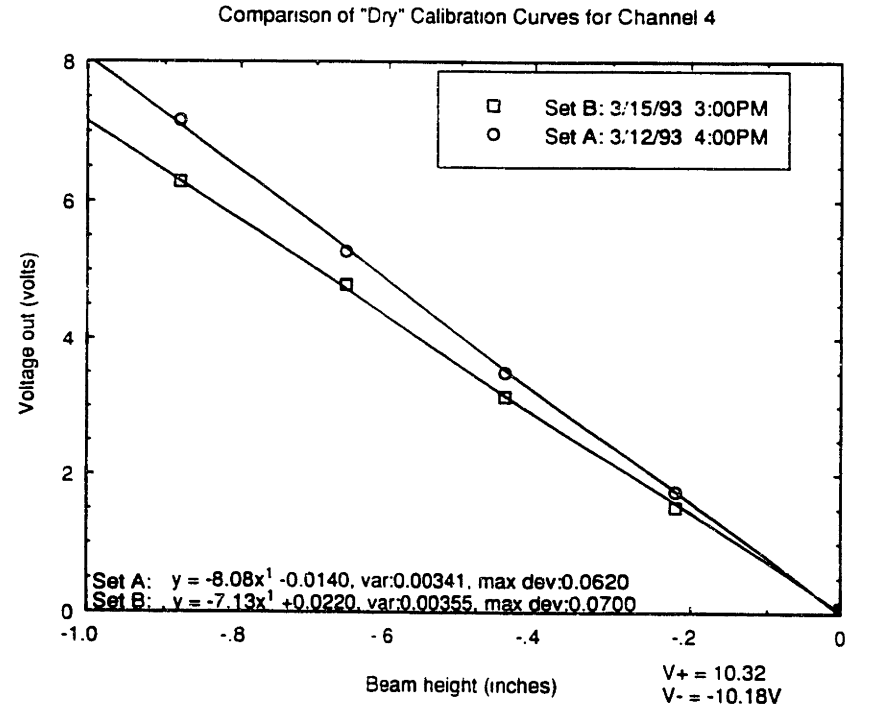

Channel 4 data

Appendix F: Deriving the Minimum Ground Wire Length Needed for Linear Saltwater Operation

Let L = total length of the probe wire (exposed and submerged sections)
h = submerged length of the probe wire
x = distance below the water's surface (along the wire)
c = conductance to the water per unit length of wire
r = resistance of the wire per unit length of wire

i(x) = current at x
v(x) = voltage at x

The electrical boundary conditions on the probe wire are the following:

Voltage at the top of the probe wire: v(x) at x = -(L-h) is V_0
Current in the exposed section of wire: I_0
Voltage at the bottom of the wire: v(h) = 0 (grounded)

So,

$$\frac{di(x)}{dx} = -cv(x) \qquad \frac{dv(x)}{dx} = -ri(x)$$

Combining these two equations, we get a differential equation for v(x):

$$\frac{d^2v(x)}{dx^2} = rc \bullet v(x)$$

One general solution for this differential equation is

$$v(x) = A \sinh\left(\sqrt{rc}\,(x+k)\right) \text{ where k = constant}$$

But, given the boundary condition that v(h) = 0, we know that k = -h, so that

$$v(x) = A \sinh\left(\sqrt{rc}\,(x-h)\right)$$

We also know that $v(0) = V_0 - I_0 (L-h)r$ so that

$$A = \frac{-V_0 + I_0(L-h)r}{\sinh\left(\sqrt{rc}\,h\right)}$$

Furthermore,

$$i(x) = -\frac{1}{r} \bullet \frac{dv}{dx} = -\frac{1}{r} \bullet A\sqrt{rc}\,\cosh\left(\sqrt{rc}\,(x-h)\right)$$

Finally, we can calculate the impedance at the water's surface as a function of h (the submerged length of probe wire).

$$z(0) = \frac{v(0)}{i(0)} = \frac{-A\sinh\left(\sqrt{rc}\,h\right)}{-\sqrt{\frac{c}{r}}\,A\cosh\left(\sqrt{rc}\,h\right)} = \sqrt{\frac{r}{c}}\,\tanh\left(\sqrt{rc}\,h\right)$$

For the resistance of the exposed section of wire to depend linearly on (-x), the hyperbolic tangent term should be close to one. We are seeking the smallest immersed depth h that will yield this result.

When the hyperbolic tangent term is close to one, there is very little change in the value of z(0) for changes in h; on the other hand, when its value is not near one (but still in the range of zero to one), z(0) varies significantly for changes in h. Ideally, we would like for the impedance at the water's surface to be constant for reasonably large changes in h.

So, if we restrict the value of the hyperbolic tangent to be as least 0.987, we have the constraint that

$$\sqrt{rc}\,h \geq 2.5 \qquad \text{or} \qquad h \geq \frac{2.5}{\sqrt{rc}}$$

In the particular case of our nichrome probe wires, we know that

$$r = \left(\frac{27\Omega}{ft}\right)\left(\frac{ft}{12in}\right) = 2.25\frac{\Omega}{in}$$

and from Eqn. 2.1, that

$$c = \frac{2\pi\sigma}{\ln\left(\frac{Rad}{rad}\right)} = \frac{2\pi\left(0.035\frac{mho}{cm}\right)}{\ln\left(\frac{20cm}{0.0056cm}\right)} \approx \left(0.027\frac{mho}{cm}\right)\left(2.54\frac{cm}{in}\right) \approx 0.07\frac{1}{\Omega \bullet in}$$

assuming that the water conductivity is 0.035 mhos/cm for T=20°C and S=25‰.

Finally, in the case of the nichrome wires,

$\sqrt{rc} \approx 0.4\frac{1}{in}$ so that we must have $h \geq 6in$ for linearity in the exposed portion.

```
/**                    SW_auto.C                                    **/
/** Written by John T. Mass                                         **/
/** Edited by David Chen                                            **/
/** Code to reconstruct the spectral energy of sea waves from       **/
/** wave height data points gathered on a circular harp             **/
/** Revision has check of autocorrelation                           **/
/** Average of autocorrelation is calculated beforehand             **/

#include <stdio.h>
#include <math.h>
#include <stdlib.h>
#include <string.h>

float ff[11], f[200][5];
float correl[100][100], xi[100][100], eta[100][100];
float avg_sum[100][100], avg_correl[100][100], sum_correl[100][100];

void main(int argc, char *argv[]) {
char ch, str[80], str2[22];
char *buffer;
FILE *f4, *f6, *f8;
int nc, np, num_pts, num_zero=55, l, m, n, o, p, q, r, scan, jout, sals;
int num_check, s_count=0;
int ns, decimal, sign, jump;
int i, j, ii, jj, iii, jjj;
unsigned long num, count, num_calcs;
float dia, radius, angle, cord;
float rho=1.02, pi=3.14159;
float rmin= - 1, rmax=1.0, tor, tpi, pio2;
float d_gama, d_gamao2, d_nu, d_r, d_theta;
float x, y;
double d_ro2, dval, ten=10.0, nn;

/*********************************************************************/
/**  # angle segments=na, # k segments=nk, # wave component          **/
/**                    CGS UNITS                                    **/
/**  rmin and rmax are log(base_10) of kmin and of kmax             **/
/*********************************************************************/

/** NEED TO DECLARE FILE NAME **/
char fname[18];
printf("Enter the number of scans you want to evaluate:  ");
```

```
scanf("%d", &ns);
for(scan=1;scan<=ns;++scan)
 {
 nn = (double) scan;
 buffer = fcvt(nn, 0, &decimal, &sign);
 strcat (buffer,".swm");
 strcpy (fname, buffer);
 /** printf("Currently Calculating File: %s  Number: %.2d of %.2d\n",fname, scan, ns); **/

                                /** Read in file information    **/
                                /** Open file for writing       **/

 if((f6=fopen(fname,"r"))==NULL)
  {
  printf("Cannot open file\n");
  exit(1);
  }

 fgets(str,80,f6);

 for(i=1;i<=7;++i)
  {
  fscanf(f6,"%s %f",str,&cord);
  ff[i]=cord;
  /**  printf("%s\t%f\n",str,ff[i]);  **/
  }

 num_pts=(int)ff[2];

 fgets(str,80,f6);
 fgets(str,80,f6);
 fgets(str,80,f6);

 for(i=0;i<=num_pts;i++)
  {
  for(j=0;j<=4;j++)
   {
   fscanf(f6,"%f",&cord);
   f[i][j]=cord;
   }
  }
```

```
/** Check input data  **/

 if(f[0][0]!=1.0 || f[1][0]!=2.0)
  {
  printf("\n\nError inputing data.\n\nCheck format of file: %s\n",fname);
  exit(1);
  }

 fclose(f6);

/**     for(i=1;i<=num_pts;++i)                                                  **/
/**     printf("%f\t%f\t%f\t%f\t%f\n",f[i][1], f[i][2], f[i][3], f[i][4], f[i][5]);  **/

/** calculate the delta gama for every segment **/

 tpi=2.0*pi;
 pio2=pi/2;
 d_gama=tpi/num_pts;
 d_gamao2=d_gama/2.0;
 d_nu=tpi/num_pts;

 radius=ff[1]/2;                                          /** Radius  **/


/*******************************************************/
/** Find AUTOCORRELATION of points on circle          **/
/*******************************************************/

 for(i=0;i<num_pts;i++)
  {
  for(j=0;j<num_pts;j++)
   {
   correl[i][j]=f[i][1]*f[j][1];
   }
  }

 for(i=0;i<num_pts;i++)
  {
  for(j=0;j<i;j++)
   {
   cord = 2*radius*sin(abs(i-j) * d_gamao2);
   xi[i][j] = cord * cos(((num_pts - i) + j) * d_gamao2 + i * d_gama);
   eta[i][j] =cord * sin(((num_pts - i) + j) * d_gamao2 + i * d_gama);
```

```
    if(i<num_pts/2 && j<num_pts/2)
     {
     ii=j + num_pts/2;
     jj=i + num_pts/2;
     avg_correl[i][j] = (correl[i][j] + correl[ii][jj])/2;
     }
    else if(i<num_pts/2 && j>=num_pts/2)
     {
     ii=j - num_pts/2;
     jj=i + num_pts/2;
     avg_correl[i][j] = (correl[i][j] + correl[ii][jj])/2;
     }
    else if(i>=num_pts/2 && j<num_pts/2)
     {
     ii=j + num_pts/2;
     jj=i - num_pts/2;
     avg_correl[i][j] = (correl[i][j] + correl[ii][jj])/2;
      }
    else
     {
     ii=j - num_pts/2;
     jj=i - num_pts/2;
     avg_correl[i][j] = (correl[i][j] + correl[ii][jj])/2;
     }

/**     printf("\ni= %.2d  j= %.2d  ii=%.2d  jj= %.2d", i, j, ii, jj);     **/
/**     printf("\ni= %.3d\tj= %.3d\tcord= %9.4f", i, j, cord);          **/

    }

   for(j=i;j<num_pts;j++)
    {
    cord = 2*radius*sin(abs((i-j)) * d_gamao2);
    xi[i][j] = cord * cos((j - i) * d_gamao2 + i * d_gama);
    eta[i][j] =cord * sin((j - i) * d_gamao2 + i * d_gama);

    if(i<num_pts/2 && j<num_pts/2)
     {
     ii=j + num_pts/2;
     jj=i + num_pts/2;
     avg_correl[i][j] = (correl[i][j] + correl[ii][jj])/2;
     }
    else if(i<num_pts/2 && j>=num_pts/2)
     {
     ii=j - num_pts/2;
```

```
      jj=i + num_pts/2;
      avg_correl[i][j] = (correl[i][j] + correl[ii][jj])/2;
      }
     else if(i>=num_pts/2 && j<num_pts/2)
      {
      ii=j + num_pts/2;
      jj=i - num_pts/2;
      avg_correl[i][j] = (correl[i][j] + correl[ii][jj])/2;
      }
     else
      {
      ii=j - num_pts/2;
      jj=i - num_pts/2;
      avg_correl[i][j] = (correl[i][j] + correl[ii][jj])/2;
      }

        /**     printf("\n%.2d\t%.2d  ii=%.2d  jj= %.2d", i, j, ii, jj);        **/
        /**     printf("\ni= %.3d\tj= %.3d\tcord= %9.4f", i, j, cord);         **/
     }

    xi[i][i] = 0;
    eta[i][i] = 0;

        /**     Calculate the 00, 11, 22, 33, 44, ... repeated points         **/

    avg_correl[i][i]=0.0;
    for(j=0;j<num_pts;j++)
     {
     avg_correl[i][i]=(avg_correl[i][i] + correl[j][j]);
     }

/**     printf("\ni= %d avg_correl[%.2d][%.2d] = %12.6f / %.2d", i, i, i,    **/
/**     avg_correl[i][i], num_pts);                                           **/

    avg_correl[i][i]=avg_correl[i][i]/num_pts;

    for(j=0;j<num_pts;j++)
     {
     sum_correl[i][j]=(sum_correl[i][j] + avg_correl[i][j]);
     }
    }
   }
```

```
/**      Turn the sum of scans into average of scans          **/

for(i=0;i<num_pts;i++)
 {
 for(j=0;j<num_pts;j++)
  {
  sum_correl[i][j] = sum_correl[i][j]/(scan - 1);
/**  printf("i %.2d\tj %.2d\txi %6.3f\teta %6.3f\tcorrel  %8.6f\tavg_correl %12.9f\n",    **/
/**  i, j, xi[i][j], eta[i][j], correl[i][j], avg_correl[i][j]);                          **/
  }
 }

/*************************************************************************/
/**                Print output file for the H.S. Olmez Solver                          **/
/*************************************************************************/
buffer = fcvt(nn, 0, &decimal, &sign); strcat (buffer,".hso"); strcpy (fname, buffer);
if((f8=fopen(fname,"w"))==NULL)
 {
 printf("Cannot open file\n");
 exit(1);
 }
                    /**          Print the 0,0 case       **/

fprintf(f8,"    %10.6f %10.6f %10.6f\n\n", xi[0][0], eta[0][0], sum_correl[0][0]);
for(i=0;i<num_pts;i++)
 {
 /**   fprintf(f8,"%.2d",i);   **/
 if(i<num_pts/2)
  {
  for(j=(i+num_pts/2);j<num_pts;j++)
   {
      /**     fprintf(f8,"    %.2d %.2d %10.6f %10.6f %10.6f",        **/
      /**     i, j, xi[i][j], eta[i][j], sum_correl[i][j]);           **/
      fprintf(f8,"    %10.6f %10.6f %10.6f", xi[i][j], eta[i][j], sum_correl[i][j]);
   }
  for(j=0;j<i;j++)
   {
      fprintf(f8,"    %10.6f %10.6f %10.6f", xi[i][j], eta[i][j], sum_correl[i][j]);
   }
  }

 if(i>=num_pts/2)
  {
  for(j=(i-num_pts/2);j<i;j++)
   {
```

```
        fprintf(f8,"    %10.6f %10.6f %10.6f", xi[i][j], eta[i][j], sum_correl[i][j]);
    }
   }
 fprintf(f8,"\n");
 }
 fclose(f8);

/*****************************************************************/
/**                    Print work file for jmass                **/
/*****************************************************************/

buffer = fcvt(nn, 0, &decimal, &sign);
strcat (buffer,".mas");
strcpy (fname, buffer);

if((f8=fopen(fname,"w"))==NULL)
 {
 printf("Cannot open file\n");
 exit(1);
 }

/**     fprintf(f8,"VARIABLES = X, Y, Autocorrelation\n");              **/
/**     fprintf(f8,"ZONE T =\"Zone One\", I=1, J=4096, F=POINT\n");     **/

/**     Print the 0,0 case              **/
fprintf(f8,"    %10.6f %10.6f %10.6f\n", xi[0][0], eta[0][0], sum_correl[0][0]);

/**     Print the rest of the cases     **/
for(i=0;i<num_pts;i++)
 {
 if(i<num_pts/2)
  {
  for(j=(i+num_pts/2);j<num_pts;j++)
   {
/**     fprintf(f8,"    %.2d %.2d %10.6f %10.6f %10.6f\n",      **/
/**     i, j, xi[i][j], eta[i][j], sum_correl[i][j]);           **/
        fprintf(f8,"    %10.6f %10.6f %10.6f\n", xi[i][j], eta[i][j], sum_correl[i][j]);
   }
  for(j=0;j<i;j++)
   {
/**     fprintf(f8,"    %.2d %.2d %10.6f %10.6f %10.6f\n",      **/
/**     i, j, xi[i][j], eta[i][j], sum_correl[i][j]);           **/
        fprintf(f8,"    %10.6f %10.6f %10.6f\n", xi[i][j], eta[i][j], sum_correl[i][j]);
   }
  }
```

```
 if(i>=num_pts/2)
  {
  for(j=(i-num_pts/2);j<i;j++)
   {
/**     fprintf(f8,"   %.2d %.2d %10.6f %10.6f %10.6f\n",      **/
/**     i, j, xi[i][j], eta[i][j], sum_correl[i][j]);          **/
        fprintf(f8,"   %10.6f %10.6f %10.6f\n", xi[i][j], eta[i][j], sum_correl[i][j]);
   }
  }

 }

x=0.0;
y=0.0;

for(i=0;i<=num_zero;i++)
 {
 for(j=0;j<=num_zero;j++)
  {
  x=i*2*radius/num_zero;
  y=j*2*radius/num_zero;
  if((2*radius*2*radius) < (x*x + y*y))
       {
       fprintf(f8,"   %10.6f %10.6f %10.6f\n", x, y, 0.0);
       fprintf(f8,"   %10.6f %10.6f %10.6f\n", x, - y, 0.0);
       fprintf(f8,"   %10.6f %10.6f %10.6f\n", - x, y, 0.0);
       fprintf(f8,"   %10.6f %10.6f %10.6f\n", - x, - y, 0.0);
       }
  }
 }

fclose(f8);

/*************************************************************************/
/** Print output file for tecplot                                       **/
/** File converts autocorrelation data into i x j matrix data for       **/
/** TECPLOT graphs. The data is printed in the format PREPLOT requires. **/
/** Data is converted by stretching the center point of the circle into a line **/
/** and using double points                                             **/
/*************************************************************************/

buffer = fcvt(nn, 0, &decimal, &sign);
strcat (buffer,".tec");
strcpy (fname, buffer);
```

```
if((f4=fopen(fname,"w"))==NULL)
 {
 printf("Cannot open file\n");
 exit(1);
 }

fprintf(f4,"TITLE = \"Autocorrelation for %d Scans\"\n",scan-1);
fprintf(f4,"VARIABLES = X, Y, Autocorrelation\n");
fprintf(f4,"ZONE T =\"Zone One\", I=%.2d, J=%.2d, F=POINT\n", num_pts+2, num_pts+1);

j=0;
p=0;

for(i=num_pts/2;i>0;i--)              /** first set of numbers **/
 {
 if(i>j)
  {
  /**  fprintf(f4,"    %.2d %.2d %10.6f %10.6f %10.6f\n",      **/
  /**  i, j, xi[i][j], eta[i][j], sum_correl[i][j]);           **/
  fprintf(f4,"    %10.6f %10.6f %10.6f\n",  xi[i][j], eta[i][j], sum_correl[i][j]);
  fprintf(f4,"    %10.6f %10.6f %10.6f\n",  xi[i][j], eta[i][j], sum_correl[i][j]);
  j++;
  p++;
  }
 else if(p=num_pts/4)
  {
  fprintf(f4,"    %10.6f %10.6f %10.6f\n", xi[0][0], eta[0][0], sum_correl[0][0]);
  fprintf(f4,"    %10.6f %10.6f %10.6f\n", xi[0][0], eta[0][0], sum_correl[0][0]);
  i=0;
  }
 }

j=num_pts/4 - 1;       /** correct the j count **/

for(i=0;i<=num_pts/2;i++)
 {
 if(i>num_pts/4)
  {
  /**  fprintf(f4,"    %.2d %.2d %10.6f %10.6f %10.6f\n",      **/
  /**  i, j, xi[i][j], eta[i][j], sum_correl[i][j]);           **/
  fprintf(f4,"    %10.6f %10.6f %10.6f\n",  xi[i][j], eta[i][j], sum_correl[i][j]);
  fprintf(f4,"    %10.6f %10.6f %10.6f\n",  xi[i][j], eta[i][j], sum_correl[i][j]);
  j--;
  }
 }
```

```
/** second set **/

ii=num_pts/2;
jj=0;
iii=num_pts/4;
jjj=num_pts/4;

p=0;
n=0;
o=0;

for(m=(num_pts - 1);m>0;m--)
 {
 if(p<num_pts/4)
  {
  j=jj;
  o=jjj;
  for(i=ii-1;p<num_pts/4;i--)
   {
   if(i<0 && j<0)
    {
    /** fprintf(f4,"    %.2d %.2d %10.6f %10.6f %10.6f\n",                  **/
    /** num_pts + i, num_pts + j, xi[num_pts + i][num_pts + j],             **/
    /** eta[num_pts + i][num_pts + j], sum_correl[num_pts + i][num_pts + j]); **/
    fprintf(f4,"    %10.6f %10.6f %10.6f\n", xi[num_pts + i][num_pts + j],
      eta[num_pts + i][num_pts + j], sum_correl[num_pts + i][num_pts + j]);
    fprintf(f4,"    %10.6f %10.6f %10.6f\n", xi[num_pts + i][num_pts + j],
      eta[num_pts + i][num_pts + j], sum_correl[num_pts + i][num_pts + j]);
    }
   else if(i>=0 && j<0)
    {
    /** fprintf(f4,"    %.2d %.2d %10.6f %10.6f %10.6f\n",                  **/
    /** i, num_pts + j, xi[i][num_pts + j], eta[i][num_pts + j],            **/
    /** sum_correl[i][num_pts + j]);                                        **/
    fprintf(f4,"    %10.6f %10.6f %10.6f\n", xi[i][num_pts + j],
      eta[i][num_pts + j], sum_correl[i][num_pts + j]);
    fprintf(f4,"    %10.6f %10.6f %10.6f\n", xi[i][num_pts + j],
      eta[i][num_pts + j], sum_correl[i][num_pts + j]);
    }
   else if(i<0 && j>=0)
    {
    /** fprintf(f4,"    %.2d %.2d %10.6f %10.6f %10.6f\n",                  **/
    /** num_pts + i, j, xi[num_pts + i][j],                                 **/
    /** eta[num_pts + i][j], sum_correl[num_pts + i][j]);                   **/
```

```
  fprintf(f4,"    %10.6f %10.6f %10.6f\n", xi[num_pts + i][j], eta[num_pts + i][j],
    sum_correl[num_pts + i][j]);
  fprintf(f4,"    %10.6f %10.6f %10.6f\n", xi[num_pts + i][j], eta[num_pts + i][j],
    sum_correl[num_pts + i][j]);
  }
 else
  {
  /** fprintf(f4,"    %.2d %.2d %10.6f %10.6f %10.6f\n",                **/
  /** i, j, xi[i][j], eta[i][j], sum_correl[i][j]);                     **/
  fprintf(f4,"    %10.6f %10.6f %10.6f\n", xi[i][j], eta[i][j], sum_correl[i][j]);
  fprintf(f4,"    %10.6f %10.6f %10.6f\n", xi[i][j], eta[i][j], sum_correl[i][j]);
  }
 j++;
 p++;
 }

fprintf(f4,"    %10.6f %10.6f %10.6f\n", xi[0][0], eta[0][0], sum_correl[0][0]);
fprintf(f4,"    %10.6f %10.6f %10.6f\n", xi[0][0], eta[0][0], sum_correl[0][0]);

for(n=iii+1;r<num_pts/4;n++)
 {
 if(n<0 && o<0)
  {
  /** fprintf(f4,"    %.2d %.2d %10.6f %10.6f %10.6f\n",                **/
  /** num_pts + n, num_pts + o, xi[num_pts + n][num_pts + o],           **/
  /** eta[num_pts + n][num_pts + o], sum_correl[num_pts + n][num_pts + o]);**/
  fprintf(f4,"    %10.6f %10.6f %10.6f\n", xi[num_pts + n][num_pts + o],
    eta[num_pts + n][num_pts + o], sum_correl[num_pts + n][num_pts + o]);
  fprintf(f4,"    %10.6f %10.6f %10.6f\n", xi[num_pts + n][num_pts + o],
    eta[num_pts + n][num_pts + o], sum_correl[num_pts + n][num_pts + o]);
  }
 else if(n>=0 && o<0)
  {
  /** fprintf(f4,"    %.2d %.2d %10.6f %10.6f %10.6f\n",                **/
  /** n, num_pts + o, xi[n][num_pts + o], eta[n][num_pts + o],          **/
  /** sum_correl[n][num_pts + o]);                                      **/
  fprintf(f4,"    %10.6f %10.6f %10.6f\n", xi[n][num_pts + o],
    eta[n][num_pts + o], sum_correl[n][num_pts + o]);
  fprintf(f4,"    %10.6f %10.6f %10.6f\n", xi[n][num_pts + o],
    eta[n][num_pts + o], sum_correl[n][num_pts + o]);
  }
```

```
  else if(n<0 && o>=0)
    {
    /** fprintf(f4,"    %.2d %.2d %10.6f %10.6f %10.6f\n",          **/
    /** num_pts + n, o, xi[num_pts + n][o],                        **/
    /** eta[num_pts + n][o], sum_correl[num_pts + n][o]);          **/
    fprintf(f4,"    %10.6f %10.6f %10.6f\n", xi[num_pts + n][o],
      eta[num_pts + n][o], sum_correl[num_pts + n][o]);
    fprintf(f4,"    %10.6f %10.6f %10.6f\n", xi[num_pts + n][o],
      eta[num_pts + n][o], sum_correl[num_pts + n][o]);
    }
  else
    {
    /** fprintf(f4,"    %.2d %.2d %10.6f %10.6f %10.6f\n",    **/
    /** n, o, xi[n][o], eta[n][o], sum_correl[n][o]);          **/
    fprintf(f4,"    %10.6f %10.6f %10.6f\n", xi[n][o], eta[n][o], sum_correl[n][o]);
    fprintf(f4,"    %10.6f %10.6f %10.6f\n", xi[n][o], eta[n][o], sum_correl[n][o]);
    }
  o--;
  r++;
  }
 jj--;
 iii++;
 }

else if(p==num_pts/4)
 {
 j=jj;
 o=jjj;
 for(i=ii - 1;p<num_pts/2;i--)
  {
  if(i<0 && j<0)
    {
    /** fprintf(f4,"    %.2d %.2d %10.6f %10.6f %10.6f\n",          **/
    /** num_pts + i, num_pts + j, xi[num_pts + i][num_pts + j],    **/
    /** eta[num_pts + i][num_pts + j], sum_correl[num_pts + i][num_pts + j]);  **/
    fprintf(f4,"    %10.6f %10.6f %10.6f\n", xi[num_pts + i][num_pts + j],
      eta[num_pts + i][num_pts + j], sum_correl[num_pts + i][num_pts + j]);
    fprintf(f4,"    %10.6f %10.6f %10.6f\n", xi[num_pts + i][num_pts + j],
      eta[num_pts + i][num_pts + j], sum_correl[num_pts + i][num_pts + j]);
    }
  else if(i>=0 && j<0)
    {
    /** fprintf(f4,"    %.2d %.2d %10.6f %10.6f %10.6f\n",          **/
    /** i, num_pts + j, xi[i][num_pts + j],                        **/
    /** eta[i][num_pts + j], sum_correl[i][num_pts + j]);          **/
```

```
  fprintf(f4,"    %10.6f %10.6f %10.6f\n", xi[i][num_pts + j],
    eta[i][num_pts + j], sum_correl[i][num_pts + j]);
  fprintf(f4,"    %10.6f %10.6f %10.6f\n", xi[i][num_pts + j],
    eta[i][num_pts + j], sum_correl[i][num_pts + j]);
  }
 else if(i<0 && j>=0)
  {
  /** fprintf(f4,"    %.2d %.2d %10.6f %10.6f %10.6f\n",                    **/
  /** num_pts+i, j, xi[num_pt +i][j], eta[num_pts+i][j], sum_correl[num_pts+i][j]);    **/
  fprintf(f4,"    %10.6f %10.6f %10.6f\n", xi[num_pts + i][j], eta[num_pts + i][j],
    sum_correl[num_pts + i][j]);
  fprintf(f4,"    %10.6f %10.6f %10.6f\n", xi[num_pts + i][j], eta[num_pts + i][j],
    sum_correl[num_pts + i][j]);
  }
 else
  {
  /** fprintf(f4,"    %.2d %.2d %10.6f %10.6f %10.6f\n",    **/
  /** i, j, xi[i][j], eta[i][j], sum_correl[i][j]);                **/
  fprintf(f4,"    %10.6f %10.6f %10.6f\n", xi[i][j], eta[i][j], sum_correl[i][j]);
  fprintf(f4,"    %10.6f %10.6f %10.6f\n", xi[i][j], eta[i][j], sum_correl[i][j]);
  }
  j++;
  p++;
 }

fprintf(f4,"    %10.6f %10.6f %10.6f\n", xi[0][0], eta[0][0], sum_correl[0][0]);
fprintf(f4,"    %10.6f %10.6f %10.6f\n", xi[0][0], eta[0][0], sum_correl[0][0]);

for(n=iii+1;r<num_pts/2;n++)
 {
 if(n<0 && o<0)
  {
  /** fprintf(f4,"    %.2d %.2d %10.6f %10.6f %10.6f\n",                  **/
  /** num_pts + n, num_pts + o, xi[num_pts + n][num_pts + o],             **/
  /** eta[num_pts + n][num_pts + o], sum_correl[num_pts + n][num_pts + o]);**/
  fprintf(f4,"    %10.6f %10.6f %10.6f\n", xi[num_pts + n][num_pts + o],
    eta[num_pts + n][num_pts + o], sum_correl[num_pts + n][num_pts + o]);
  fprintf(f4,"    %10.6f %10.6f %10.6f\n", xi[num_pts + n][num_pts + o],
    eta[num_pts + n][num_pts + o], sum_correl[num_pts + n][num_pts + o]);
  }
 else if(n>=0 && o<0)
  {
  /** fprintf(f4,"    %.2d %.2d %10.6f %10.6f %10.6f\n",              **/
  /** n, num_pts + o, xi[n][num_pts + o], eta[n][num_pts + o],        **/
  /** sum_correl[n][num_pts + o]);                                    **/
```

```
      fprintf(f4,"    %10.6f %10.6f %10.6f\n", xi[n][num_pts + o], eta[n][num_pts + o],
        sum_correl[n][num_pts + o]);
      fprintf(f4,"    %10.6f %10.6f %10.6f\n", xi[n][num_pts + o], eta[n][num_pts + o],
        sum_correl[n][num_pts + o]);
      }
     else if(n<0 && o>=0)
      {
      /** fprintf(f4,"    %.2d %.2d %10.6f %10.6f %10.6f\n",          **/
      /** num_pts + n, o, xi[num_pts + n][o], eta[num_pts + n][o],    **/
      /** sum_correl[num_pts + n][o]);                                **/
      fprintf(f4,"    %10.6f %10.6f %10.6f\n", xi[num_pts + n][o], eta[num_pts + n][o],
        sum_correl[num_pts + n][o]);
      fprintf(f4,"    %10.6f %10.6f %10.6f\n", xi[num_pts + n][o], eta[num_pts + n][o],
        sum_correl[num_pts + n][o]);
      }
     else
      {
      /** fprintf(f4,"    %.2d %.2d %10.6f %10.6f %10.6f\n",          **/
      /** n, o, xi[n][o], eta[n][o], sum_correl[n][o]);               **/
      fprintf(f4,"    %10.6f %10.6f %10.6f\n", xi[n][o], eta[n][o], sum_correl[n][o]);
      fprintf(f4,"    %10.6f %10.6f %10.6f\n", xi[n][o], eta[n][o], sum_correl[n][o]);
      }
     o--;
     r++;
     }
   p=0;
   r=0;
   ii--;
   jjj++;
   }
 }

q=0;
j=num_pts/2;
p=0;

/** last set of numbers **/

for(i=0;i<num_pts/2;i++)
 {
 if(i<j)
  {
  /** fprintf(f4,"    %.2d %.2d %10.6f %10.6f %10.6f\n",          **/
  /** i, j, xi[i][j], eta[i][j], sum_correl[i][j]);               **/
  fprintf(f4,"    %10.6f %10.6f %10.6f\n", xi[i][j], eta[i][j], sum_correl[i][j]);
```

```
    fprintf(f4,"    %10.6f %10.6f %10.6f\n", xi[i][j], eta[i][j], sum_correl[i][j]);
    j--;
    p++;
    }
   else if(p=num_pts/4)
    {
    fprintf(f4,"    %10.6f %10.6f %10.6f\n", xi[0][0], eta[0][0], sum_correl[0][0]);
    fprintf(f4,"    %10.6f %10.6f %10.6f\n", xi[0][0], eta[0][0], sum_correl[0][0]);
    i=num_pts/2;
    }
  }

  j=num_pts/4 + 1;        /** correct the j count **/

  for(i=num_pts/4 - 1;i>=0;i--)
   {
   /** fprintf(f4,"    %.2d %.2d %10.6f %10.6f %10.6f\n",        **/
   /** i, j, xi[i][j], eta[i][j], sum_correl[i][j]);             **/
   fprintf(f4,"    %10.6f %10.6f %10.6f\n", xi[i][j], eta[i][j], sum_correl[i][j]);
   fprintf(f4,"    %10.6f %10.6f %10.6f\n", xi[i][j], eta[i][j], sum_correl[i][j]);
   j++;
   }

fclose(f4);

}
```

```
C "DFSUM.F"
C Written by John T. Mass
C Least Squares Solver --- written by Hasan S. Olmez
C Edited by David Chen

program dfsum
parameter(m=4893,n=17)
C
C*****************************************************************
C
C    n must be odd for current count a(k,ip)
C
C*****************************************************************
C
C
C    2317=2049+268 (268 zeroes)
C    m : # of points on the surface
C    n : # of points for the Fourier sum
C
C    R(x,y)=sum(1,nx) sum(1,ny) A(nx,ny) cos(nx pi x/Lx) cos(ny pi y/Ly)
C    where nx=ny=n
C

dimension aux(2*n*n,1),ipiv(n),x(m),y(m),r(m),sol(n*n,1)
dimension a(m,n*n),b(m,1),skx(n,1),sky(n,1),spp(n,n)
dimension rn(m)

real lx,ly
data pi /3.141592654/

C    DIAMETER OF WIRE CAGE
diameter = 20
C    RADIUS OF AUTOCORRELATION SPACE
radius = diameter

lx=diameter
ly=diameter

open(10,file='correl.mas',status='unknown')
open(20,file='z.dat',status='unknown')
open(30,file='s.dat',status='unknown')
open(40,file='spec.dat',status='unknown')
open(50,file='foo.dat',status='unknown')
```

```
do 1 i=1,m
        read(10,*) x(i),y(i),r(i)
        if(x(i).eq.0.0 .and. y(i).eq.0.0) r0=r(i)

C*****************************************************************
C    convolve the auto correlation with a smoothing window
C       wn =  sqrt(x(i)*x(i) + y(i)*y(i))
C       rn(i)=r(i)*(1.0 - wn/diameter)
C       rn(i)=r(i)
C*****************************************************************
C    Second window
C       rn(i)=r(i)*2/pi(acos(r/R-r/Rsqrt(1-(pow(2,r/R))
        wn =  (sqrt(x(i)*x(i) + y(i)*y(i)))/radius
        if(wn.le.1.0) then
                rn(i)=r(i)*(2./pi)*(acos(wn) - wn*sqrt(1. - (wn*wn)))
        else
                rn(i) = 0.0
        end if
C       write(*,*) rn(i)

1   continue

do 30 k=1,m
        ip=0
        do 20 i=-n/2,n/2
                do 10 j=1,n
                ip=ip+1
                a(k,ip)=cos((i)*pi*x(k)/lx)*cos((j)*pi*y(k)/ly)-
&                       sin((i)*pi*x(k)/lx)*sin((j)*pi*y(k)/ly)

10              continue
20      continue
        b(k,1)=rn(k)
30  continue

C do 32 i=1,m
C               write(50,'(25E12.4)') (a(i,j),j=1,25)
C 32  continue

nsq=n*n
write(*,*) 'nsq: ',nsq
call llsq(a,b,m,nsq,1,sol,ipiv,0.00000000000001,ier,aux)

write(*,*) 'Error warning: ',ier
```

```
C*****************************************************************
C     Regenerate the autocorrelation
C
C    For regeneration to work, producing equally spaced points,
C    the original autocorrelation file must be padded with zeros
C    in the corners
C
C
C*****************************************************************

write(20,*) 'TITLE = "Reconstructed Autocorrelation"'
write(20,*) 'VARIABLES = X, Y, Autocorrelation'
write(20,*) 'ZONE T = "Zone One", I=64, J=64, F=POINT'

do 70 ix=1,64
        xn=-lx+((ix-0.5)*2.*lx/64.0)
C       xn=((ix-0.5)*lx/64.0)
        do 60 jy=1,64
                ip=0
                sum=0.0
                yn=-ly+((jy-0.5)*2.*ly/64.0)
C               yn=((jy-0.5)*ly/64.0)
                do 50 i=-n/2,n/2
                        do 40 j=1,n
                                ip=ip+1
                                sum=sum+(sol(ip,1)*
&                                       (cos((i)*pi*xn/lx)*cos((j)*pi*yn/ly)-
&                                       sin((i)*pi*xn/lx)*sin((j)*pi*yn/ly)))
40                      continue
50              continue
                write(20,*) xn,yn,sum
60      continue
70 continue

C*****************************************************************
C                       Calculate the spectra from the solution matrix          *
C*****************************************************************

write(30,*) 'TITLE = "Spectral Energy"'
write(30,*) 'VARIABLES = X, Y, S'
write(30,*) 'ZONE T = "Zone One", I=21, J=21, F=POINT'

ip=0
sum=0.0
fac=2.*pi*pi/(lx*ly)
```

```
do 90 i=1,n
        do 80 j=1,n
                ip=ip+1
C               skx(i,1)=(i)*pi/lx
                skx(i,1)=(-n/2 + i - 1)*pi/lx
                sky(j,1)=(j)*pi/ly
                sum=sum+sol(ip,1)
                sq=sol(ip,1)
                spp(i,j)=2.*(sol(ip,1)/fac)
C               spp(i,j)=sol(ip,1)
C               sq=sol(ip,1)*sol(ip,1)
C               write(30,*) i,j,sq/fac
                write(30,*) skx(i,1),sky(j,1),sq/fac

C    Question about the factor of two in spp(i, j)

80      continue
90 continue

write(40,'(22E12.4)')(sky(i,1),i=1,n)

do 100 i=1,n
        write(40,'(22E12.4)') skx(i,1),(spp(i,j),j=1,n)
100 continue

write(*,*) 'r0  sum ', r0,sum
stop
end

    SUBROUTINE LLSQ(A,B,M,N,L,X,IPIV,EPS,IER,AUX)
C*************************************************************************
C
C       Purpose
C         To solve linear least squares problems, i.e. to minimize
C         the Euclidean norm of B-A*X, where A is a M by N matrix
C         with M not less than N. In the special case M=N systems of
C         linear equations may be solved.
C
C       Usage
C         CALL LLSQ (A,B,M,N,L,X,IPIV,EPS,IER,AUX)
C
C       Description of parameters
C         A     - M by N coefficient matrix (destroyed).
C         B     - M by L right hand side matrix (destroyed).
C         M     - row number of matrices A and B.
```

```
C       N    - column number of matrix A, row number of matrix X.
C       L    - column number of matrices B and X.
C       X    - N by L solution matrix.
C       IPIV - integer output vector of dimension n which
C                   contains informations on column interchanges
C                   in matrix A. (see remark no.3).
C       EPS  - input parameter which specifies a relative
C                   tolerance for determination of rank of matrix A.
C       IER  - a resulting error parameter.
C       AUX  - auxiliary storage array of dimension MAX(2*N,L).
C                   on return first L locations of AUX contain the
C                   resulting least squares.
C
C     Remarks
C       (1) no action besides error message IER=-2 in case
C          M less than N.
C       (2) no action besides error message IER=-1 in case
C          of a zero-matrix A.
C       (3) if rank K of matrix A is found to be less than N but
C          greater than 0, the procedure returns with error code
C          IER=K into calling program. the last N-K elements of
C          vector IPIV denote the useless columns in matrix A.
C          the remaining useful columns form a base of matrix A.
C       (4) if the procedure was successful, error parameter IER
C          is set to 0.
C
C     Subroutines and function subprograms required
C       none
C
C     Method
C       Householder transformations are used to transform matrix A
C       to upper triangular form. After having applied the same
C       transformation to the right hand side matrix B, an
C       approximate solution of the problem is computed by
C       back substitution. For reference, see
C       G. Golub, Numerical Methods for Solving Linear Least
C       Squares Problems, Numerische Mathematik, vol.7,
C       iss.3 (1965), pp.206-216.
C
C*************************************************************************
      INTEGER IPIV(*)
      DIMENSION A(*),B(*),X(*),AUX(*)

C.....Error test
      IF(M .GE. N) THEN
```

```
C.....Generation of initial vector S(K) (K=1,2,...,N) in storage
C.....locations AUX(K) (K=1,2,...,N)
      PIV=0.0
      IEND=0
      DO 20 K=1,N
            IPIV(K)=K
            H=0.0
            IST=IEND+1
            IEND=IEND+M
            DO 10 I=IST,IEND
                  H=H+A(I)*A(I)
10          CONTINUE
            AUX(K)=H
            IF(H .GT. PIV) THEN
                  PIV=H
                  KPIV=K
            END IF
20    CONTINUE

C.....Error return in case of zero-matrix A
      IF(PIV .LE. 0) THEN
            IER=-1
            RETURN
      END IF

C.....Define tolerance for checking rank of A
      SIG=SQRT(PIV)
      TOL=SIG*ABS(EPS)

C.....Decomposition loop
      LM=L*M
      IST=-M
      DO 110 K=1,N
            IST=IST+M+1
            IEND=IST+M-K
            I=KPIV-K

            IF(I .GT. 0) THEN
C.....Interchange K-th column of A with KPIV-th in case KPIV.GT.K
6                 H=AUX(K)
                  AUX(K)=AUX(KPIV)
                  AUX(KPIV)=H
                  ID=I*M
                  DO 30 I=IST,IEND
                        J=I+ID
```

```
                    H=A(I)
                    A(I)=A(J)
                    A(J)=H
30                  CONTINUE
                    END IF

C.....Computation of parameter SIG
                    IF(K .GT. 1) THEN
                        SIG=0.0
                        DO 40 I=IST,IEND
                            SIG=SIG+A(I)*A(I)
40                      CONTINUE
                        SIG=SQRT(SIG)

C.....Error return in case of rank of matrix A less than N
                        IF(SIG .LE. TOL) THEN
                            IER=K-1
                            RETURN
                        END IF
                    END IF

C.....Generate correct sign of parameter SIG
                    H=A(IST)
                    IF(H .LT. 0.0) SIG=-SIG

C.....Save interchange information
                    IPIV(KPIV)=IPIV(K)
                    IPIV(K)=KPIV

C.....Generation of vector UK in K-th column of matrix A and of
C.....parameter BETA
                    BETA=H+SIG
                    A(IST)=BETA
                    BETA=1.0/(SIG*BETA)
                    J=N+K
                    AUX(J)=-SIG
                    IF(K .LT. N) THEN

C.....Transformation of matrix A
                        PIV=0.0
                        ID=0
                        JST=K+1
                        KPIV=JST
                        DO 70 J=JST,N
                            ID=ID+M
```

```
                                H=0.0
                                DO 50 I=IST,IEND
                                    II=I+ID
                                    H=H+A(I)*A(II)
50                              CONTINUE
                                H=BETA*H
                                DO 60 I=IST,IEND
                                    II=I+ID
                                    A(II)=A(II)-A(I)*H
60                              CONTINUE

C.....Updating of element S(J) stored in location AUX(J)
                                II=IST+ID
                                H=AUX(J)-A(II)*A(II)
                                AUX(J)=H
                                IF(H .GT. PIV) THEN
                                    PIV=H
                                    KPIV=J
                                END IF
70                          CONTINUE
                            END IF

C.....Transformation of right hand side matrix B
                            DO 100 J=K,LM,M
                                H=0.0
                                IEND=J+M-K
                                II=IST
                                DO 80 I=J,IEND
                                    H=H+A(II)*B(I)
                                    II=II+1   80
                                CONTINUE
                                H=BETA*H
                                II=IST
                                DO 90 I=J,IEND
                                    B(I)=B(I)-A(II)*H
                                    II=II+1
90                              CONTINUE
100                         CONTINUE
110                 CONTINUE

C.....Back substitution and back interchange
                    IER=0
                    I=N
                    LN=L*N
                    PIV=1.0/AUX(2*N)
```

```
                DO 120 K=N,LN,N
                    X(K)=PIV*B(I)
                    I=I+M
120             CONTINUE

                IF(N .GT. 1) THEN
                    JST=(N-1)*M+N
                    DO 150 J=2,N
                    JST=JST-M-1
                    K=N+N+1-J
                    PIV=1.0/AUX(K)
                    KST=K-N
                    ID=IPIV(KST)-KST
                    IST=2-J
                    DO 140 K=1,L
                        H=B(KST)
                        IST=IST+N
                        IEND=IST+J-2
                        II=JST
                        DO 130 I=IST,IEND
                            II=II+M
                            H=H-A(II)*X(I)
130                     CONTINUE
                        I=IST-1
                        II=I+ID
                        IF (II .GT. I) X(I) = X(II)
                        X(II)=PIV*H
                        KST=KST+M
140                 CONTINUE
150             CONTINUE
            END IF

C.....Computation of least squares
            IST=N+1
            IEND=0
            DO 170 J=1,L
                IEND=IEND+M
                H=0.0
                IF(M .GT. N) THEN
                    DO 160 I=IST,IEND
                        H=H+B(I)*B(I)
160                 CONTINUE
                    IST=IST+M
                END IF
                AUX(J)=H
```

```
170         CONTINUE
            RETURN
      ELSE

C.....Error return in case M less than N
            IER=-2
            RETURN
      END IF
C(((((((((((((((((((( end of subroutine LLSQ )))))))))))))))))))
      END

      FUNCTION DOT(A,B)
      DIMENSION A(3),B(3)
      DOT=0.0
      DO 10 J=1,3
            DOT=DOT+A(J)*B(J)
      10 CONTINUE
      RETURN
      END

      SUBROUTINE CROSS(A,B,C)
      DIMENSION A(3),B(3),C(3)
      C(1)=A(2)*B(3)-A(3)*B(2)
      C(2)=A(3)*B(1)-A(1)*B(3)
      C(3)=A(1)*B(2)-A(2)*B(1)
      RETURN
      END
```